NTNU

Norwegian University of
Science and Technology

Oxidation of silicon in aqueous media

Håkon Trygve Strøm Jørgensen

Materials Science and Engineering
Submission date: June 2011
Supervisor: Mari-Ann Einarsrud, IMTE
Co-supervisor: Tor Grande, IMTE
Johan Svanem, Elkem
Harry Rong, Elkem

Norwegian University of Science and Technology
Department of Materials Science and Engineering

Preface

The work of this master thesis has been conducted at the Department of Materials Science and Engineering at the Norwegian University of Science and Technology (NTNU) during spring 2011, and has been in collaboration with Elkem. This thesis presents the results obtained during studies of the oxidation of silicon in aqueous media.

The master thesis has been carried out independently, honest and in accordance with the guide lines given.

Trondheim, June 2011

Håkon Trygve Strøm Jørgensen

Acknowledgement

During my work with this thesis I have gained a lot of knowledge and been fortunate enough to try a lot of different techniques for analysis. Being a metallurgist, the (phase) transition from metallurgy to inorganic chemistry has not been without strains and a certain expansion of volume. A number of people have been involved in my work, and they all deserve my uttermost gratitude for their effort and contribution.

First of all I want to express my sincere gratitude to my supervisor Professor Mari-Ann Einarsrud for her supervision of this work, the frequent feedback, suggestions and input during our weekly meetings and whenever I needed guidance.

M. Sc. Johan S. Svanem from Elkem deserves a lot of credit for his great support and many useful discussions both in person and through email.

I am grateful to Elkem AS for the financial support during this investigation and for providing me with the silicon powder and particles needed.

The ceramic group I have been involved with during this work has been an important forum for discussion and transfer of knowledge.

Great thanks are also addressed to M. Sc. Jan-Otto Hoel from Elkem, divisional engineer Julian Tolchard, Anne Støre at SINTEF, Syverin Lierhagen, Yingda Yu, Jianying He, Professor Tor Grande, Dr. Harry Rong, Lotte Skolem and Anne-Jorunn Enstad for their help and support.

Last but not least, I would like to thank my dear Magni Mauset for keeping up my spirits when the ordeals seemed endless.

Abstract

Silicon is used in the production of various ceramic products. As the solar industry is advancing, the need for reusable crucibles for the casting of solar grade silicon has arisen. One idea is to produce silicon nitride crucibles by slip casting. During slip casting, silicon powder is mixed with water at high alkaline conditions to ensure good dispersion of the powder and a stabilized slip. This may lead to oxidation of the silicon and the evolution of hydrogen gas. The hydrogen evolution introduces porosity in the final product, thereby ruining the mechanical properties. Gaining knowledge on how to inhibit the oxidation of silicon in slurries would therefore prove valuable for producing defect-free silicon based ceramics.

In this thesis the main objective is to gain knowledge about the oxidation of silicon in aqueous media, emphasizing on the formation of oxides with respect to initiation point, initiation time and characterizing of the oxide. Silicon powder and coarse silicon particles delivered by Elkem was oxidized in a purpose built apparatus. The effects on the powder and the coarse particles were examined by the several techniques, including among other: SEM, Colorimetry, HR ICP-MS and LECO. The mechanical properties of oxidized single crystal and polycrystalline silicon were also investigated, using nanoindentation.

The most important results, indicates that the oxidation of silicon results in formation of silica and hydrogen gas evolution. Firstly silicic acid is formed until the solubility limit is reached. Further oxidation leads to silicic acid condensing to form; colloidal silica which adsorbs on the silicon particles and dispersed colloidal silica in the suspension. The oxide layer formation on the coarse silicon particles were studied and confirmed using SEM. The oxide is the result of silicic acid condensing

to form silica and adsorbing on to the surface of the silicon. Initiation points for the oxidation were not found. A more controlled oxidation is needed and the study of the oxide layer must be performed with high resolution techniques like Atomic Force Microscopy and/or Auger Electron Spectroscopy.

The oxidation of silicon in aqueous media can be summarized as described in the figure below:

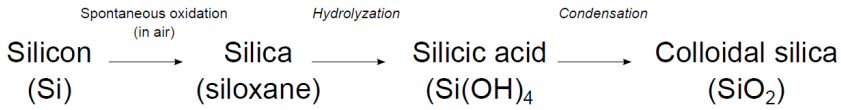

Oxidation of silicon in aqueous media, step-by-step.

There were some problems related to reproducing the results with respect to the hydrogen evolution from the silicon powder. Storage of the powder seemed to be a key factor as the powder behaved differently from one week to another. Storage in a desiccator for two weeks lead to earlier and more intense hydrogen evolution. Any reasonable cause for this was not found, and is subject for further investigations. The initiation time for hydrogen evolution was therefore difficult to determine, as it is dependent on unknown parameters.

Nanoindentation was found to be a useful technique for studying the mechanical properties of oxidized silicon. The results indicated that the single crystal samples were homogeneous with respect to mechanical properties, as each of the indents of the respective samples produced more or less the same value. The E-modulus for the oxidized single crystal sample was about 10 GPa lower than for the unoxidized sample, the hardness was not affected. The results for the polycrystalline sample is more difficult to interpret, but nanoindentation indicates that the oxidized sample is not as homogeneous as the single crystal particles with respect to mechanical properties. The hardness was equal to the single crystal samples, and the E-modulus was close to that of the unoxidized single crystal sample.

List of abbreviation and terminology

- **Silica** - Silicon dioxide.
- **Silanol** - Used for any OH group attached to silicon.
- **Siloxane** - Chemical compound composed of units of the form X_2SiO, where X is a hydrogen atom or a hydrocarbon group.
- **Silicate** - A compound containing an anion in which one or more central silicon atoms are surrounded by electronegative ligands (e.g. SiO_4^{4-}).
- **Silicic acid** - General name for a family of chemical compounds of the element silicon, hydrogen, and oxygen, with the general formula $[SiO_x(OH)_{4-2x}]_n$.
- **Hydrophilic** - The property of bonding with water through hydrogen bonding.
- **Suspension** - A heterogeneous fluid containing solid particles that are sufficiently large for sedimentation.
- **Slurry** - Dispersion of powder, solvent and a dispersant.
- **Slip** - Suspension in water of clay and/or other materials used in the production of ceramics.
- **Colloid** - A substance microscopically dispersed evenly throughout another substance.
- **PZC** - Point of Zero Charge (no net electric charge at the surface of a particle).

- **Zeta potential** - The potential at the surface of the shear plane (Stern plane) of a particle.
- **IEP** - Isoelectric point (The zeta potential is zero, i. e. no charge at the surface of the shear plane).
- **PSD** - Particle size distribution.
- **Darvan C-N** - Ammonium Polymethacrylate and water.
- **Polymerization** - In this context it means the condensation of the monomer, $Si(OH)_4$, to form a polymer and the subsequent $(SiO2)_n$.
- **Green body** - A ceramic compound before it has been sintered.
- **BET** - Method of measuring the specific surface area of particles.
- **SEM** - Scanning Electron Microscope.
- **XRD** - X-ray Diffraction.
- **LECO** - Combustion analysis for determination of elements such as carbon, nitrogen, oxygen and sulfur in inorganic samples.
- **Colorimetry** - Determination of the concentration of coloured compounds in solution.
- **HR ICP-MS** - High Resolution Inductively Coupled Plasma Mass Spectrometry.
- **EBSD** - Electron backscatter diffraction.
- **Nanoindentation** - Technique for measuring hardness of small volumes of material.

Contents

Chapter 1

Introduction

1.1 Motivation

Silicon is used to produce various ceramic products. As the solar industry is advancing, the need for reusable crucibles for solar grade silicon has arisen. One idea is to make crucibles out of silicon nitride. There are many different ceramic routes one could follow, whereas slip casting is one of them. Slip casting is an easy and inexpensive consolidation process to produce materials with high green density and homogeneous micro structure, even for complex geometries [1].

There are many challenges connected to slip casting, but one area of interest is the unwanted hydrogen evolution from silicon slurries. The hydrogen evolution is initiated by the addition of an alkaline in order to raise the pH of the slurry; this is done in order to stabilize the slurry. Hydrogen evolution originates from the oxidation of silicon and is the source of several unwanted effects. The main problem is that the hydrogen gas produces macro pores in the green body, which leads to porosity in the final material, ruining the mechanical properties. Gaining knowledge on how to inhibit the oxidation of silicon in slurries would therefore prove valuable for producing defect free silicon based ceramics.

1.2 Aim of work

During the work with [2], hydrogen evolution from different silicon powders at different pH and temperature was carried out. It was determined that a more fundamental study of the oxidation of silicon in aqueous media was necessary, and thus was the foundation for the current thesis laid. In order to obtain this, silicon powders and coarse silicon particles delivered by Elkem will be oxidized in a purpose-built apparatus. The silicon powders and particles, and the slurries produced, will be examined before and after oxidation in order to discover any changes and trends, utilising a number of different techniques. Nanoindentation will also be performed in order to gain knowledge about the mechanical properties of oxidized silicon.

To summarize, the overall important aim is to gain knowledge of the oxidation of silicon in aqueous media, hopefully developing a step-by-step guide to how the oxidation elapses. Important targets are:

- How the oxide develops.
- Characterization of the oxide.
- Initiation time for the oxide formation.
- Preferred sits for oxidation on the silicon particles.

Chapter 1 provides the motivation and aim of work for the thesis. Chapter 2 explains the chemistry of silicon and silica in water, stabilization of suspensions and the theory behind nanoindentation. Chapter 3 describes the experimental work performed. Chapter 4 displays the results obtained. Chapter 5 provides a thorough discussion of the results. Chapter 6 concludes the thesis, and chapter 7 describes further work. The references used are listed. The appendices contain calculations and data for some of the measurements.

Chapter 2

Theory

2.1 Silicon in general

Silicon is a metalloid, meaning that it possesses properties of both metals and non-metals, and a semiconductor. It is a tetravalent element, which means that its most important valence is 4^+. Silicon is the second most abundant element after oxygen in the earth's crust, making up 27.7 % of the crust by mass. Silicon rarely occurs as the pure free element in nature, the most common forms are silica and silicates. Silicon will spontaneously oxidize in air at room temperature, this results in a passivation layer of a thin oxide film on the surface [3, 4]. The chemical behaviour of the silicon surface should thus be comparable with that of silica. It is also worth mentioning that silicon and silica exhibit similar dispersion behaviour [5].The chemistry of silicon in tetravalent state is quite complex since there a number of different reactions occurring simultaneously dependent on pH of the solution. The reaction between silicon powder and water, Equation 2.1, should lead to intensive hydrolysis, since the standard electro potential is strongly negative, $E_0 = -0.888V$ according to [6]. This paragraph is primarily based on [7], [8] and [9].

$$Si(s) + H_2O(l) = SiO_2(s) + H_2(g) \tag{2.1}$$

$$\Delta G^0_{298} = -382kJ/mol$$

2.2 Silica surface

This section is primarily based on [10] and [11].

As explained in the previous section, silicon oxidizes spontaneously in air and is therefore covered with a layer of silica. The silica layer is often referred to as siloxane (SiOSi) which reacts with water at ordinary temperature. According to Equation 2.2 the surface is hydrolyzed by chemisorbed water molecules, this results in the formation of hydrophilic silanol (SiOH) groups at the surface.

$$Si - O - Si + H_2O = 2Si - OH \tag{2.2}$$

Surface hydrolysis followed by dissolution will continue until solid-solution equilibrium is reached [12]. Figure 2.1 illustrates the dissolution of silica in aqueous solution.

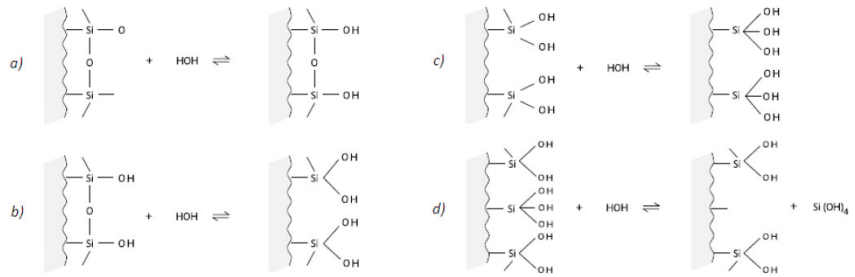

Figure 2.1: *The hydrolysis of the surface species of silica. a) Hydrolysis of the surface takes place as fresh silica is introduced to water giving rise to silanol groups at the surface. b) When silica is exposed to water for longer intervals, its surface tends to hydrolyze further to form $SiOH_2$. c) Formation of more silanol groups is possible, particularly under low bulk concentration of alkali metal. d) Further hydrolysis of the surface can result in the dissolution of the surface species to form silicic acid, thus exposing new silicon atoms to the solute. The figure is adapted from [12].*

When silica particles are formed in water, the number of OH^- groups can be affected in several ways [11]. One effect depends on the particle size, this is shown in Figure 2.2. Particles with small positive radius tends to hold SiOH groups on the surface further apart so they can form fewer hydrogen bonds between them. Larger particles with a larger positive radius has more interactions between the SiOH groups on the surface and thus creates a more stable layer. On a particle with large positive radius, there is a binding force between a specific atom of the adsorbate and an atom on the surface, hence hindering the dissolution process to a greater extent [11].

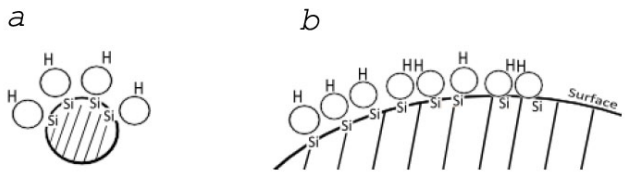

Figure 2.2: *Factors affecting the number of hydroxyl (silanol) groups on a silica particle formed in water. a) Hydroxyl groups on very small (under 100nm) particles are less crowded per unit area. b) Hydroxyl groups on a larger particle are closer together and can form more stable hydrogen-bonded pairs. The figure is adapted from [1].*

There are many different forms of silica present when silica dissolves, a brief description of these are given underneath based on [11]:

- Silicic acid - also referred to as dissolved silica or monomeric silica
- Polysilicic acid - also referred to as oligomers. These are polymers with molecular weight (as SiO_2) up to 100 000, whether consisting of highly hydrated silica or dense spherical particles less than about 50 Å in diameter.
- Colloidal silica - is a more highly polymerized species or particles larger than about 50 Å, although sometimes down to 10-20 Å.

2.3 Mechanisms of dissolution of silica

This section is primarily based on [11].

The rate at which silica dissolves in water is influenced by many factors, but the dissolution process requires the presence of a catalyst. The dissolution of silica in water is a depolymerisation through hydrolysis, and the "solubility" is the concentration of $Si(OH)_4$, reached as a steady state in the depolymerisation-polymerization equilibrium following Equation 2.3.

$$SiO_2(s) + 2H_2O(l) = Si(OH)_4(aq) \tag{2.3}$$

The "catalyst" is a material that can be chemisorbed and increases the coordination number of silicon atom on the surface to more than four, thus weakening the oxygen bonds to the underlying silicon atoms. In alkaline solutions this catalyst is the hydroxyl ion OH^- , thus the dissolution rate is expected to be strongly affected by pH. The first step is the adsorption of OH^- ion, after which a silicon atom goes into solution as a silicate ion, shown in Figure 2.3. If the pH is much below 11, the silicate ion hydrolyzes to silicic acid, $Si(OH)_4$, and OH^- ions and the process is repeated [11].

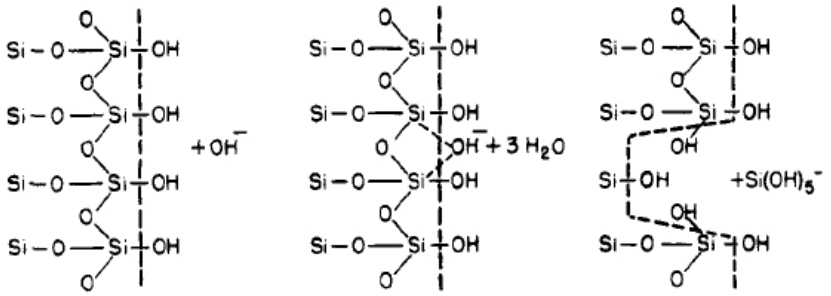

Figure 2.3: *Proposed mechanism of dissolution of silica surface in alkaline solution. The dotted line represents the interface between silica on the left and alkaline solution on the right. The figure is adapted from [11].*

As the silica layer dissolves, the silicon underneath will be exposed to the solution. In an alkaline environment silicon and OH^- will react

and yields a silicate ion and hydrogen gas according to Equation 2.4.

$$Si(s) + 4OH^{-}(aq) = SiOH_4^{4-}(aq) + 2H_2(g) \tag{2.4}$$

The main reaction is though 2.5, which is based on water hydrolyzing the surface, resulting in silicic acid and hydrogen.

$$Si(s) + 4H_2O(l) = Si(OH)_4(aq) + 2H_2(g) \tag{2.5}$$

Figure 2.4 displays the dependence of solubility of silica (amorphous) versus both pH and temperature. The figure predicts that the solubility of silica increases with increase of pH, temperature or both.

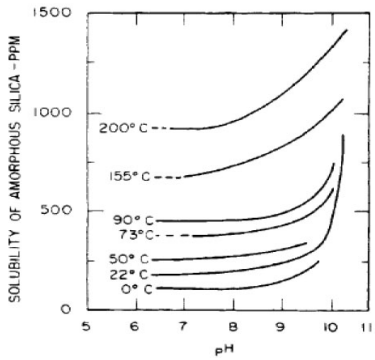

Figure 2.4: *Solubility of amorphous silica versus pH and temperature. Adapted from [11].*

The effect of particle size, as briefly discussed in Figure 2.2, also affects the solubility with regards to the radius of curvature, as seen in Figure 2.5.

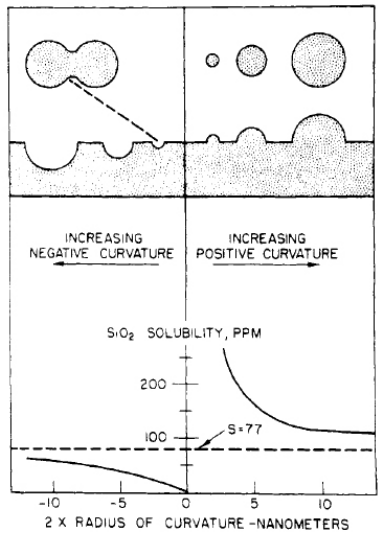

Figure 2.5: *Solubility of silica versus radius of curvature of surface (saturation concentration of 77 ppm). The positive radii of curvature are shown in cross-section as particles and projections from a silica surface. Negative radii are shown as depressions or holes in the silica surface, and in the crevice between two holes. Adapted from [11].*

The overall hydrodynamic shape of a particle defines its surrounding shear plane boundary, thus smaller particle surface can have varying local diffusion layer thickness. The preferred dissolution of convex versus concave surface structures can be concluded on the basis of thinner diffusion layers of convex features, as they extend from the surface toward the shear plane, whereas concave features will have thicker diffusion layers because they are recessed on the surface.

2.4 Condensation of silica

This section is based on [11].

As mentioned earlier, the silicic acid is a monomer which can polymerize. In Iler [11] the polymerization can be summed up in three steps:

1. Polymerization of monomer to form particles.

2. Growth of particles.

3. Linking of particles together into branched chains, then networks, finally extending throughout the liquid medium, thickening it to a gel.

If the concentration of silicic acid is greater than about 100-200 ppm as SiO_2, which is greater than the solubility limit of the solid phase of amorphous silica, and with the absence of solid phase where the silica might be deposited, the monomer can polymerize by condensation to form dimer and high molecular weight species of silicic acid. This is displayed in Figure 2.6.

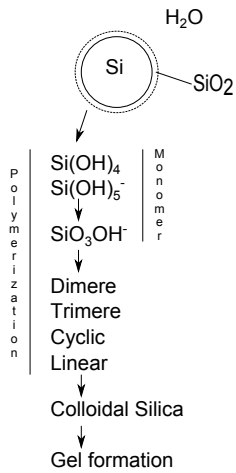

Figure 2.6: *Polymerization of silicic acid and silicates from the dissolution of silica, resulting in colloidal silica or eventually silica gel. Based on [13].*

The growth of the condensed silica particles are controlled by both pH, temperature and initial size of condensed silica. Since smaller particles have a larger solubility than larger particles, the particles grow in average size and diminish in numbers. This is due to Ostwald ripening, where the smaller particles dissolve and are deposited on the larger ones. This effect is pronounced only when the particles are smaller than 5 nm. When above pH 7, the rate of dissolution and deposition of silica is high, the particle growth will continue until the

particles are 5-10 nm in diameter and then slow down.

When there is solid phase present, the silicic acid will prefer to condense to silica directly on the solid phase when solubility of the silicic acid is reached. The silica will be adsorbed on the solid phase as colloidal silica.

2.5 Charging of silicon in aqueous solutions

This section is based on [14].

Introducing silicon to an acidic or alkaline solution will lead to a charging of the silicon surface, due to the fact that the silanols covering the surface will react with either H^+ or OH^- respectively. In the low pH range, the silanols react with H^+ and yields $SiOH_2^+(s)$, this gives a net positive charge on the surface of the silicon particle which results in a positive zeta potential. In the high pH range, the silanols react with OH^- and yields $SiO^-(s)$, this gives a net negative charge on the surface of the silicon particle which results in a negative zeta potential. The reactions are as following, according to [15]:

$$SiOH(s) + H^+(aq) = SiOH^+(s) \tag{2.6}$$

$$SiOH(s) + OH^-(aq) = SiO^-(s) + H_2O(l) \tag{2.7}$$

The charging of the silicon surface depending on the pH of the solution can also be observed in Figure 2.7.

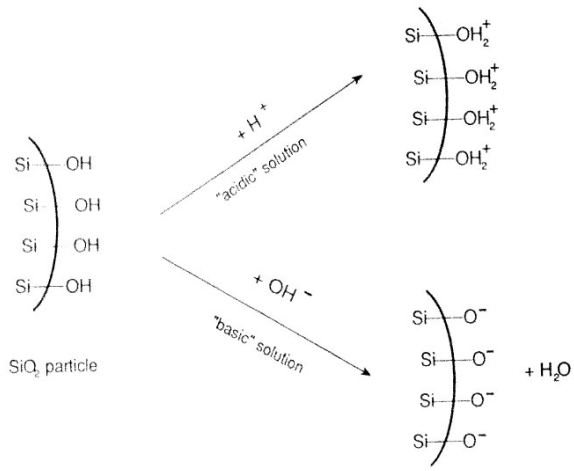

Figure 2.7: *The production of surface charges on SiO_2 particles by adsorption of ions from acidic or basic solutions. Adapted from [14].*

Charging of the silicon surface is an important effect for stabilizing a suspension, this will be explained more carefully in the next section.

2.6 Stabilization of suspensions

This section is based on [14].

As mentioned in the previous section, a particle surface can have a net positive, neutral or negative surface charge varying with the pH of the solution. At some intermediate pH a particle has a net neutral surface charge, it means that the adsorption of H^+ and OH^- balance each other. This pH is referred to as the point of zero charge (PZC). For oxides the PZC is related to the acidity or alkalinity of the surface groups. Acidic oxides like SiO_2 have a low PZC, and basic oxides like Al_2O_3 have high PZC, respectively 2 and 8-9 according to [14].

When dealing with ceramic suspensions, it is more convenient to measure and use the zeta potential to describe the charge of a particle. The zeta potential is the potential (or charge) a short distance from the surface of the particle (at the surface of the Stern layer), Figure

2.8. At a pH where the charge at the Stern layer is zero, the zeta potential will be zero, this is known as the isoelectric point (IEP).

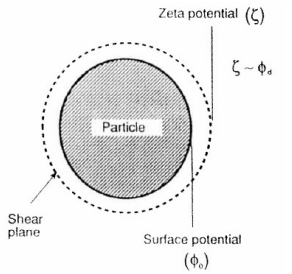

Figure 2.8: *The zeta potential (ζ) is taken to be the electric potential at the surface of the shear plane surrounding the particle, this is approximately equal to the potential at the Stern layer. The shear plane between the particle and the liquid develops because the particle moves with an attached layer of liquid. Adapted from [14].*

The zeta potential curve for a silicon powder is displayed in Figure 2.9. A minimum is observed at about pH 10.5, in accordance with earlier results [10]. There are results that indicate two separate minima at pH 4 and 8 [16]. This difference could arise from silicon particles with different surface states.

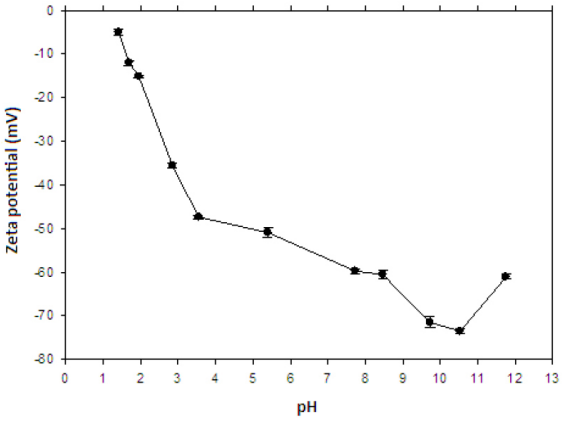

Figure 2.9: *The Zeta potential of a silicon powder from Elkem, adapted from [17].*

When altering the surface charge of a particle, there must exist an

equal and opposite counter charge in the solution, this gives rise to the electrical double layer as seen in Figure 2.10. The theory concerning electrical double layers and interactions between them is far to comprehensive to present in this report, readers are requested to read "Ceramic processing and sintering"' by Rahaman [14] to get a more detailed description.

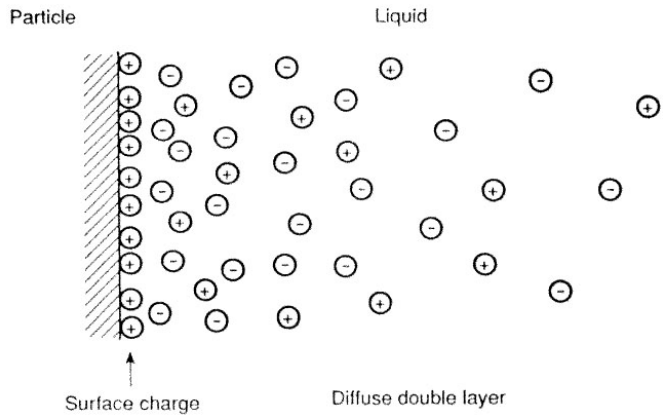

Figure 2.10: *The distribution of positive and negative charges in the electrical double layer associated with a charged surface in liquid. Adapted from [14].*

In a ceramic suspension there are attractive Van der Waals forces between the particles, if these forces are large enough they will lead to flocculation (M2) or coagulation (M1) of the particles and render a useless suspension, see Figure 2.11. The purpose of stabilizing a suspension is to prevent the particles from "sticking" together by overcoming the Van der Waals forces, by for instance increasing the double layer repulsion. There are three common methods of stabilizing a suspension: Electrostatic, steric and electrosteric.

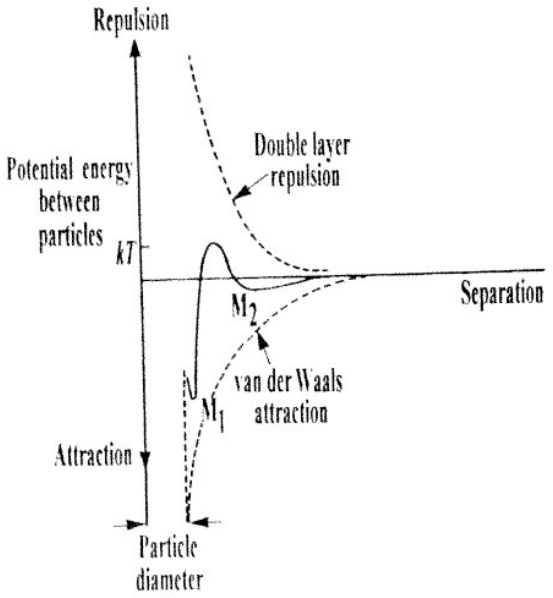

Figure 2.11: *The potential energy between to particles in a liquid resulting from the effects of the Van der Waals attraction and the double layer repulsion. Adapted from [14].*

Electrostatic stabilization utilizes the charging mechanism of particle surfaces discussed above. When charging the particles, they all get the same charge which makes them repel each other. If the absolute value of the zeta potential is large enough, typically larger than 35 mV [18], the repelling forces will overcome the attractive forces and thus give a stable suspension.

Steric stabilization uses organic (nonionic) polymers to stabilize a suspension. Stability is achieved by adsorbing or attaching polymers to the colloidal particles in the suspension. The polymer molecule must consist of two parts; one part is nominally insoluble and anchors (chemically or physically) onto the particle, and the other part is soluble in the liquid. Attachment of a polymer chain to the surface of a Silica particle is illustrated in Figure 2.12.

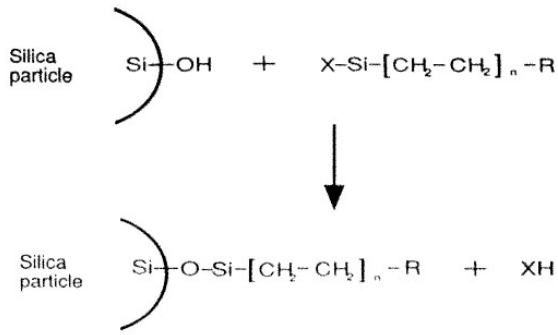

Figure 2.12: *Chemical attachment of a polymer chain to the surface of a silica particle. Adapted from [14].*

The origins of steric stabilization is a mixing effect and an elastic effect. When two particles with polymer chains attached approach each other, they will start to interact. At a given distance the polymer chains may interpenetrate, the concentration of polymers is increased in the interpenetration region, in certain solvents this can lead to repulsion between the particles. The repulsion is said to arise from a mixing effect (or rather a demixing effect) due to the need of the polymer chains to avoid other chains in the interpenetration region of increased concentration. If the distance between the particles becomes even smaller, the polymer chain on one particle may be compressed by the rigid surface of the other particle. The compression gives an elastic contribution to the stabilization which always opposes flocculation. The elastic contribution could also be regarded as an entropic effect or a volume restriction effect. When the particle distance is this short, there are regions of space that are no longer accessible to a given chain. Conformations that would otherwise have been accessible are excluded, so there is a loss of configurational entropy. In summary, as long as the sum of the mixing and elastic effects energy is larger than that of the Van der Waals energy of attraction, the suspension will be stabilized.

Electrostatic stabilization is a combination of electrostatic and steric stabilization, it requires an adsorbed polymer and a significant double layer repulsion. To achieve this polyelectrolytes are used, i.e. polymers that have ionisable groups that dissociate to produce charged polymers. Dissociation of the polymer and adsorption onto the par-

ticles is dependent on the pH, and needs to be determined in order to achieve the requested properties for the suspension. If used to its full potential, suspensions with over 60 vol% particles and low viscosity can be prepared and consolidated to produce green bodies with over 65 % of theoretical density. A well known polyelectrolyte is Darvan C-N, this is an ammonium-polymethacrylate. It is well suited for specialty-ceramics requiring low sodium content and spray dried slurries [19].

2.7 Nanoindentation - determination of mechanical properties

This section is based on an introduction to nanoindentation written by Jianying He [20].

Nanoindentation is a well established tool for probing the mechanical properties of materials, for example E-modulus and hardness at micro- and nano-scales. During indentation, the indentation load and displacement are simultaneously monitored. From these data, load vs. displacement curves can be plotted. The material hardness and reduced modulus can be calculated from the contact area determined by the contact depth. Figure 2.13 displays a load versus displacement curve.

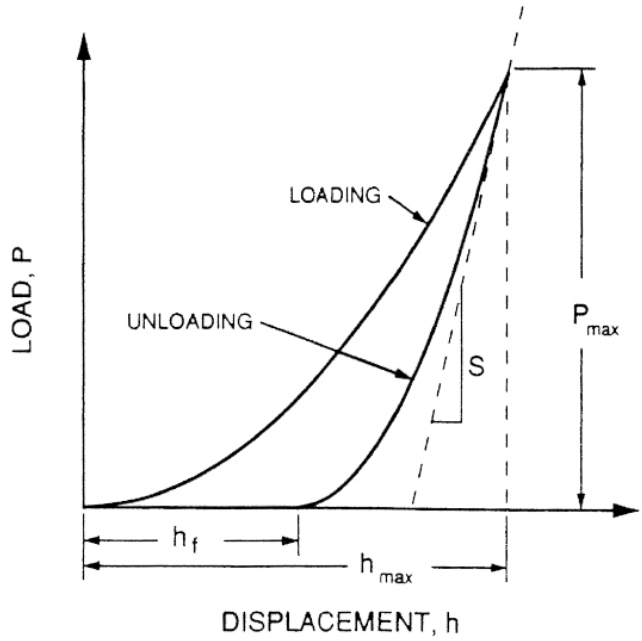

Figure 2.13: *A schematic representation of load versus indenter displacement data for an indentation experiment. The quantities shown are P_{max}:the peak indentation load, h_{max}: the indenter displacement at peak load, h_f: the final depth of the contact impression after unloading and S:the initial unloading stiffness. Adapted from [21].*

From the information obtained during the indentation, the hardness (H) and the reduced elastic modulus (E_r) can be calculated.

The reduced modulus is defined by Equation 2.8:

$$E_r = \frac{\sqrt{\pi}}{2}\frac{S}{\sqrt{A}} \tag{2.8}$$

S is the unloading stiffness ($\frac{dP}{dh}$) and A is the projected contact area.

The reduced modulus (E_r) is related to the modulus of elasticity through Equation 2.9:

$$\frac{1}{E_r} = \frac{(1-\nu_1^2)}{E_1} + \frac{(1-\nu_2^2)}{E_2} \tag{2.9}$$

Subscript 1 corresponds to the indenter, subscript 2 refers to the specimen and ν is the Poisson's ratio. For a diamond indenter tip, E_1 is typically 1140 GPa and ν_1 is 0.07. For these values the first term of Equation 2.9 is close to zero, this leads to an approximation of the E-modulus for the material which is given in Equation 2.10:

$$E_2 = E_r(1 - \nu_2^2) \tag{2.10}$$

The unloading stiffness (S) is calculated by fitting the unloading curve to the power law relation in Equation 2.11:

$$P = A(h - h_f)^m \tag{2.11}$$

A, h_f and m are arbitrary fitting parameters. The stiffness can be calculated from the derivative of Equation 2.11 which yields Equation 2.12:

$$S = \frac{dP}{dh}(h_{max}) = mA(h_{max} - h_f)^{m-1} \tag{2.12}$$

The hardness is defined by Equation 2.13

$$H = \frac{P_{max}}{A} \tag{2.13}$$

P_{max} is the maximum load and A is the projected contact area. The contact area is determined from a tip calibration function $A(h_c)$ where the contact depth h_c is found by using Equation 2.14:

$$h_c = h_{max} - \varepsilon\frac{P_{max}}{S} \tag{2.14}$$

To account for edge effects, the deflection of the surface at the contact perimeter is estimated by taking the geometric constant ε as 0.75.

Chapter 3

Experimental

The experimental procedures carried out can be divided in to three different sections. The first part was intended to characterize the Silicon powder received prior to any experiments. The second part was the oxidation of silicon powder and particles in a purpose-built apparatus and the investigation of the silicon particles, powder and the aqueous solutions from the oxidation experiments. The last part is meant to gain knowledge of the mechanical properties of silicon and how the oxidation affect these, by performing nanoindentation on single crystal and polycrystalline silicon samples that have been oxidized.

3.1 Silicon powders and coarse particles

Two different silicon powders and one batch of coarse silicon particles were investigated, all delivered by Elkem. An overview of the samples and the respective sample codes are given in Table 3.1, the chemical analysis of the samples are given in Table 3.2. The JET1 powder was collected by a cyclone and milled by jet milling. The 2-10 powder is based on a commercial powder which is jet milled to a size of 0-10 μm. Air classification was used to remove the fraction below 2 μm, effectively giving it a size of 2-10 μm. Both powders were acid treated, this could affect the materials surface [22]. The Coarse silicon particles called COARSE, is based on commercial silicon which has been crushed

with a jaw crusher.

Table 3.1: *Silicon samples delivered by Elkem. *The JET1 powder was collected from a cyclone and then jet milled.*

Sample	Size	Mechanical treatment	Chemical treatment
JET1	0-75 μm	Jet milled*	Acid treated
2-10	2-10 μm	Jet milled	Acid treated
COARSE	< 1 cm	Jaw crusher	-

Table 3.2: *Chemical analysis of the different samples, all measurements were performed by Elkem*

Sample	Si (%)	Fe (%)	Al (%)	Ti (%)	Ca (%)
JET1	97.8	1.1	0.79	0.14	0.12
2-10	99.7	0.055	0.112	0.001	0.013
COARSE	99.521	0.271	0.175	0.015	0.018

3.2 Powder characterisation

The 2-10 powder was initially meant to be used in the oxidation experiments which are more thoroughly explained in 3.3.1. Due to the fact that hydrogen evolution was hard to achieve from the 2-10 powder, the JET1 powder was used instead. Since the 2-10 powder was intended used, it was tested quite extensively. The results for the JET1 was acquired during the work with [2].

3.2.1 pH of aqueous suspensions

To measure the pH, the aqueous suspensions was prepared as following. First 10 g of Si powder was weighed out, and then 100 ml of distilled

water was added. The suspension was stirred for 5 minutes with the use of a magnetic stirrer at 400 RPM. A Mettler Toledo S20 Seven easy pH-meter with an Inlab 413 SG electrode was used for the measurements. This procedure is based on the procedure Elkem uses [22].

3.2.2 Surface area measurements

The surface area of the different Si powders, were examined by nitrogen adsorption, using a Tristar 3000 from Micromeritics. Firstly the empty sample tube was weighed, then the powder was added and it was weighed again. The amount of powder used was mostly 2 g for each sample. The sample tube with powder was then degassed overnight under vacuum and at a temperature of 150 ℃. The sample tube with powder was weighed again after degassing to determine the mass of the powder, in case any weight was lost due to volatile species. It was important during preparations to never touch the sample tube with bare hands, thus cotton gloves and lint-free cloth was used during handling of the sample tube. The sample tubes with isothermal jackets were then mounted in to the Tristar 3000 machine. Liquid nitrogen was added to a cold-bath inside the machine. The machine was then ready to start the measurements.

The adsorption of gas molecules onto the particles is measured by performing a 5-point BET. The surface area is then calculated according to the BET method [23]. Based on the BET surface area, average particle size can be calculated assuming spherical particles. Assumptions and calculations are accounted for in Appendix A

3.2.3 Particle size distribution

All particle size distributions were measured by a Mastersizer 2000 by Malvern Instruments. The Mastersizer 2000 uses laser diffraction for measuring particle size, and therefore relies on the refractive index of the powder measured. Thus it is important to know what the powder consists of before doing any measurements. The term particle size distribution is simply referred to from here on as "PSD".

The JET1 powder was prepared by weighing out 1 g of powder, adding it to a beaker with 100 ml of tap water and then adding 1 wt% of Darvan C-N in relation to the amount of powder. An ultrasonic probe was used for 5 minutes to break agglomerates. The suspension was then added to the wet-cell of the Mastersizer 2000 and the ultrasound in the machine was applied for 1 minute, then the particle size distribution was measured. This was performed as a part of [2].

The 2-10 powder was prepared by weighing out 0.5 g of powder and adding it to a beaker with 50 ml of distilled water, beakers with distilled water and adjusted pH, a beaker with distilled water and 2 wt% of Darvan C-N and a beaker with distilled water and 2 wt% of Polyethyleneimine. An ultrasonic probe was used for 5 minutes to break agglomerates. The suspension was then added to the wet-cell of the Mastersizer 2000 and the ultrasound in the machine was applied for 30 seconds, then the particle size distribution was measured.

This was done in order to examine how pH and dispersing agents affect the measured PSD. Hydrochloric acid was used to prepare acidic solutions and ammonium hydroxide was used to prepare alkaline solutions. The different pH values were chosen according to the zeta-potential curve, Figure 2.9. Darvan C-N and polyethyleneimine was added by 2 wt% according to the amount of powder.

The pH of the Darvan C-N and the polyethyleneimine was measured before and after addition of the 2-10 silicon powder, the change was negligible.

3.2.4 Ultrasonic treatment during PSD measurements

During the work with [2], the use of ultrasound during the PSD measurements was much discussed. It was suggested that the use of ultrasound would not only break agglomerates, but also break the silicon particles and therefore compromise the PSD measurements. It was therefore decided to do PSD measurements of the JET1 powder using different amounts of ultrasonic treatment with and without Darvan C-N.

0.5 g of JET1 powder was added to a beaker containing 50 ml of distilled water and 2 wt% of Darvan C-N in relation to the amount of powder. Several beakers were made and they were each subjected to various amounts of ultrasonic treatment ranging from 0 to 10 minutes by an ultrasonic probe. All of samples, except for one of the 0 minutes samples, were then subjected to 0.5 minutes of ultrasonic treatment in the wet cell of the Mastersizer 2000.

The same procedure was then repeated, but Darvan C-N was not added. This was to examine whether or not Darvan C-N had any effect on the result and kept the particles from agglomerating.

3.2.5 Particle morphology

The powders were studied in a Hitachi S-3400N Scanning Electron Microscope, this is a low vacuum SEM. To prepare the samples for SEM examination, two different techniques were used.

The first technique was to sprinkle dry silicon powder on to carbon tape glued to the top of a copper stud. The second technique used was to disperse the powder in ethanol, before dispersing it in an ultrasonic bath for 3 minutes. The solution was then applied to a copper stud with a pipette and left to dry in air.

Both the secondary electron detector and the backscatter detector was used to examine the particles. EDS analysis using the Oxford EDS detector attached to the SEM was also carried out to get a qualitatively result of the composition of the particles. It is important to remember that the samples were not polished, the EDS results can therefore not be used for quantitative analysis.

The SEM investigation of the silicon particles COARSE will be presented in 3.3.2.

3.3 Oxidation of silicon

The main focus of this thesis is the oxidation of silicon in aqueous media. To examine this, a purpose-built apparatus has been used to

oxidize a slurry of water and silicon powder, including a coarse silicon particle. The coarse silicon particles were examined in SEM before and after oxidation. The slurry was centrifuged to separate the powder and the aqueous solution. The powder from these experiments were then dried and examined by BET surface area measurements, LECO and SEM. Some powders were examined by XRD. The aqueous solutions were examined by colorimetry and ICP-MS.

The purpose of using these techniques is to find out where the oxide layer initiates growth on the COARSE particles, initiation time, how the oxide grows, characterization of the oxide, what species are present in the aqueous solutions after the oxidation and how the silicon powder has been affected by the oxidation.

3.3.1 The oxidation experiments

An apparatus was built by Rune Nilsen and Jan Otto Hoel from Elkem, to measure hydrogen evolution from silicon slurries [1]. The apparatus was modified to be used in the project thesis [2], but the results were not reproducible and included a lot of scatter. Before commencing any oxidation experiments to be used in this thesis, an extensive testing an rebuilding had to be carried out to get results that could be trusted. This took a lot of time, a further description of the process is given in Appendix E.

The purpose of the oxidation experiments is to oxidize the silicon particles, COARSE, at different time intervals. This is done in order to expose where the oxidation starts on the particles, time for initiation and how the oxide layer grows. The COARSE particles are oxidized in a slurry consisting of distilled water and JET1 silicon powder. In order to oxidize the particles, the temperature of the slurry is increased and pH is adjusted to the alkaline area. Figure 3.1 describes the apparatus.

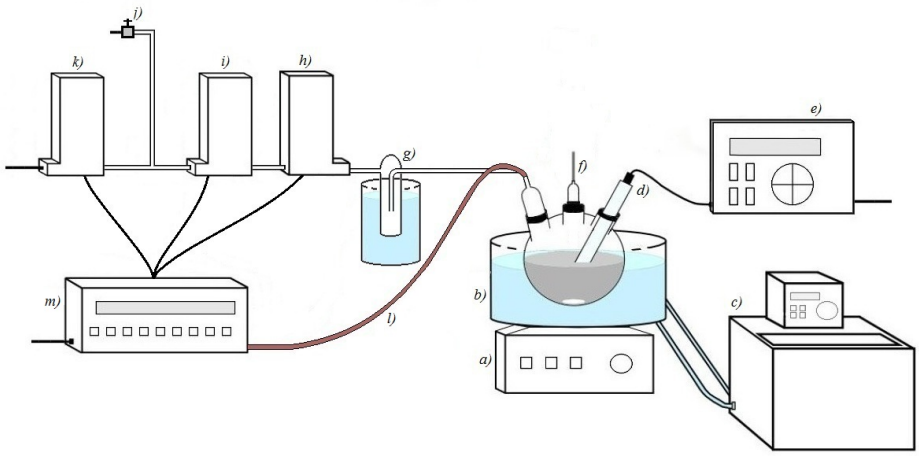

Figure 3.1: *Apparatus for oxidation of silicon slurries. a) Magnetic stirrer, b) Water bath with fixed temperature, c) Heat circulator, d) pH-electrode), e) pH-meter with computer output, f) Nitrogen input, g) Cold trap, h) Pressure sensor, i) Flow meter with large range, j) Ball valve, k) Flow meter with small range, l) Thermocouple type K, m) Data logger with computer output.*

The flask contains the slurry which consists of water, silicon powder and a COARSE particle. Ammonium hydroxide was added with a pipette through the Nitrogen input (f). A magnetic stirrer (a) was used to agitate the slurry. A heat circulator (c) from Julabo , Germany, was used to heat up the water bath (b). The apparatus was flushed with nitrogen gas through input (f) The pH was measured with a Inlab 413SG pH-electrode (d) connected to a Seven easy S20 pH-meter (e) from Mettler Toledo. The pH was continuously logged by a computer with the LabX pH-direct software from Mettler Toledo. The flow of gas was directed through a cold trap (g) cooled with liquid nitrogen in order to remove water vapour and ammonia from the gas flow, so that hydrogen was the only gas that would keep on through the apparatus. The gas was then lead through a pressure sensor (h) from Ellison Sensors International, Wales to measure any changes in the pressure. All of the hydrogen gas was measured by a flow meter (i) from Bronkhorst High Tech, which has a limit of 180 ml/min. If the flow of hydrogen was small, i.e. less than 3.2 ml/min, it was also lead through the flow meter (k) from Bronkhorst High Tech too get a more accurate result. If the flow was greater than 3.2 ml/min, the ball

valve (j) was opened to let the gas flow freely. Failure to do this would lead to pressure build up as the flow meter (k) was too narrow to let large gas flows through. In practice the flows were always larger than 3.2 ml/min, so all experiments were carried out with the ball valve (j) open. To measure the temperature directly in the slurry, a type K thermocouple (l) was used. Logging of Hydrogen flow, temperature and pressure was executed by an Agilent34970A data acquisition/switch unit (m) connected to a computer with Benchlink logging software.

To ensure that the results could be compared directly and to avoid a possible source of error, all measurements were carried out as equal as possible.

1. An amount of 2 g of silicon powder was mixed with 50 ml of distilled water in a 100 ml beaker.
2. The slurry was poured into the flask which was placed in the preheated water bath.
3. The magnetic stirrer was set to a rotational speed of 1000 RPM for the whole duration of the experiment
4. A COARSE silicon particle was added
5. The apparatus was flushed with nitrogen gas
6. When the slurry had reached the desired temperature, ammonium hydroxide solution was added until the suspension reached the desired pH

A test experiment was conducted where six COARSE particles were added to the slurry and removed at the time intervals 10, 20, 30, 40 and 90 minutes. The last particle was left in the slurry and dried in a furnace at 110 ℃. All particles were rinsed with distilled water and dried with a tissue before being put in to separate small bottles. The oxidation was performed at a temperature of 60 ℃, pH 9.4 and for a duration of 90 minutes.

The main oxidation experiments were conducted with only one COARSE particle at the time. Durations were 10, 30, 40, 60, 90, 120 and 240 minutes. The oxidations were performed at a temperature of 60 ℃ and pH 9.4. All particles were rinsed with distilled water and dried

with a tissue before being put in to separate small bottles in a desiccator. Table 3.3 summarizes the oxidation experiments performed. An experiment without a COARSE particle was performed at a temperature of 60 ℃ and pH 9.4 for 90 minutes. This gives an indication of the reproducibility of the 90 minutes experiment with a COARSE particle.

Table 3.3: *A list of all oxidation experiments performed. *The experiment was performed without a COARSE particle, using only a slurry of JET1. **The experiment was performed with six COARSE particles, removed at time intervals 10, 20, 30, 40 and 90 minutes. The last particle was left in the slurry and dried in a furnace at 110 ℃.*

Sample	**Duration** (min)	**Number of COARSE particles**
10 min	10	1
30 min	30	1
40 min	40	1
60 min	60	1
90 min	90	1
90* min	90	0*
120 min	120	1
240 min	240	1
Test experiment	90	6**

3.3.2 Coarse silicon particles - COARSE

Several coarse silicon particles from the sample COARSE were examined in a Hitachi S-3400N Scanning Electron Microscope, this is a low vacuum SEM. The particles were examined before and after oxidation, by attaching them to carbon tape glued to the top of a copper stud.

Both the secondary electron detector and the backscatter detector was used to examine the particles. It was discovered that in order to get a good view of the oxide layer and achieve phase contrast when using the BSE detector, a low accelerating voltage of 3 keV had to be applied.

This is explained in the results. EDS analysis using the Oxford EDS detector attached to the SEM was also carried out to get a qualitatively result of the composition of the particles. It is important to remember that the samples were not polished, the EDS results can therefore not be used for quantitative analysis. Also for the EDS analysis low accelerating voltage had to be utilized to get results from the oxide layer.

3.3.3 Separation of slurry

To separate the slurry in to powder and aqueous solution a centrifuge, Heraeus Biofuge Stratos, was used. The slurry was added to tubes which was then centrifuged two times for ten minutes at 15 000 RPM. The aqueous solution was removed from the tube with a pipette and put into a small bottle. The wet powder was put back in to a beaker and was dried overnight in a furnace, Termaks, at 110 ℃ before being ground in a mortar.

3.3.4 Surface area measurements

The powders from the oxidized slurries were all measured by BET surface area, the method is the same as described in Section 3.2.2.

3.3.5 LECO

The LECO analysis was performed by Anne Støre at SINTEF Materials and Chemistry. The instrument used was a LECO TC436-DR, the procedure used was as following.

The samples are weighed out in a small tin capsule. The capsule is then closed and the air i pushed out by using a pincer. The oxygen content in the capsule is by then so low, a few ppm, compared to the content of the material that it is negligible. The capsule is then placed in the instrument. At first the capsule is in a chamber by oneself which is flushed by He 6.0. A graphite crucible is then placed between two electrodes, the crucible acts as a heating element. The furnace chamber

is firstly flushed with He (used as carrier gas) at room temperature and then at a temperature a bit above the temperature at which the measurements are going to be performed. This is done to remove any oxygen in the crucible itself. The temperature is then lowered to the level of which the measurements are performed, it is flushed with He for some seconds to assure that all oxygen is removed from the system. The sample is then dropped in to the crucible. The oxygen in the sample reacts with the carbon from the crucible and forms CO and CO_2 which is measured by two separate IR-cells. Calibration factors are used to convert the amount of CO and CO_2 in to amount of oxygen. Steel samples with known oxygen content is used to calibrate the instrument.

3.3.6 Particle morphology of the oxidized JET1 powder

The JET1 powders from the oxidized slurries were examined in a Hitachi S-3400N Scanning Electron Microscope, this is a low vacuum SEM. The dry silicon powder was sprinkled on to carbon tape glued to the top of a copper stud, and then examined in the SEM. This was done to determine whether or not there was any visual differences between the different the oxidized powders with respect to the difference in oxidation time.

3.3.7 XRD

XRD analysis was applied to check one batch of oxidized JET1 powder from the test run described in 3.3.1. Two samples were made, one containing the oxidized JET1 powder, the other one containing what was believed to be amorphous silica precipitated during the drying of the slurry. Since the amount of each sample was quite small, only a small amount of each sample was added to separate small bottles containing ethanol. The suspensions were shaken by hand and then applied with a pipette onto sample holders made of single crystal silicon. The samples were then put in to a Bruker AXS D8 Focus for XRD analysis. Since these samples were not of great importance, a large step size of 0.1° was chosen and a scan time of five minutes. The wavelength was

1.5406 nm. The obtained data i therefore quite noisy, but should give a qualitatively description of what the powders consists of.

3.3.8 Colorimetry

Colorimetry was applied to determine the amount of silicic acid in the aqueous solutions, also known as dissolved silica. The analysis was carried out with a spectrophotometer, Spectroquant Pharo 100 from Merck. The reactants needed for this analysis was included in the kit "'silicic acid test"' 1.14794.0001 from Merck. These reactants were meant for analysis of seawater, which contain only small amounts of silicic acid. This implied that the samples from the oxidation experiments had to be diluted to be able of measuring the concentration of soluble silica. Lotte Skolem, student at NTNU, performed the analysis.

Firstly 5 ml of sample solution was added to a test tube, it was then diluted a hundred times with distilled water. Three drops of reagent Si-1 from the Merck test kit was then added to the test tube and mixed. After three minutes the pH was measured, this should be between pH 1.2 - 1.6. If not, more of reagent Si-1 had to be added. Then the Si-2 reagent was added by three drops and mixed, and finally 0.5 ml of reagent Si-3 was added with a pipette and mixed. The solution was then added to a cell and put in to the spectrophotometer to determine the concentration of silicic acid.

The pH of the aqueous solutions were measured with a Inlab Science Pro pH-electrode and a Seven easy S20 pH-meter from Mettler-Toledo.

3.3.9 HR ICP-MS

HR ICP-MS was applied to determine the total amount of silica in the aqueous solutions. Subtracting the results from the colorimetry, in effect dissolved silica, the amount of colloidal silica can be determined. The analysis was carried out with an HR ICP-MS instrument, ELEMENT 2 from Thermo Electronics. The analysis was performed by Syverin Lierhagen at the Department of Chemistry, NTNU.

The samples delivered were diluted ten times and conserved with 0.1M HNO_3 and 0.2 %v/v HF. Three samples of distilled water were used as "'blanks"'. The concentrations of silica found in the blanks were subtracted from the results of the other samples. The analysis was set up to measure the amount of ^{30}Si isotope.

3.4 Mechanical properties of silicon

Studies of the mechanical properties of the oxide layer formed during oxidation was planned from the beginning of the thesis. Later it came to attention that the surface of the particle needed to be flat in order to get reliable results. A new approach to the problem was therefore needed, leading to the following procedure.

To obtain good and reliable data, single crystal silicon was chosen as material. One polycrystalline specimen, based on a COARSE particle was included to combine earlier results and the new approach together. The samples were prepared by grinding and polishing to make a flat surface and prepare the polycrystalline sample for EBSD analysis. The EBSD analysis was carried out in order to identify the crystallographic directions of the sample. One of the single crystal samples were oxidized for five hours while the other one was not oxidized in order to have a reference. The polycrystalline sample was oxidized for four hours. Nanoindentation was performed afterwards on the three samples in order to investigate the mechanical properties of silicon and the oxide layer.

3.4.1 Samples and sample preparation

Two different types of silicon were prepared. Two samples were made from a solar cell ingot of single crystal silicon with crystallographic direction (100). The third sample was a COARSE particle with unknown crystallographic directions, this was later determined by applying EBSD. The samples are listed inn Table 3.4.

Table 3.4: *Info regarding the silicon samples prepared for nanoindentation.*

Sample	Origin
Single crystal	Ingot drawn in the (100) direction
Polycrystal	COARSE particle

To prepare the samples, especially with EBSD analysis in mind, a thorough sample preparation was performed. This included embedding in epoxy, plane grinding, fine grinding, polishing and chemical polishing. The COARSE sample was ground so that a large flat surface was exposed, in contradiction to the original rough and edgy appearance. The single crystal only needed grinding to remove the abrasion marks from the cutting of the ingot. The plane grinding was carried out manually in two steps with SiC paper of 500 and 1200 grit. The fine grinding, polishing and chemical polishing was performed on a Struers Tegrapol-31 with a Tegradoser-5 to dispense the abrasives and chemicals. The methods used to prepare the samples are listed in Table 3.5.

The samples were examined in a Hitachi S-3400N Scanning Electron Microscope in order to compare the surfaces of the samples before and after oxidation.

3.4.2 EBSD

In order to obtain information about the crystallographic directions and grain size of the polycrystalline sample, an EBSD analysis was conducted. This was performed using a Zeiss Supra Field Emission Scanning Electron Microscope equipped with a EBSD On-Line detector and ISL OIM Data Collection software. This was performed by Yingda Yu at the Department of Materials Science and Engineering, NTNU.

To obtain conduction for the sample which was embedded in epoxy, aluminium foil was wrapped around it. There were made marks in the x and y direction of the sample in order to know where the EBSD scan was performed. Upon the EBSD scan, the sample was tilted 70 °. An

Table 3.5: *Mechanical preparation of the samples before EBSD and nanoindentation. The force listed is for six samples at a time in the Struers Tegrapol-31, the value for one sample is in the parenthesis*

	Plane grinding	**Fine grinding**	**Polishing**	**Chemical polishing**
Surface	SiC paper	MD Allegro	MD-Dac	MD-Chem
Suspension	Water	Diapro Allegro/Largo	Diapro Dac	OP-U
Grit/grain size	500, 1200	9 μm	3 μm	-
RPM	-	150	150	150
Force (N)	-	120 (20)	180 (30)	60 (10)
Time (min)	Until plane	5	8	2

accelerating voltage of 20 keV was used with an aperture of 30 μm. An area of approximately 0.5 mm^2 was scanned and mapped.

3.4.3 Oxidation of samples

The samples where oxidized in the same apparatus as mentioned in section 3.3.1. The oxidations were performed at a temperature of 60 ℃ and pH 9.8. These experiments were performed with one sample at the time in distilled water, JET1 powder was not used. Ammonium hydroxide was used to alter the pH. The single crystal sample was oxidized for 300 minutes, while the polycrystal was oxidized for 240 minutes. One single crystal sample was not oxidized, in order to be used as a reference. After oxidation, the samples were rinsed with ethanol and dried with a lint-free cloth. The oxidized samples are listed in Table 3.6.

Table 3.6: *A list of the samples oxidized before nanoindentation, a temperature of 60 ℃ and pH 9.8 was used.*

Sample	**Oxidation time** (min)
Single crystal	300
Polycrystal	240

The samples were examined in a Hitachi S-3400N Scanning Electron Microscope to compare the surfaces before and after oxidation.

3.4.4 Nanoindentation

In order to examine the mechanical properties of the oxidized silicon particles, a Hysitron Triboindenter with a Berkovich standard tip was used to map the surface and perform the nanoindentation. A magnet was glued onto the underside of the samples in order for the samples to keep still during the nanoindentation. Before the samples were put in to the apparatus, they were "flushed" with air to clean them. Firstly the area of the specimen was measured an plotted in to the software,

then the distance between the indenter and the sample was measured. This was done by moving the indenter in to the sample until a force of 100 μN was measured. An area of interest measuring 20x20 μm was then chosen and mapped. This was done by letting the indenter scan the surface of the area while touching it, similar to the technique used in Atomic Force Microscopy. Finally the number of indents and load parameters were determined, the rest of the procedure was automated. The most important properties obtained from each indent was the E-modulus and the hardness value. The nanoindentation procedure was performed by Jianying He at the Department of Structural Engineering, NTNU.

Table 3.7: *List of the samples and the indents made on each. The nanoindentation was performed on a Hysitron Triboindenter with a Berkovich standard tip. Maximum load was 2000 μN, linear loading/unloading rate of 400 $\mu N/s$, area tested was 20x20 μm.*

Sample	Number of indents
Single crystal oxidized	10
Polycrystal oxidized	16
Single crystal unoxidized	9

Chapter 4

Results

In this chapter, the aim is to present the results obtained. The results include the powder characterization, the oxidation experiments, the analysis performed on the particles, powders and aqueous solutions before and after oxidation, and the nanoindentation performed on the single crystal and polycrystalline silicon samples. The results are meant to display how the oxidation affects the JET1 powder and the COARSE particles with respect to oxide layer growth, silica species formed in the slurry and mechanical properties.

4.1 Powder Characterisation

The powder characterisation results is meant to give an overview of the powder properties, especially to be able to compare the powder before and after oxidation.

4.1.1 pH of aqueous suspensions

The pH of the aqueous suspensions prepared are listed in Table 4.1.

As seen in Table 4.1, both the JET1 and 2-10 powder is quite acidic. This is probably because of the chemical treatment with acid, per-

Table 4.1: *pH of the aqueous suspensions of the different powders. *The pH value for JET1 powder was measured in [2].*

Samples	pH
JET1*	3.9
2-10	4.7

formed by Elkem during the production process. The JET1 suspension was kind of "lumpy", comparable to the early stages of a silicon suspension that polymerizes. Nothing out of the ordinary was noted about the aqueous suspension of the 2-10 powder.

4.1.2 Surface area measurements

The results from the BET surface area analysis and average diameter of the particles are given in Table 4.2. The average diameter of the particles are based on the BET surface area values, the density of silicon and the assumption of spherical particles. The formulas and assumptions need for the calculations are given in Appendix A. The 5-point BET surface area plots are given in Appendix C.

Table 4.2: *BET surface area and average diameter of the two different silicon powders as-received. The average diameter is based on the density of silicon.*

Sample	Surface area S_0 (m^2/g)	Average diameter (μm)
JET1	2.2	1.2
2-10	2.4	1.1

Although the JET1 powder has a much larger particle size range, 0-75 μm, compared to the size range of the 2-10 powder, 2-10 μm, the difference in BET surface area is quite small. Smaller size should correspond to a larger surface area, thus should there be a great difference in the BET surface area. The JET1 powder has a very large surface

area compared to the size distribution, this is thought to arise from the fact that the surface of the powder is very rough from the jet milling as mentioned in [2].

4.1.3 Particle size distribution

The PSD measurements for the JET1 powder is shown in Figure 4.1, the cut-off values are given Table 4.3 The measurement in dry state was performed by Elkem. Darvan C-N was added to the measurement in wet state. The results were initially measured in [2].

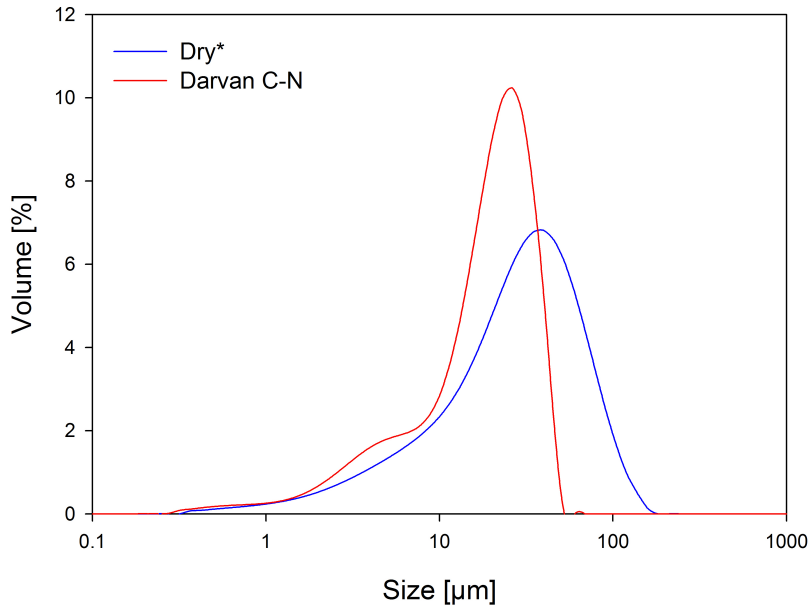

Figure 4.1: *Particle size distribution of the JET1 powder in dry and wet state.*

Table 4.3: *Cut-off values for the PSD measurements of JET1 in dry state and wet with Darvan C-N, these were per. *The dry state measurement was performed by Elkem. **The PSD value for JET1 powder was measured in [2]*

Sample	**d (0.1)** (μm)	**d (0.5)** (μm)	**d (0.9** (μm)
Dry*	5.3	27.2	67.2
Darvan C-N**	4	18.5	33

The results in Table 4.3 indicates that the results from PSD measurements are dependent on the state in which the measurement is performed. The measurement in dry state displays larger values than for the measurements in wet state with Darvan C-N. From Figure 4.1 it is seen that the measurement in dry state has large particles and a more broad distribution than the measurement performed with Darvan C-N. As suggested in [2], performing measurements in dry state is not desirable because the powder is agglomerated, thus leading to a larger powder with a smaller amount of small particles or lack of small particles. Performing the measurements in wet state with Darvan C-N and the use of ultrasound breaks the agglomerates and therefore yields a higher amount of small particles and smaller particles in general.

The results of the more extensive PSD measurements of the 2-10 powder, with different dispersing agents and suspensions with adjusted pH, is displayed in Figure 4.2.

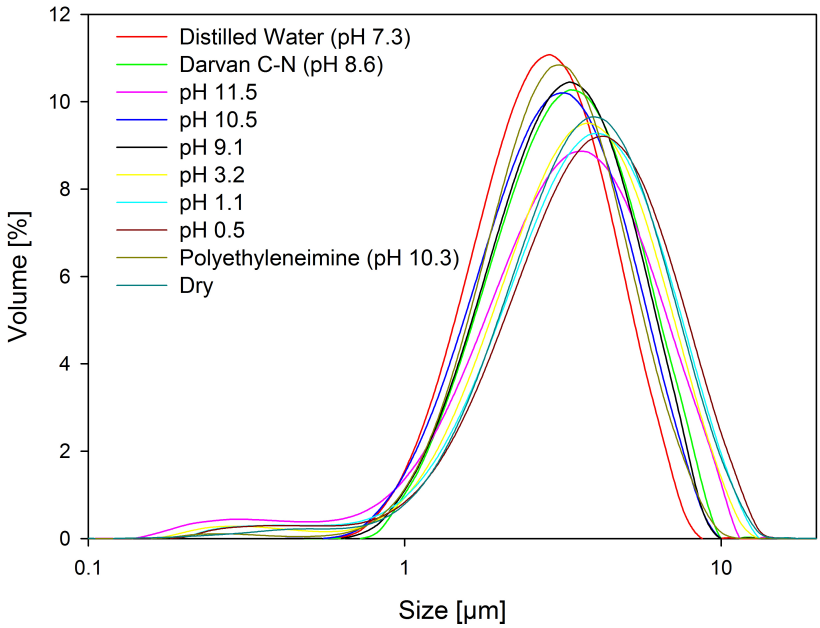

Figure 4.2: *Particle size distribution of the 2-10 powder in suspensions of different pH, with added Darvan C-N and polyethyleneimine.*

The dry state measurement was performed by Elkem. From Figure 4.2 it seems that distilled water is the best dispersing agent, since it gives the highest volume of particles in the range of 1 - 10 μm. The second best is polyethyleneimine.

Table 4.4: *Cut-off values for the various PSD measurements of the 2-10 powder including dry and wet with different pH and additives. *The dry state measurement were performed by Elkem.*

Sample	**d (0.1)** (μm)	**d (0.5)** (μm)	**d (0.9)** (μm)
Dry*	1.6	3.5	6.7
Distilled water (pH 7.3)	1.3	2.6	4.6
Darvan C-N (pH 8.6)	1.5	3.0	5.6
Polyethyleneimine (pH 10.3)	1.4	2.8	5.0
pH 11.5	1.2	3.0	6.2
pH 10.5	1.4	2.8	5.2
pH 9.1	1.5	2.9	5.4
pH 3.2	1.5	3.3	6.4
pH 1.1	1.5	3.4	6.8
pH 0.5	1.5	3.6	7.1

Table 4.4 lists the cut-off values for the results given in Figure 4.2. The cut-off values are a measure on how large a portion of the suspension is beneath the given size. A d (0.1) value off 1.2 μm denotes that 10 volume % of the suspension has a particle size less than 1.2 μm in diameter.

The results listed in Table 4.4 indicates that distilled water has the smallest d (0.1), d(.5) and d (0.9) values, which would indicate that it is the best dispersive medium of all the aqueous suspensions prepared. The d (0.5) values, also known as volume median diameter for each aqueous suspension is plotted versus the pH of the suspension in Figure 4.3.

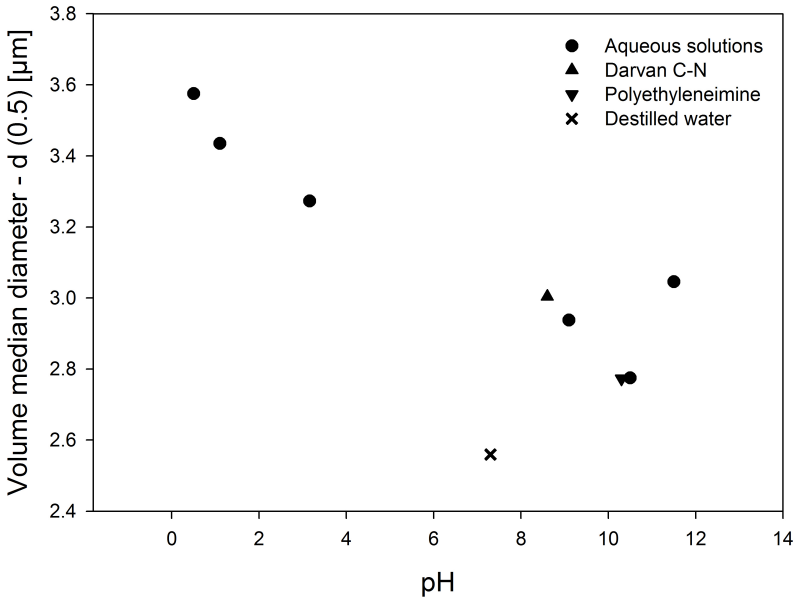

Figure 4.3: *Volume median - d (0.5) vs. pH of the various aqueous suspensions of 2-10 silicon powder.*

Figure 4.3 indicates that distilled water has the lowest d (0.5) value. The acidic region of the pH scale seems to have the highest d (0.5) values, with a seemingly linear decrease in d (0.5) until pH 10.5, if the result for distilled water is neglected. There is an increase in the d (0.5) value for pH 11.5.

4.1.4 Ultrasonic treatment during PSD measurements

As mentioned earlier, ultrasonification of the suspensions before PSD measurements was suspected of breaking not only agglomerates, but also the particles themselves. To verify whether or not there was any reason for this concern, suspensions of JET1 with and without Darvan C-N was prepared and given various amounts of ultrasonic treatment. The Cut-off values for the measurements performed without Darvan C-N are given in Table 4.5.

Table 4.5: *Table of cut-off values for the aqueous suspensions without Darvan C-N treated with various amount of ultrasound. *The sample was not treated with an ultrasonic probe, nor with ultrasound in the PSD machine.*

Sample	**d (0.1)** (μm)	**d (0.5)** (μm)	**d (0.9)** (μm)
0 min*	5.9	27.5	68.1
0 min	6.2	27.8	84.0
1 min	5.3	27.1	106.6
2 min	4.5	24.4	61.2
5 min	3.7	22.0	58.9
7 min	5.1	24.1	58.3
10 min	4.6	25.1	63.1

The PSD curves for the measurements in Table 4.5 are given in Figure 4.4.

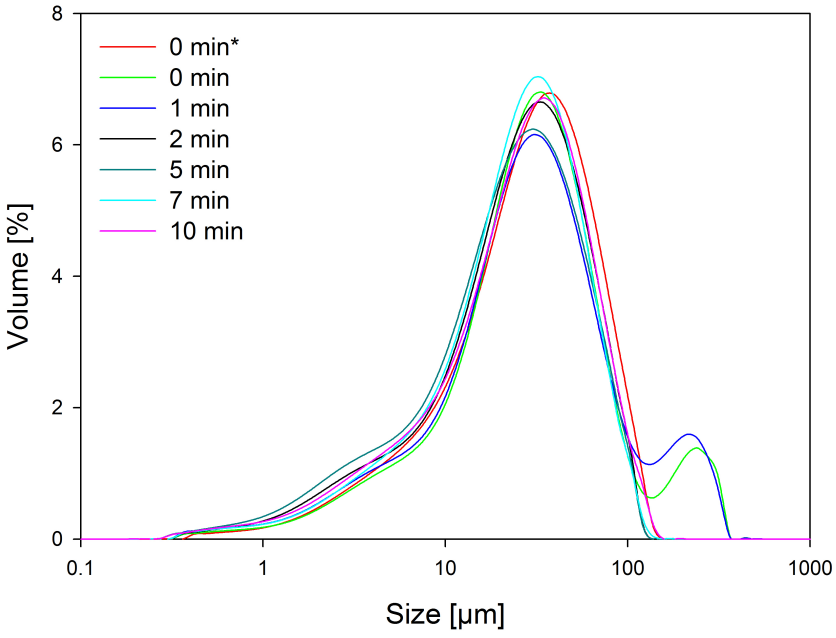

Figure 4.4: *JET1 silicon powder, various amount of ultrasonic treatment.*

From the curves in Figure 4.4, a bimodal distribution for the 0 min and 1 min measurements is observed, this is thought to arise from the ultrasonic treatment. As the ultrasonic treatment increases the distribution is shifted to the left towards smaller particles, and the peak decreases and increases in height. The 10 min measurement has the broadest distribution with both the smallest and the largest particles of all of the measurements.

Table 4.6 displays the results from the PSD measurements performed on the suspensions consisting of JET1 and Darvan C-N, treated with various amount of ultrasound.

Table 4.6: *Cut-off values for the aqueous suspensions with Darvan C-N treated with various amount of ultrasound. *The sample was not treated with an ultrasonic probe, nor with ultrasound in the PSD machine.*

Sample	**d (0.1)** (μm)	**d (0.5)** (μm)	**d (0.9)** (μm)
0 min*	5.157	23.836	59.064
0 min**	5.103	23.788	56.827
1 min	2.434	19.825	61.725
2 min	4.524	26.123	70.088
5 min	5.037	27.082	70.314
7 min	3.745	25.778	71.889
10 min	2.232	24.412	74.501

The PSD curves for the measurements in Table 4.6 are given in Figure 4.5.

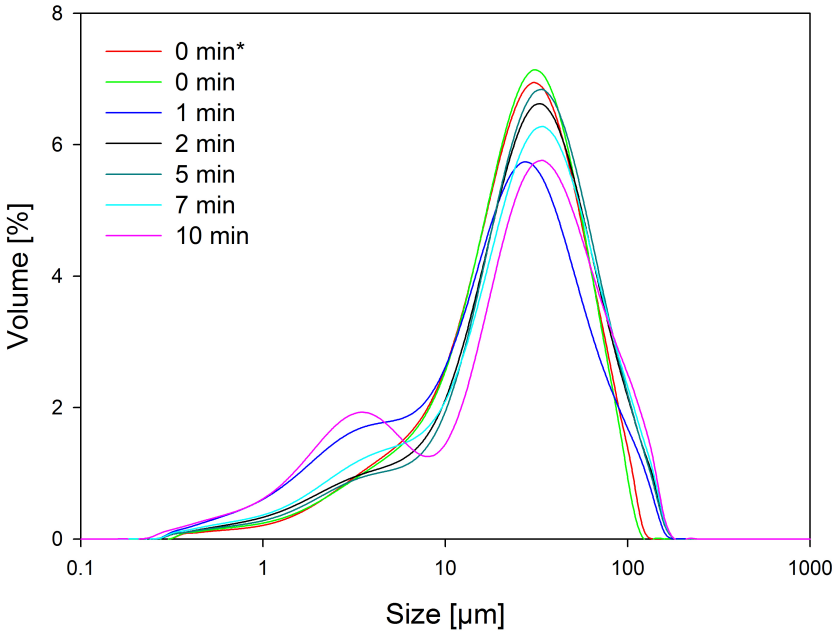

Figure 4.5: *JET1 silicon powder and Darvan C-N, various amount of ultrasonic treatment.*

Plotting of the PSD measurements in Figure 4.5 makes i easier to interpret the results. The 0 min* and 0 min has the most narrow curves, and therefore the highest peaks. As the ultrasonic treatment is increased a broadening of the curve with a decrease in the peak value is observed. For the 10 min measurement a bimodal distribution is observed. This indicates that the amount of small particles, range of 1 - 10 μm, and the amount of large particles, range of 10 - 100 μm, is increasing with increasing amount of ultrasonic treatment. It is also observed that the 10 min measurement has both the largest and the smallest particles. The smallest particles are observed because the Darvan C-N keeps them from agglomerating.

Comparing the measurements performed with and without Darvan C-N, the most important observation is that the 10 min observation has the broadest distribution whether or not Darvan C-N was used. What separates them the most is that with Darvan C-N there is a build up of small particles and a bimodal distribution is observed, while in the measurement without Darvan C-N this build-up of smaller particles is

not seen. The measurements without Darvan C-N at 0 min and 1 min show a bimodal distribution with a build up of large particles which is not seen for the same measurements with Darvan C-N.

4.1.5 Particle morphology

The two silicon powder samples JET1 and 2-10 were examined in a Hitachi S-3400N Scanning Electron Microscope in order to investigate the particle morphology. The results are displayed in Figure 4.6 and 4.7.

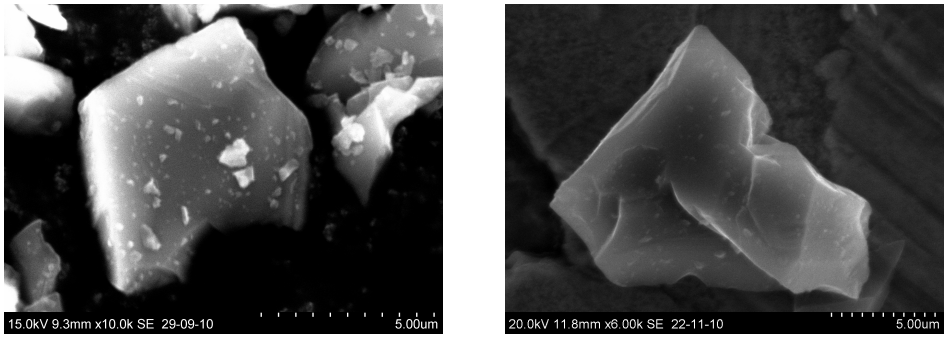

(a) **(b)**

Figure 4.6: *JET1 powder (a) Dry, (b) Dispersed in ethanol*

The JET1 powder is quite rough and edgy. The dry powder has small particles attached to the surface of the larger particles, Figure 4.6a. The JET1 powder dispersed in ethanol lacks the small particles attached to the surface of larger particles, Figure 4.6b

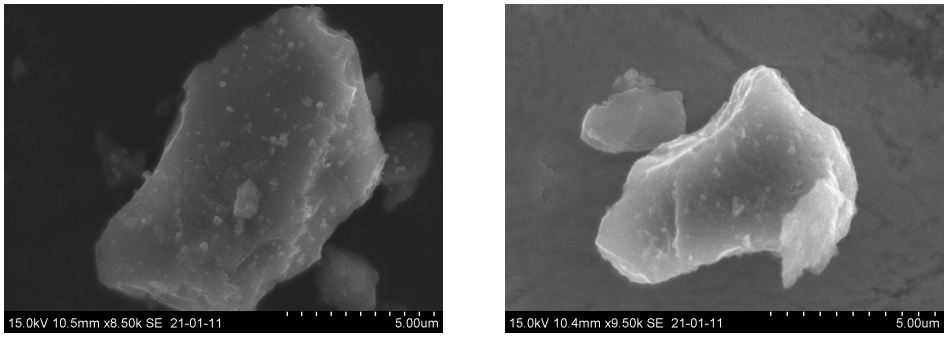

(a) **(b)**

Figure 4.7: *2-10 powder (a) Dry, (b) Dispersed in ethanol*

The 2-10 powder seems to not be that rough. The dry powder has small particles attached to the surface of the large particles, Figure 4.7a. The 2-10 powder dispersed in ethanol lacks the smallest particles attached to the surface of larger particles, Figure 4.7b

To summarize, both powders consist of particles with smaller particles attached to the surface, when dispersed in ethanol the smaller particles seems to detach. The JET1 powder seems to be more rough and edgy than the 2-10 powder.

4.2 Oxidation of silicon

The reason for the oxidation experiments, was to investigate how silicon is oxidized. Oxide growth on the COARSE particles, how the JET1 powder is affected and silica species formed in the slurry was the main focus.

4.2.1 Oxidation experiments

The oxidation experiments were performed in order to oxidize COARSE particles in a slurry consisting of JET1 powder and water, the pH was adjusted with ammonium hydroxide.

Several oxidation experiments were performed, all at a temperature of 60 ℃ and pH 9.4. The first experiment, referred to as test experiment, was performed with six COARSE particles in one slurry, removed at different time intervals. The main experiments were a set of experiments performed at different time intervals, ranging from 10 to 240 minutes, with one COARSE particle at a time in a slurry of JET1. An experiment without a COARSE particle was performed at a temperature of 60 ℃ and pH 9.4 for 90 minutes, this indicates the reproducibility of the result for the 90 minutes oxidation experiment with a COARSE particle. These experiments formed the base for the further analysis. In Table 4.7, a list of the different oxidation experiments with the total amount of hydrogen evolved is displayed.

Table 4.7: *Total amount of hydrogen evolved from the different oxidation experiments with a temperature of 60 ℃ and pH 9.4. *The experiment contained only JET1 silicon powder, not a COARSE particle.*

Sample	**Total amount of hydrogen evolved** (ml)
10 min	0
30 min	31.4
40 min	0
60 min	0
90 min	128
90* min	180.6
120 min	1289
240 min	1207
Test experiment	13.3

All of the hydrogen evolution curves and the pH measurements for each experiment will be displayed and explained in the following section. The hydrogen evolution is plotted as a cumulative curve with the denomination ml, since the hydrogen flow curves [ml/min] contain more scatter. All of the curves displaying the hydrogen flow [ml/min] are given in Appendix D. The cumulative curves are calculated from the hydrogen flow curves [ml/min] using the trapezoidal method.

The hydrogen evolution and pH measurements for the test experiment is displayed in Figure 4.8.

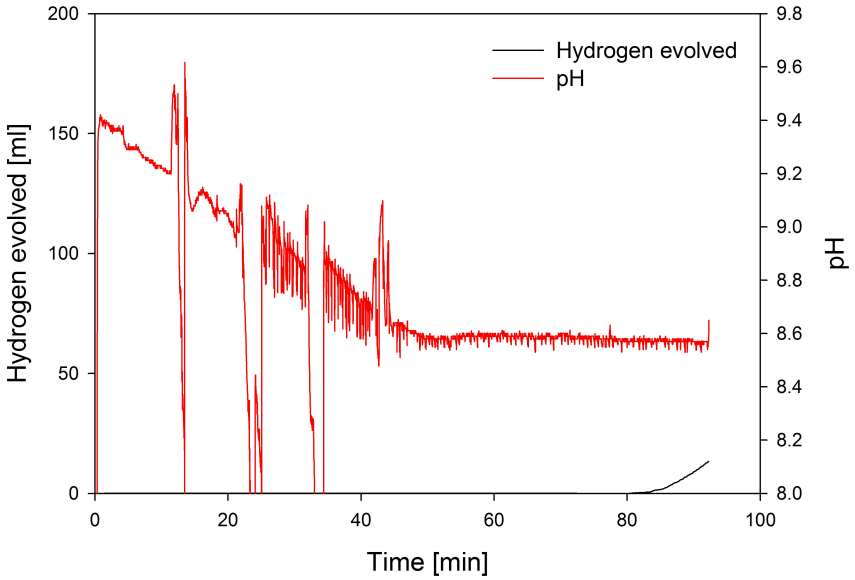

Figure 4.8: *Test experiment, oxidation of six COARSE particles and JET1 silicon powder.*

As observed in Figure 4.8, the pH decreased until about 50 minutes and was then stable for the rest of the experiment. The sudden drops in pH observed are caused by the removal of COARSE particles, since the slurry had to be poured out of the flask in order to remove a particle. This was done at 10, 20 30 and 40 minutes. One particle was removed at 90 minutes and the last one was left in the slurry and dried in a furnace overnight. The constant disturbance of the slurry caused the experiment to not evolve hydrogen until after 80 minutes, about 30 minutes after the pH had settled.

The hydrogen evolution and pH measurements for the main experiments are displayed and commented on in the rest of this section.

The 10 minutes oxidation, Figure 4.9, did not evolve hydrogen, but the pH dropped from about 9.5 to 9.3. The pH should have been 9.4, but achieving the exact pH proved quite difficult.

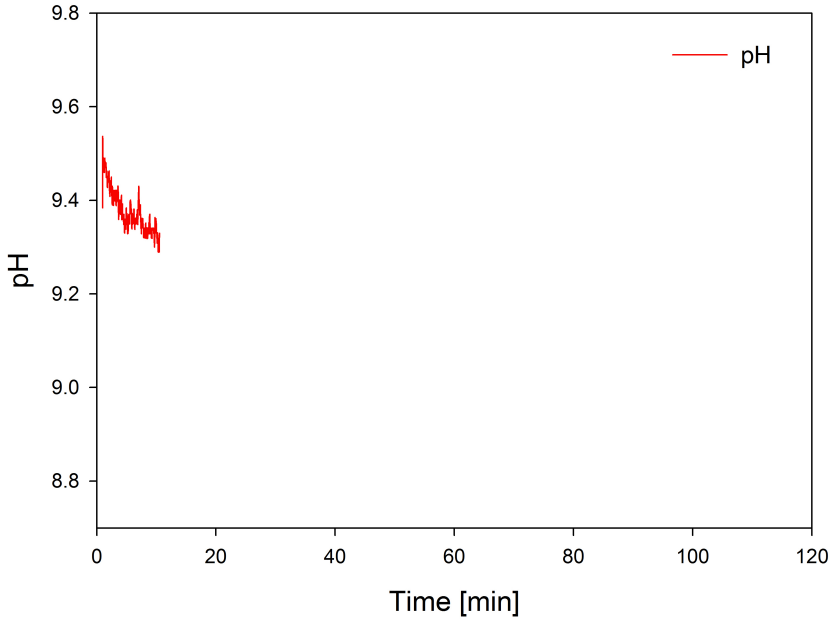

Figure 4.9: *Oxidation experiment - 10 minutes.*

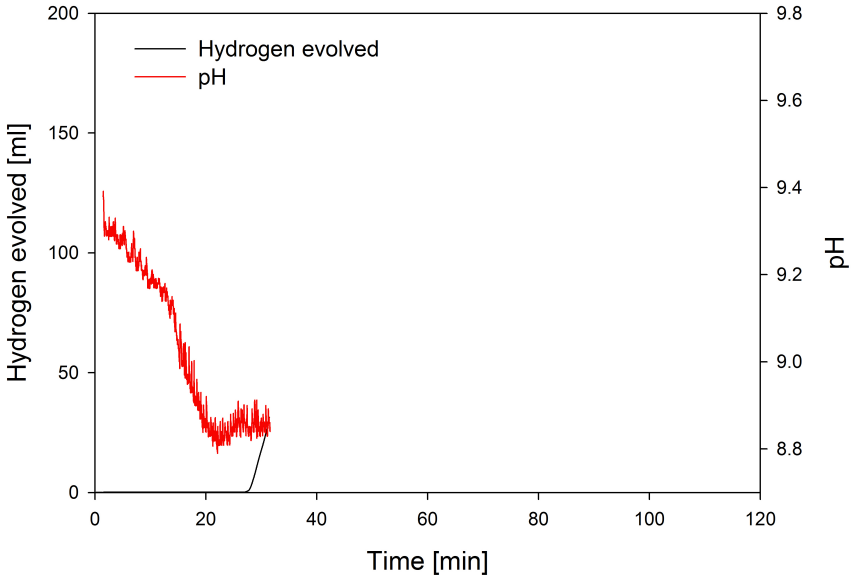

Figure 4.10: *Oxidation experiment- 30 minutes.*

The 30 minutes oxidation, Figure 4.10, evolved 31.1 ml of hydrogen. This experiment was performed after the powder had been stored in a desiccator for some time, this is thought to be the reason for the early initiation of hydrogen evolution compared to the experiments performed at 40 and 60 minutes. The pH dropped from 9.4 to 8.8 in about 20 minutes, it then increased some before the hydrogen evolution initiated after about 25 minutes.

The 40 minutes oxidation, Figure 4.11, did not evolve any hydrogen. The pH dropped from 9.4 to 8.8 in 35 minutes and then increase some.

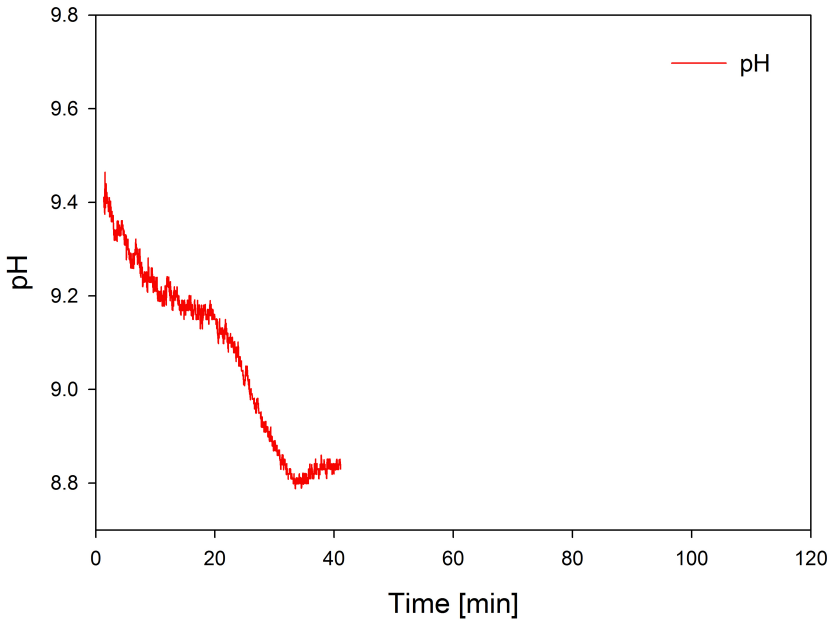

Figure 4.11: *Oxidation experiment - 40 minutes.*

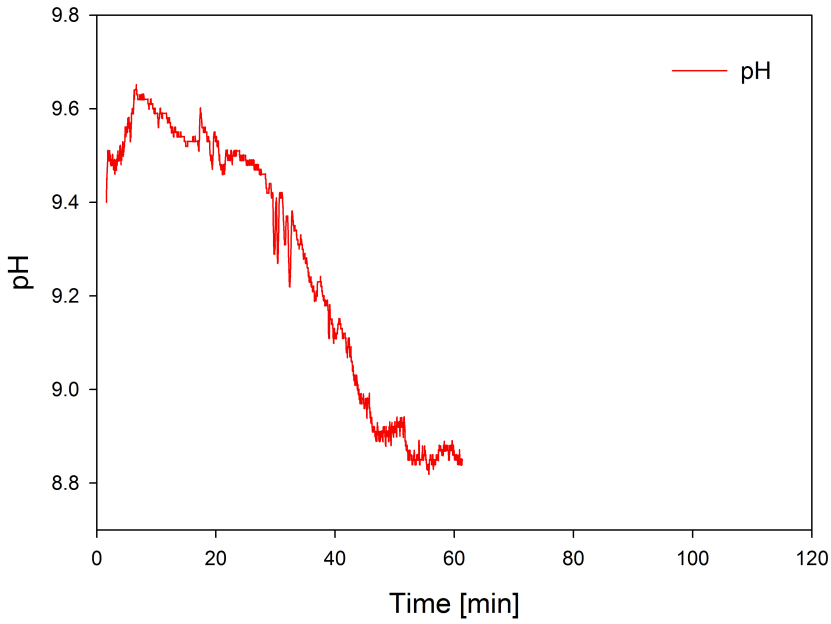

Figure 4.12: *Oxidation experiment - 60 minutes.*

The 60 minutes oxidation, Figure 4.12, did not evolve any hydrogen. The pH was a bit too high, about 9.6. The pH decreased from 9.6 to about 8.9, it then increased some before it decreased to about 8.8. Comparing with the 90 minutes and 90* minutes experiments, Figure 4.13 and 4.14, the hydrogen evolution should have initiated after about 50 minutes, this did not happen. An explanation for this might be that the JET1 powder proved quite difficult to obtain reproducible results from, and that the pH was higher than it was supposed to.

The 90 minutes oxidation, Figure 4.13,evolved 128 ml of hydrogen. The pH decreased from 9.4 to about 8.8 in 50 minutes and then increased some before it was quite stable. The hydrogen evolution initiated at 50 minutes, at the same time as the pH as dropped to its minimum. The hydrogen evolution was quite stable, but decreased some after 75 minutes.

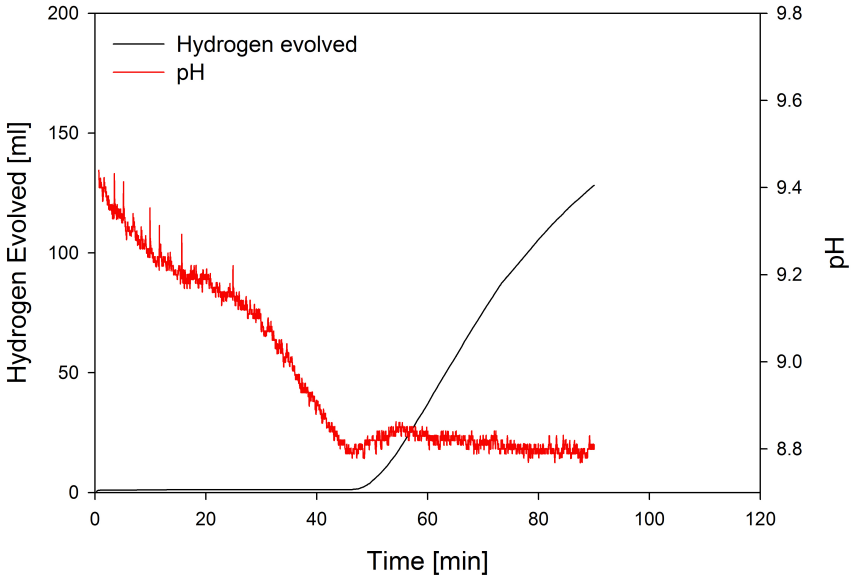

Figure 4.13: *Oxidation experiment- 90 minutes.*

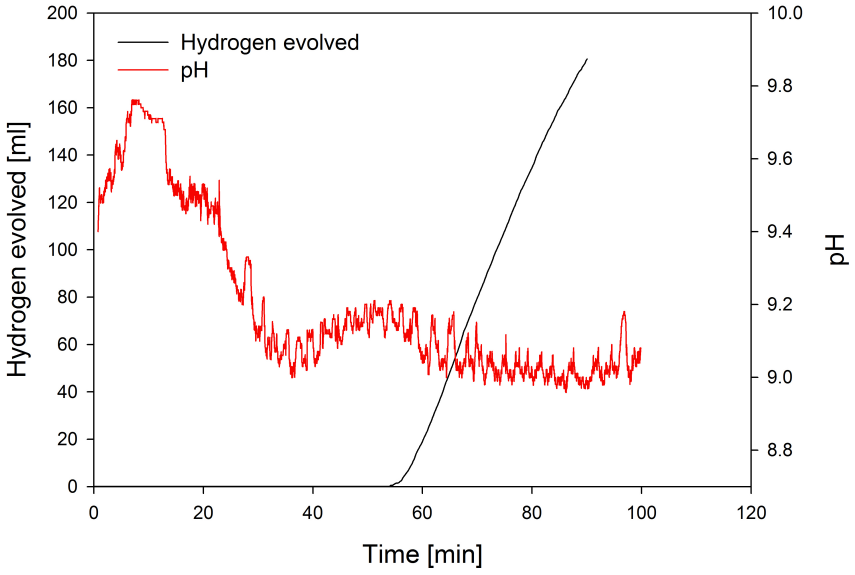

Figure 4.14: *Oxidation experiment - 90* minutes. This experiment contained only JET1 silicon powder, not a COARSE particle.*

The 90* minutes oxidation experiment, Figure 4.14, evolved 180 ml

of hydrogen. The pH was too high, 9.8 compared to 9.4 as it should have been. This is due to the difficulties of adding the correct amount of ammonium hydroxide to a slurry and getting the exact desired pH. Looking at the trends, it is observed that the pH decreased until about 40 minutes, it then increased until about 50 minutes, before it decreased to about 9.0 and was stable for the rest of the experiment. At about 50 minutes the hydrogen evolution from the slurry initiated and continued evolving for the duration of the experiment.

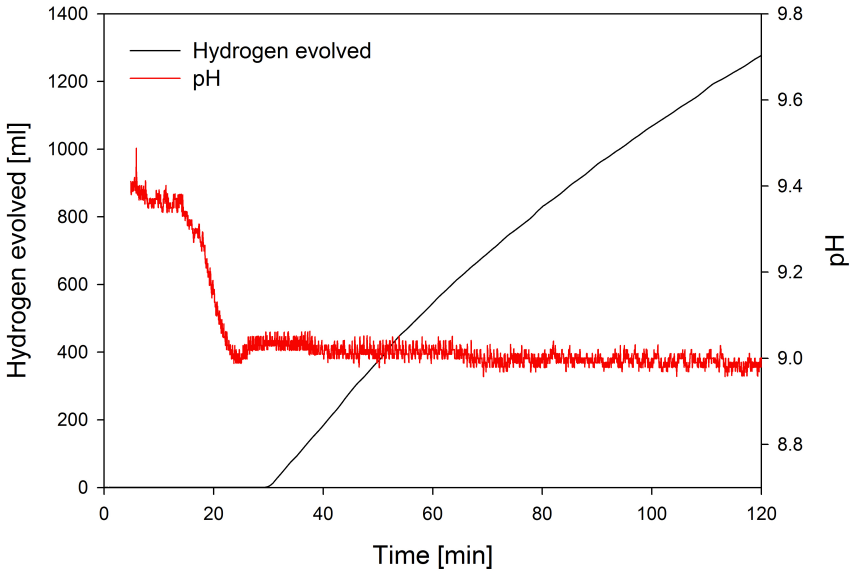

Figure 4.15: *Oxidation experiment - 120 minutes.*

The 120 minutes oxidation experiment, Figure 4.15, evolved 1289 ml of hydrogen. The pH decreased from 9.4 to about 9.0 in about 20 minutes and then increased some. The hydrogen evolution initiated after 30 minutes and was quite stable for the rest of the experiment. The pH dropped less than in the 90 minutes oxidation experiment, Figure 4.13, but the characteristic decrease of pH followed by an increase was observed. The hydrogen evolution initiated about 20 minutes earlier than for the 90 minutes oxidation experiment. The initiation time is more comparable with the 30 minutes oxidation experiment. It should also be pointed out that the 120 minutes experiment was the first to be run after keeping the JET1 powder in a desiccator for some weeks.

This is believed to cause this experiment to have an earlier hydrogen evolution initiation an such a large hydrogen evolution.

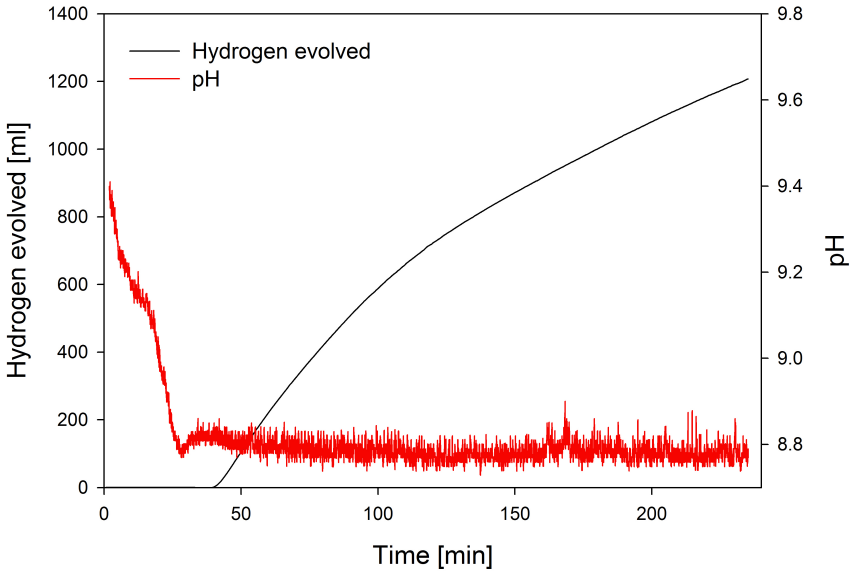

Figure 4.16: *Oxidation experiment - 240 minutes.*

The 240 minutes oxidation experiment, Figure 4.16, evolved 1207 ml of hydrogen. The pH decreased from 9.4 to about 8.8 in 30 minutes, and then increased some. The hydrogen evolution initiated after about 40 minutes, some time after the small increase in pH. The hydrogen evolution was quite stable until 100 minutes, where it decreased a bit. The 240 minutes experiment was the last experiment to be performed after keeping the JET1 powder in a desiccator, approximately 24 hours after the 120 and 30 minutes experiments. Comparing it to the 120 minutes oxidation experiment, it initiated hydrogen evolution about 10 min later and the amount of hydrogen evolved was about 100 ml less.

Comparing all of the experiments from 10 to 240 minutes, the 30 and 120 minutes oxidation experiments distinguishes. There is no hydrogen evolution for the 10, 40 and 60 minutes oxidation experiments, but the 30 minutes oxidation experiment evolved 31.4 ml. The 90, 90*, 120 and 240 minutes oxidation experiments evolved hydrogen, but the 120 minutes experiment evolved more hydrogen than the 240 minutes

experiment, even though it was run for half the time. This indicates that the storage of the JET1 powder in a desiccator has influenced the JET1 powder, resulting in earlier initiation of hydrogen evolution and more hydrogen evolving totally. All of the experiments have in common that the pH needed to drop considerably before the hydrogen evolution initiated, and it is thus a good indicator for whether or not hydrogen should have evolved.

The cumulative curves for each of the experiments that evolved hydrogen is displayed in Figure 4.17.

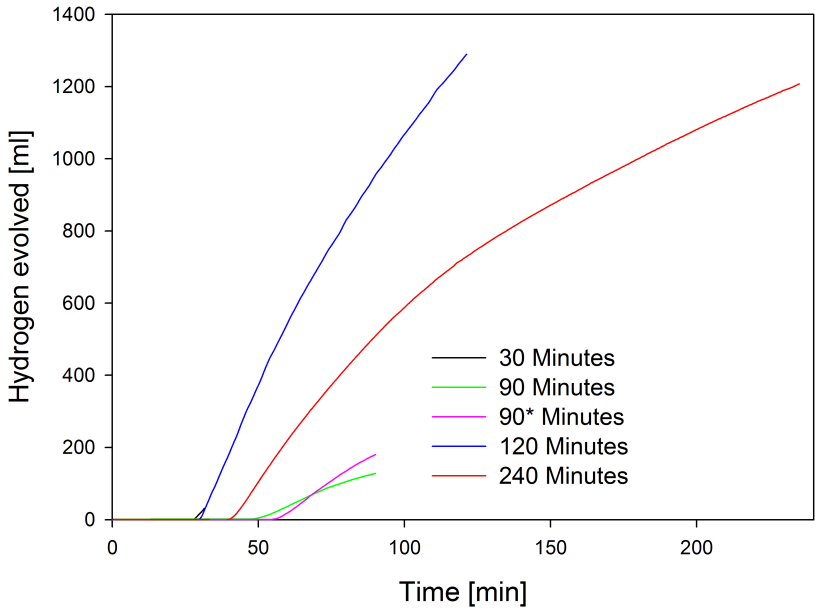

Figure 4.17: *Oxidation experiments - Cumulative Curves for the experiments that evolved hydrogen.*

From Figure 4.17 it is observed that the 30 and 120 minutes oxidation experiments initiated hydrogen evolution at approximately the same time and had a similar slope. The 120 minutes oxidation experiment initiated hydrogen evolution about 10 minutes later and had a smaller slope. The 90 and 90* minutes initiated even later and had an even smaller slope compared to the previous experiments. There was some difference between the 90 and 90* minutes experiments considering initiation time and amount of hydrogen evolved. This could arise from

one experiment using a COARSE particle, and the other one not, but might as well arise from the problems with reproducing results. In short, the pH had to decrease about 0.8 units before hydrogen evolution initiated, the total amount of hydrogen evolved does not seem to be entirely dependent on oxidation time. The powders that was used immediately after being stored in a desiccator had a short initiation time for hydrogen evolution and evolved hydrogen more rapidly than powders that were not stored for a longer time in a desiccator. The amount of hydrogen evolved therefore is dependent not only on oxidation time, but also on how the powder has been stored.

4.2.2 SEM studies - Oxidized JET1 powder

Oxidized JET1 powder from the test experiment and the main experiments were examined using SEM. Even though the powders had been oxidized for very different intervals of time, there was no visible difference between them. The oxidized powders from the 10 and the 240 minutes oxidation experiments are shown in Figure 4.18.

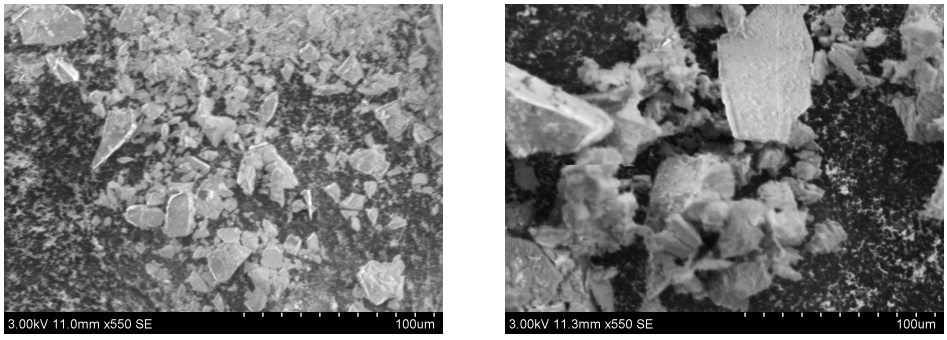

(a) **(b)**

Figure 4.18: *JET1 powder oxidized for various amount of time (a) 10 minutes, (b) 240 minutes.*

It was quite difficult to achieve good pictures, because the particles were covered with a layer of what is assumed to be silica, thus yielding them non-conductive. The scale of the particles has a good resemblance to what was observed for the reacted powders in [2]. The main

difference lies in the fact that the powders from the current experiments were dried with a minimum of water from the slurry, while the powders in [2] were dried together with all of the slurry. This results in a much thinner layer of silica on the powder in Figure 4.18, compared to the powder in [2].

4.2.3 SEM studies - COARSE particles

The COARSE particles were examined prior to oxidation and after oxidation in order to determine whether or not there was a difference between oxidized and unoxidized particle, and if the oxidation time had any influence. It was anticipated that a longer oxidation time would yield more oxides on the surface. It was also desirable to observe the initiation points for the oxidation. The oxide is believed to be silica, and can therefore be referred to as both oxide and silica.

To examine the COARSE particles, both the SE (Secondary electron) detector and the BSE (Back scattered Electron) detector of the SEM was used. The SE detector was used for topographic examinations, the BSE detector was utilized in order to observe any atomic number contrast between the silicon and the oxide layer. The atomic contrast is yielded by difference in mean atomic number. For pure silicon the mean atomic number is 28, while for the oxide which is silica, the mean atomic number is approximately 20. The phase with the highest atomic number will appear brighter than one with lower atomic number, thus will silicon appear brighter than silica in the pictures using the BSE detector as described in [24]. The EDS results presented were collected from unpolished samples, and therefore should not be used qualitatively. The results should only be used as an indication of whether or not there is a difference in the oxygen content between measured points, the exact values of the oxygen content is not reliable.

During the early SEM investigations, what seemed to be a silicon surface with surrounding silica in the SE detector, showed no contrast when using the BSE detector for several samples. After much trial and failure, it was decided to examine the same spot on a COARSE particle at different accelerating voltages, ranging from 15 - 3 keV. As the accelerating voltage was lowered, the surface of the particle came

in to view and at 3 keV a clear atomic contrast between silicon and the oxide layer was observed. Figure 4.19 displays the difference between the accelerating voltage and the resulting picture.

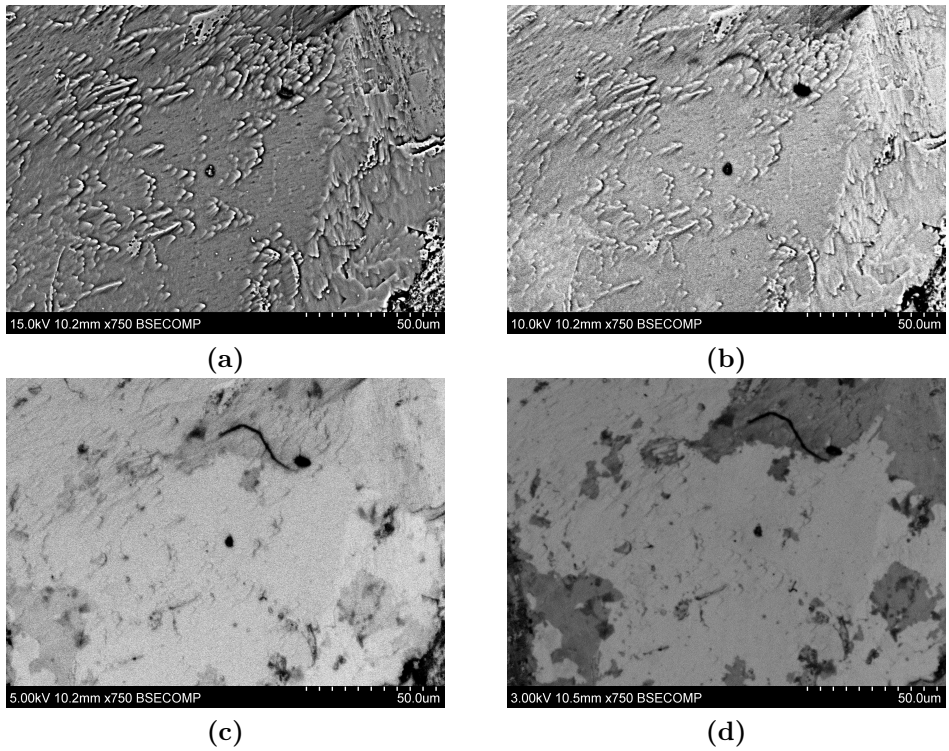

Figure 4.19: *Variation of the accelerating voltage to achieve atomic number contrast between the silicon and the oxide for the 120 minutes COARSE particle (a) 15 keV, (b) 10 keV, (c) 5 keV, (d) 3 keV*

Using an accelerating voltage of 15 keV and 10 keV as seen in Figure 4.19a and 4.19b, reveals nothing of interest. At 5 keV some slight contrast is observed, Figure 4.19c. Applying 3 keV gives a good atomic contrast between silicon and the oxide layer, Figure 4.19d These results lead to 3 keV being the standard accelerating voltage for SEM examinations of both the COARSE particles and the JET1 powder. This is in good agreement with the theory of SEM investigations. As the accelerating voltage is lowered, the emission volume is decreased [24], when looking at samples with thin layers it is therefore necessary to decrease the accelerating voltage. Using too high voltage the electrons

coming from the substrate will overshadow the signals from the thin layer, and therefore hide the information from the oxide layer.

Test experiment

For the test experiment where all of the particles where oxidized together and removed at different time intervals, the actual hydrogen evolution initiated after 80 minutes. The particles that were removed at 10, 20, 30 and 40 minutes display little of interest and all of them look similar. The 10 minutes particle is displayed in Figure 4.20 to compare with the 90 and 90+ particles.

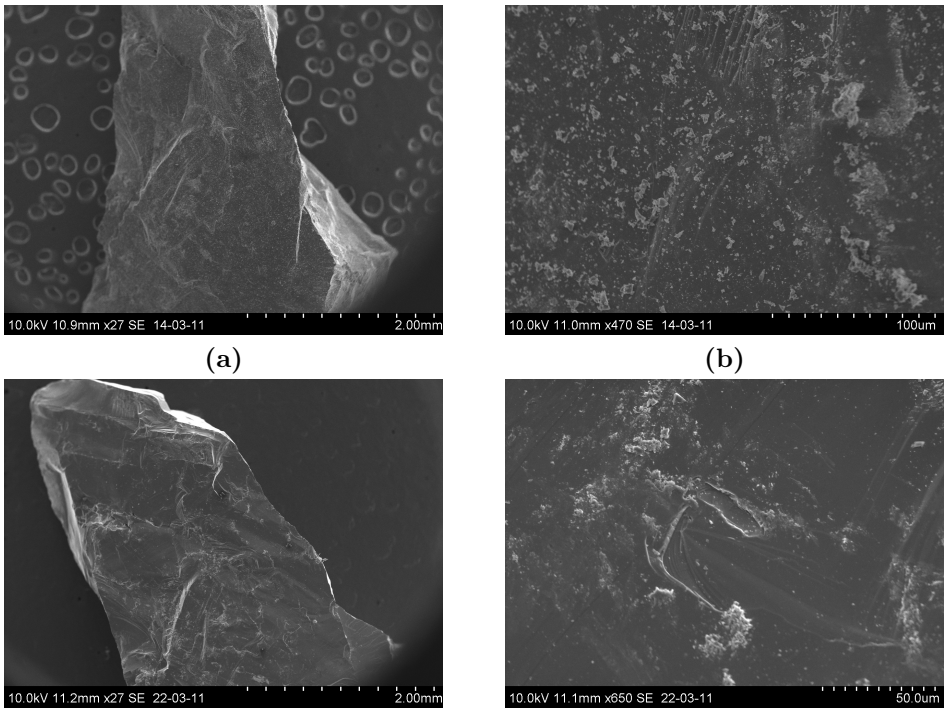

Figure 4.20: *The COARSE particle from the test experiment, before and after 10 minutes oxidation time (a) Overview of the unoxidized particle, (b) Close-up of the unoxidized particle, (c) Overview of the oxidized particle, (d) Close-up of the oxidized particle*

The unoxidized particle has a lot of smaller silicon particles attached to it as seen in Figures 4.20a and 4.20b , similar to the JET1 and 2-10 powder in Figure 4.6a and 4.7a. After the 10 minutes oxidation, these small particles are removed and a more smooth surface appears as seen in Figures 4.20c and 4.20d. There is nothing that indicates an oxide layer of any kind. EDS analysis was not performed.

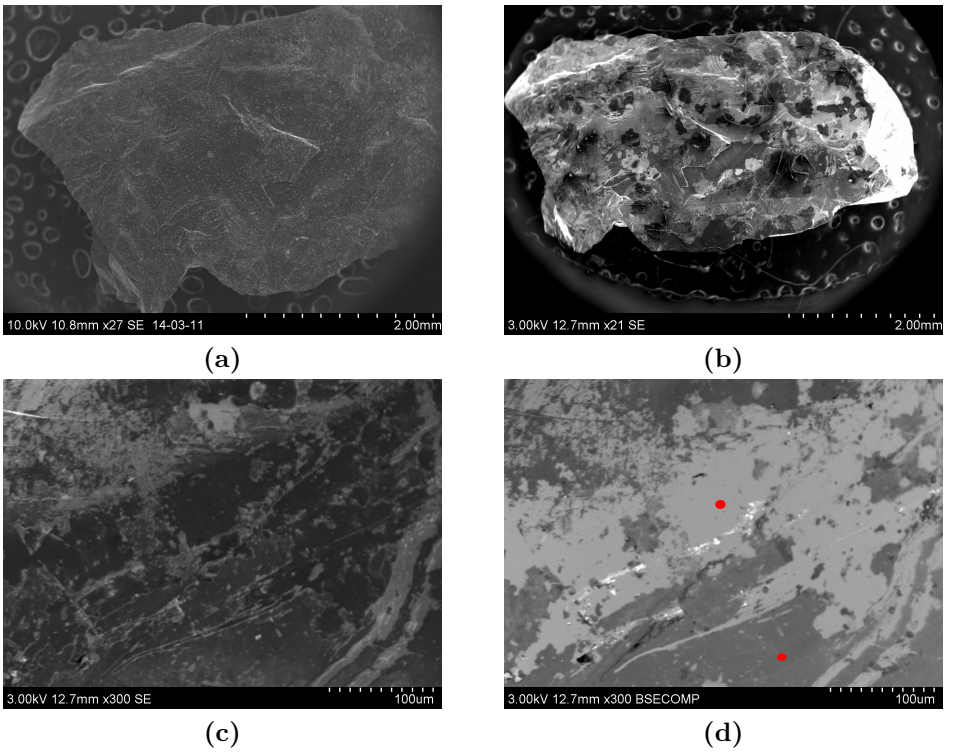

Figure 4.21: *The COARSE particle from the test experiment, before and after 90 minutes oxidation time (a) Overview of the unoxidized particle, (b) Overview of the oxidized particle, the black dots are carbon tape, (c) Close-up of the oxidized particle with SE detector, (d) Close-up of the oxidized particle with BSE detector, the red dots are the EDS analysis points.*

The unoxidized particle, Figure 4.21a is similar to the 10 minutes particles, Figure 4.20a. After oxidation, Figure 4.21b, the surface is free of smaller particles and a white layer of what is believed to be silica appears. The black dots observed is carbon tape from earlier examinations. In Figure 4.21c a close-up of the oxidized particle is displayed,

the white layer believed to be silica and the dark grey the silicon surface. According to theory, the white layer observed in Figure 4.21c should be darker than the substrate when using the BSE detector. Using the BSE detector, Figure 4.21d, there is a clear difference in contrast between the oxide and the substrate, indicating that the substrate is silicon and that the oxide layer is silica. The EDS analysis indicated an oxygen content of 1 wt% in the bright area of Figure 4.21d and an oxygen content of about 26 wt% in the dark area. This confirms the indication that the substrate is silicon and that the oxide layer is silica.

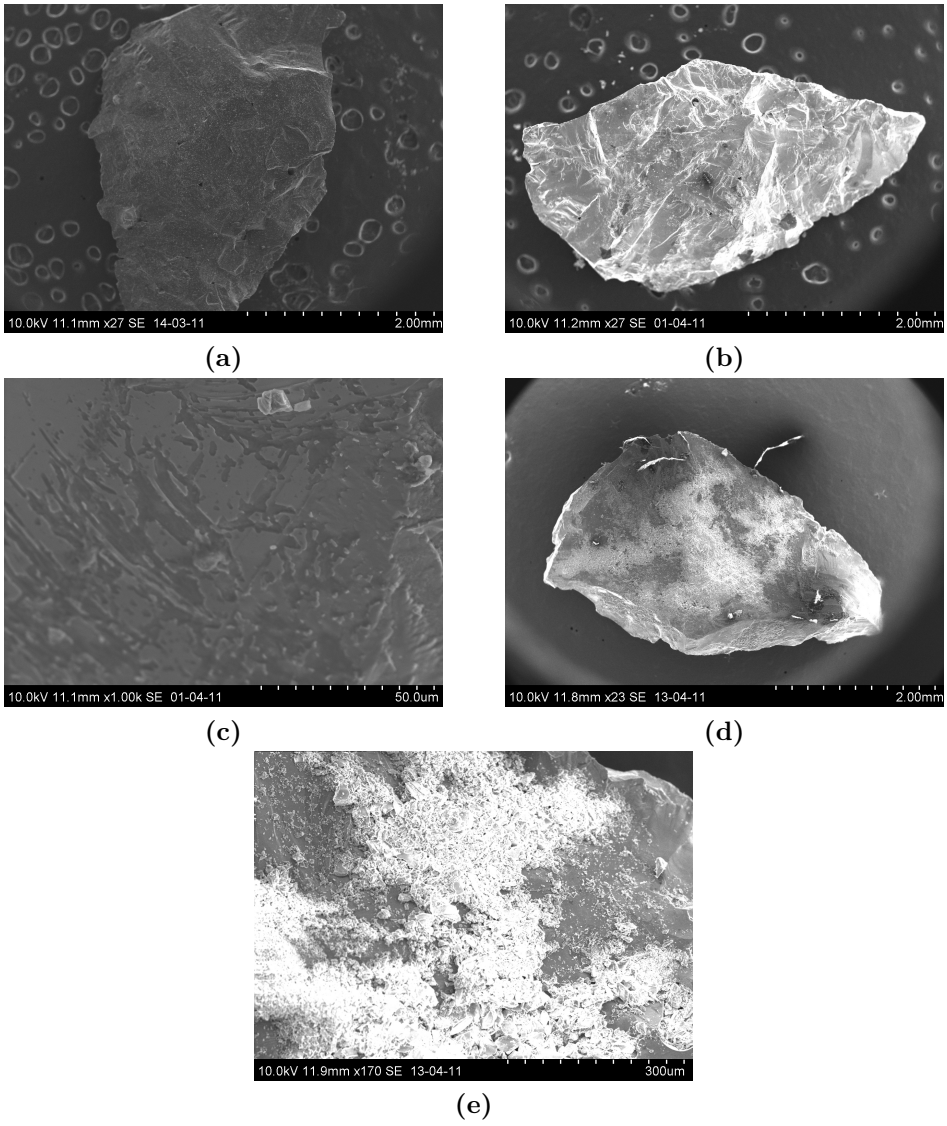

Figure 4.22: *The COARSE particle from the test experiment, before and after 90+ minutes oxidation time (a) Overview of the unoxidized particle, (b) Overview of the oxidized particle, (c) Close-up of the oxidized particle, (d) Overview of oxidized particle after some days storage, (e) Close-up of oxidized particle after some days of storage.*

The unoxidized particle, Figure 4.22a is similar to the previous unoxidized particles, Figures 4.20a and 4.21a. After oxidation the particle

was left in the slurry and dried in a furnace at 110 ℃. This resulted in a particle covered with a layer of something that seemed to be non-conducting, thus leading to a charge build-up, Figure 4.22b. A closer view, Figure 4.22c, unveiled that the surface was covered with at thick layer, similar to what was observed in [2] on reacted powder which had been dried from slurries. Examining the particle with the BSE detector was also intended a few days later. Upon examining the particle again, the result can be observed in Figure 4.22d. The layer which had covered the surface had now cracked an consisted of several smaller particles, a close-up is displayed in Figure 4.22e. It is believed that the thick layer was amorphous silica which acted as a drying agent and thus cracked after absorbing moisture. The particle was stored in a small beaker with a lid, but not in a desiccator. EDS analysis indicated that the small particles were a mixture of silicon and oxygen and it is thus plausible that it was silica.

In short, this experiment showed that it is possible to oxidize the COARSE particle and examine the oxide layer with SEM using the SE and BSE detectors. Using the BSE detector it is possible to achieve an atomic contrast between the silicon and the silica. EDS analysis can provide information about difference in oxygen content between measured points. The drying of the slurry together with a particle resulted in a thick layer of what is believed to be amorphous silica on the surface of the particle.

Main oxidation experiments

For the main oxidation experiments, one COARSE particle in a slurry of JET1 was oxidized for a given amount of time. This resulted in a total of seven particle to investigate. In the following section each of the particles will be presented in unoxidized and oxidized state. All of the particles in unoxidized state look similar, and is therefore not commented on any further than for the 10 minutes particle.

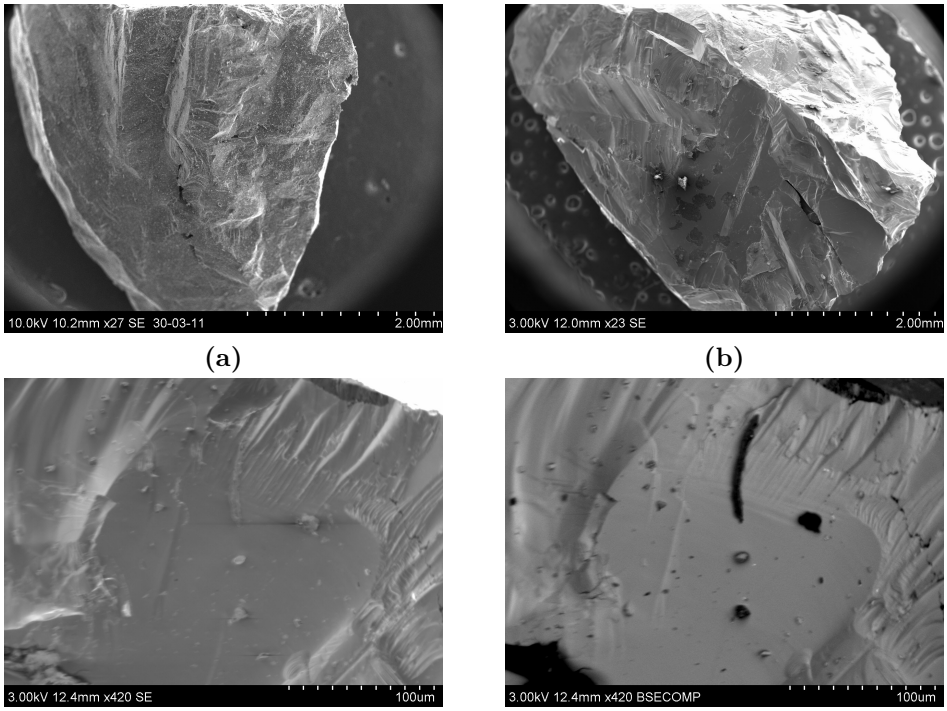

Figure 4.23: *The COARSE particle from the main experiment, before and after 10 minutes oxidation time (a) Overview of the unoxidized particle, (b) Overview of the oxidized particle, (c) Close-up of the oxidized particle with SE detector, (d) Close-up of the oxidized particle with BSE detector.*

The unoxidized particle has a lot of smaller silicon particles attached to it as seen in Figure 4.23a, similar to the JET1 and 2-10 powder in Figure 4.6a and 4.7a. The surface of the particle is quite rough with defect points and marks from the jaw crushing. The oxidized particle, Figure 4.23b, have only small amounts of small particles attached to the surface, the black dots seen on the surface is carbon tape from earlier investigations. The surface seems quite smooth, except for the deformations from the jaw crushing. There is no sign of oxidation as displayed in Figure 4.23c. The Figure 4.23d show that there is no atomic contrast, which would indicate that there is no oxidation. The black points seen in figure 4.23d is probably dust. EDS analysis was not performed.

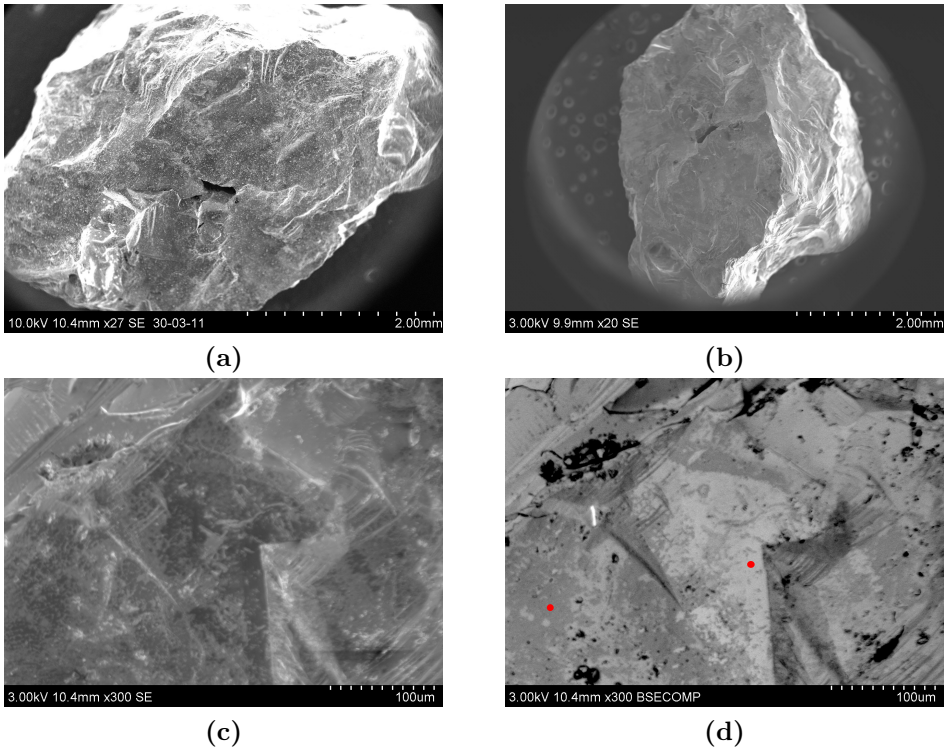

Figure 4.24: *The COARSE particle from the main experiment, before and after 30 minutes oxidation time (a) Overview of the unoxidized particle, (b) Overview of the oxidized particle, (c) Close-up of the oxidized particle with SE detector, (d) Close-up of the oxidized particle with BSE detector, the red dots are the EDS analysis points.*

The unoxidized particle, Figure 4.24a resembles the other unoxidized particles mentioned earlier. The oxidized particle, Figure 4.24b, is quite smooth and does not have small particles attached to the surface. There seems to be islands of a white layer on the surface. The close-up in Figure 4.24c reveals that the particle is partly covered with a white layer and have areas that a dark grey. The BSE detector, Figure 4.24d gives a clear atomic contrast between these areas, indicating that the dark grey area in Figure 4.24c which is white in Figure 4.24d is silicon, while the white layer in Figure 4.24c which is dark grey in Figure 4.24d is silica. The EDS analysis shows a concentration of 5 wt% oxygen in the grey area of Figure 4.24d, compared to 1 wt% oxygen in the white area. As displayed in Figure 4.10 this experiments evolved hydrogen.

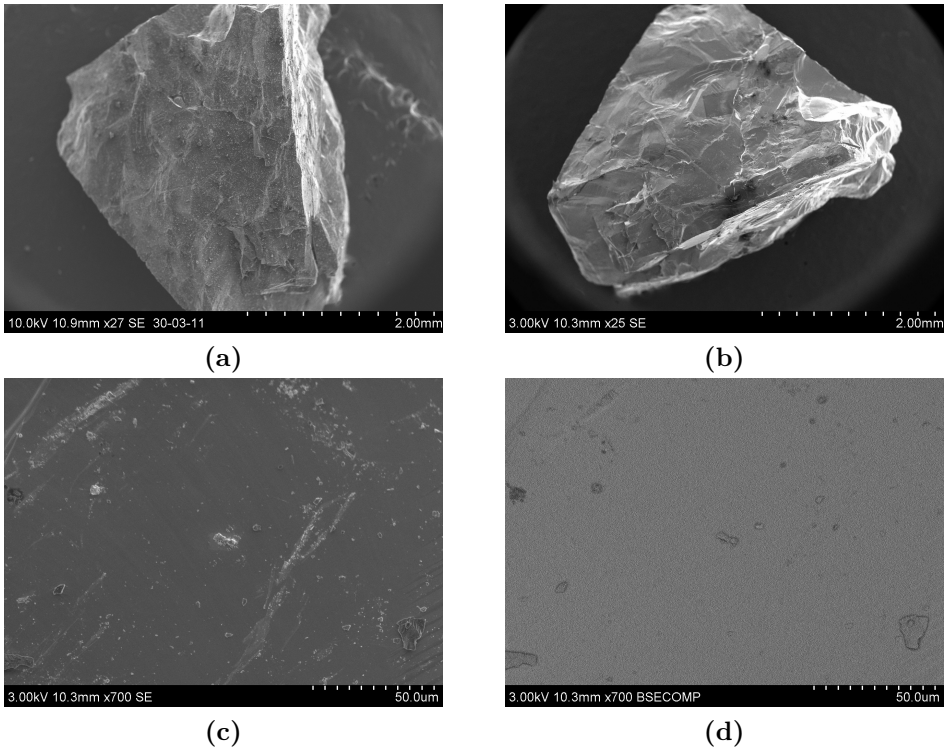

Figure 4.25: *The COARSE particle from the main experiment, before and after 40 minutes oxidation time (a) Overview of the unoxidized particle, (b) Overview of the oxidized particle, (c) Close-up of the oxidized particle with SE detector, (d) Close-up of the oxidized particle with BSE detector.*

The unoxidized particle, Figure 4.25a resembles the other unoxidized particles mentioned earlier. The oxidized particle, Figure 4.25b, is quite smooth but no white layer is present on the surface. In Figure 4.25c, the surface has some small particles attached to the surface, but no white areas like observed in Figure 4.24c is present. The BSE detector, Figure 4.25d, gives no atomic contrast. EDS analysis was not performed. The particle seems to not have any oxide layer, this agrees with Figure 4.11 which indicates that no hydrogen has evolved.

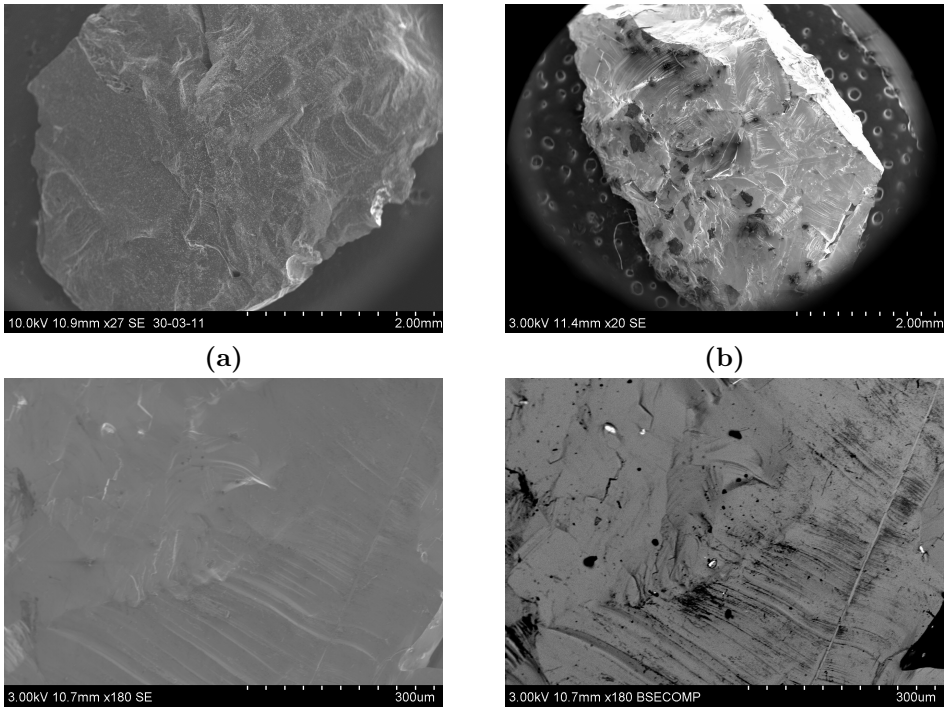

Figure 4.26: *The COARSE particle from the main experiment, before and after 60 minutes oxidation time (a) Overview of the unoxidized particle, (b) Overview of the oxidized particle, the black dots are from carbon tape, (c) Close-up of the oxidized particle with SE detector, (d) Close-up of the oxidized particle with BSE detector.*

The unoxidized particle, Figure 4.26a resembles the other unoxidized particles mentioned earlier. In Figure 4.26b , the surface has some small particles attached to the surface, but no white areas like observed in Figure 4.24c is present. The black spots observed are from carbon tape from earlier examinations. The close-up in Figure 4.26c reveals no oxide white layer. The BSE detector, Figure 4.26d gives no atomic contrast. EDS analysis was not performed. The particle seems to not have any oxide layer, this agrees with Figure 4.12 which indicates that no hydrogen has evolved.

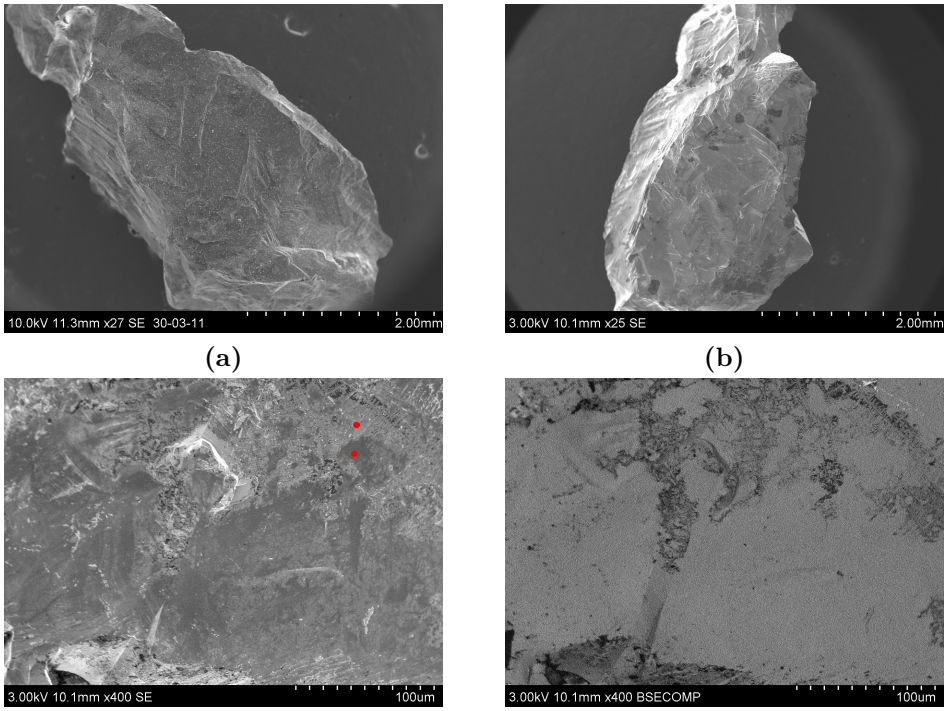

Figure 4.27: *The COARSE particle from the main experiment, before and after 90 minutes oxidation time (a) Overview of the unoxidized particle, (b) Overview of the oxidized particle, the black dots are from carbon tape, (c) Close-up of the oxidized particle with SE detector, the red dots are the EDS analysis points, (d) Close-up of the oxidized particle with BSE detector.*

The unoxidized particle, Figure 4.27a resembles the other unoxidized particles mentioned earlier. In Figure 4.27b the particle seems to be covered partly with a very thin white layer, with some areas showing a dark grey colour. The black spots are due to carbon tape from earlier investigations. The close up in Figure 4.27c reveals what seems to be a very thin white layer on the particle surface. The BSE detector, Figure 4.27d produces no atomic contrast. The EDS analysis is inconclusive, as the oxygen content in the white area is 1.4 wt%, while the oxygen content in the gray area is 1 wt%. The oxide layer is perhaps too thin to perform EDS on. Figure 4.13 indicates that hydrogen has evolved, and thus should the particle be oxidized.

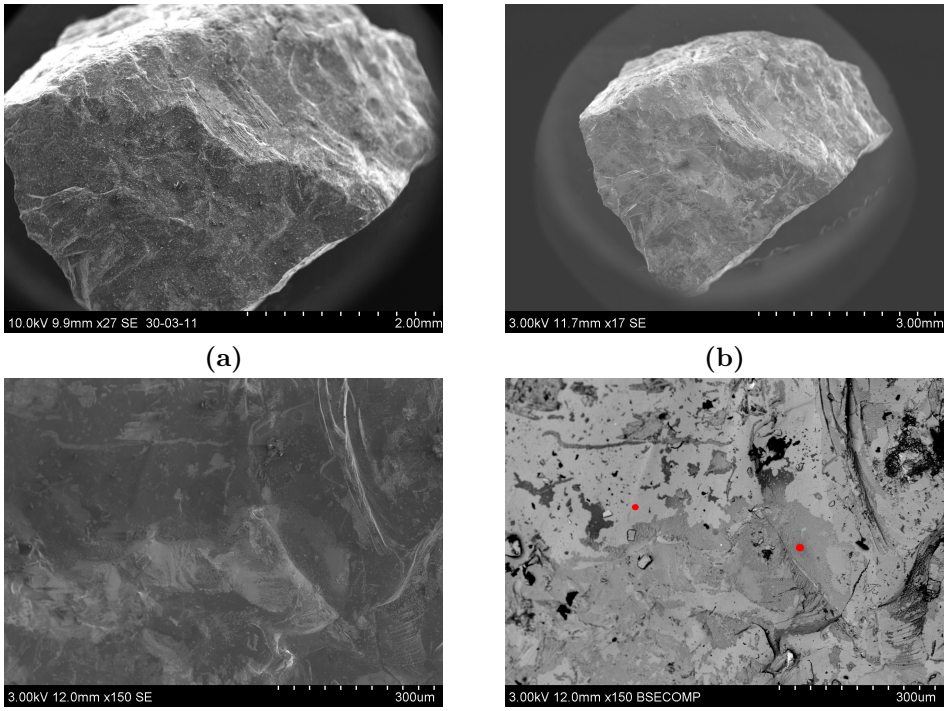

Figure 4.28: *The COARSE particle from the main experiment, before and after 120 minutes oxidation time (a) Overview of the unoxidized particle, (b) Overview of the oxidized particle, (c) Close-up of the oxidized particle with SE detector, (d) Close-up of the oxidized particle with BSE detector, the red dots are the EDS analysis points.*

The unoxidized particle, Figure 4.28a, resembles the other unoxidized particles mentioned earlier. In Figure 4.28b the particle seems to be partly covered with a white layer, with some areas showing a dark grey colour. The Close-up in Figure 4.28c reveals white, light grey and dark grey areas. Examining the same area with the BSE detector, Figure 4.28d, reveals that the white and light grey areas from Figure 4.28c are probably silica with various thickness. The dark grey areas in Figure 4.28c appears to be the silicon. The EDS analysis indicates that the grey area in Figure 4.28d has a concentration of 9 wt% oxygen compared to the white area with 1 wt% of oxygen, thus is it plausible that the particle has been oxidized and have some areas with silica and some with bare silicon surface.

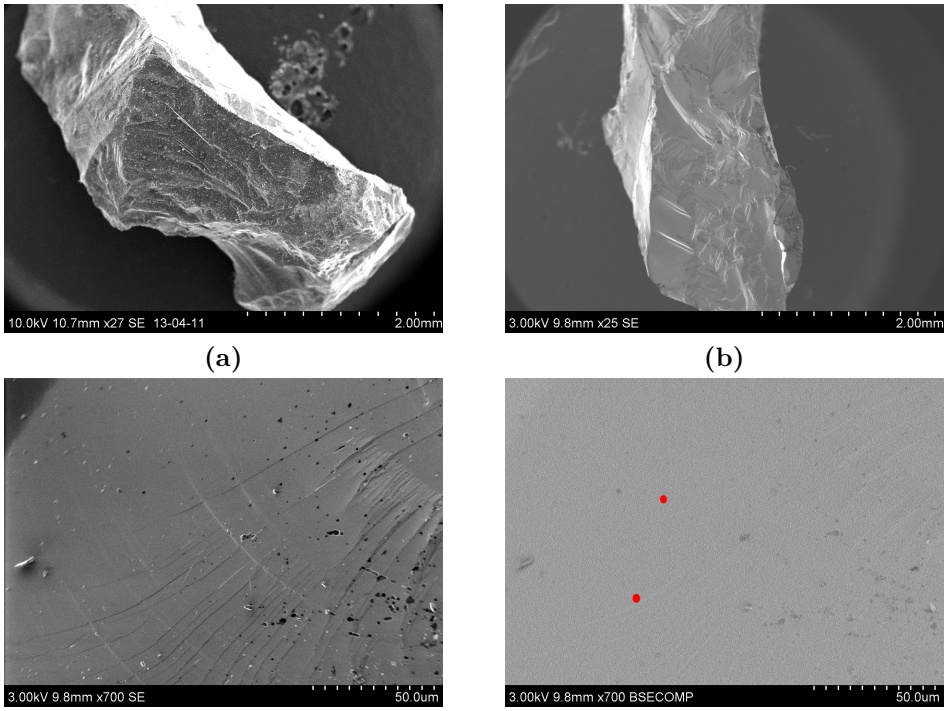

Figure 4.29: *The COARSE particle from the main experiment, before and after 240 minutes oxidation time (a) Overview of the unoxidized particle, (b) Overview of the oxidized particle, the black dots are from carbon tape, (c) Close-up of the oxidized particle with SE detector, (d) Close-up of the oxidized particle with BSE detector, the red dots are the EDS analysis points.*

The unoxidized particle, Figure 4.29a resembles the other unoxidized particles mentioned earlier. In Figure 4.29b the particle seems to be completely covered with a white layer. The Close-up in Figure 4.29c indicates that there is no dark grey areas present, and the BSE detector, Figure 4.29d does not produce any atomic contrast. The EDS show little difference in oxygen concentration, both points have about 5 wt% oxygen, but it is a higher concentration than on the surface of an unoxidized COARSE particle. This indicates that the particle is completely covered with silica.

In short, the oxidation of the particles seems to be in agreement with the hydrogen evolution curves, as the presence of silica is found only

on the particles where hydrogen was evolved during the experiment. It is important to remember that the hydrogen evolution primarily originates from the JET1powder used in the slurries, not the COARSE particles, as the powder has a much larger surface area and smaller curvature which leads to higher solubility.

4.2.4 Surface area measurements

The surface area of the oxidized JET1 powders from the various experiments were measured by a 5-point BET method. The results for the oxidized JET1 powders are listed in Table 4.8, the unoxidized powder is listed as a point of reference. After drying of the powders removed from the slurry, glass clear rods was found in the beakers together with the powder. It was assumed that this was amorphous silica, BET surface area measurements were performed. It was also studied with XRD to confirm the suspicion of it being amorphous silica. The amorphous silica is mainly included in Table 4.8 to display the large area amorphous silica obtains, which is what mainly increases the surface area of all the powder samples.

Table 4.8: *BET surface area and average diameter of the JET1 powders from the different oxidation experiments. The surface area is based on the density of silica, except for unoxidized JET1 which is based on density of silicon. **The sample was degassed at 300 ℃ compared to 150 ℃ for the other samples.*

Sample	**Surface area** S_0 (m^2/g)	**Average diameter** (nm)
10 min	17.2	134.2
10m min**	19.1	120.8
30 min	23.6	97.8
40 min	16.8	137.4
40 min**	17.2	134.2
60 min	11.5	200.7
60 min**	12.1	190.7
90 min	25.9	89.1
90* min	37.9	60.9
120 min	37.3	61.9
240 min	46.3	49.8
Test experiment	18.6	124.1
Amorphous JET1	238	9.7
JET1 unoxidized	2.2	1.2 (μm)

From the results in Table 4.8 it is clear that the surface area has increased when comparing the oxidized JET1 with the unoxidized JET1 powders. It is also indicated that a higher degas temperature yields a higher surface area, probably because more water is removed. Because of the JET1 powders problems with reproducing results with respect to hydrogen evolved, plotting the BET surface area versus the oxidation time would be hard to interpret. The BET surface area is therefore plotted versus the total hydrogen evolved, Figure 4.30, to remove the uncertainty's connected to the reproducibility of the powder.

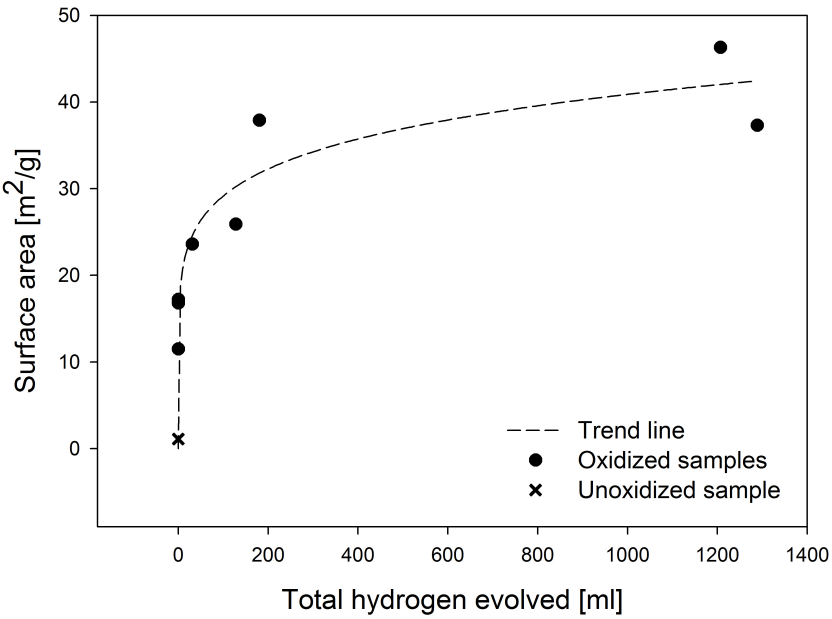

Figure 4.30: *Surface area of oxidized JET1 silicon powder vs. total hydrogen evolved.*

From Figure 4.30 it is observed that the surface area increases as a function of total hydrogen evolved, but there is also a great increase even though no hydrogen has evolved. The slope of the increase in surface area seems to decline a bit as the amount of total hydrogen evolved increases.

4.2.5 LECO

The oxygen content in the oxidized JET1 powders and the unoxidized JET1 powder was determined by performing a LECO analysis. The results are listed in Table 4.9.

Table 4.9: *Oxygen content of the JET1 powders from the different oxidation experiments.*

Sample	Weight (g)	Amount of Oxygen (wt%)
10 min	0.12	5.9
30 min	0.10	7.0
40 min	0.14	4.7
60 min	0.13	4.1
90 min	0.10	7.1
90* min	0.12	9.5
120 min	0.12	10.4
240 min	0.07	9.9
Test experiment	0.14	6.0
Jet1 unoxidized	0.14	1.4

From Table 4.9 it is observed that the oxidized JET1 powders have a larger oxygen content than the unoxidized JET1 powder. Because of the JET1 powders problems with reproducing results with respect to total hydrogen evolved, plotting the oxygen content versus the oxidation time would be hard to interpret. The oxygen content is therefore plotted versus the total hydrogen evolved, Figure 4.31.

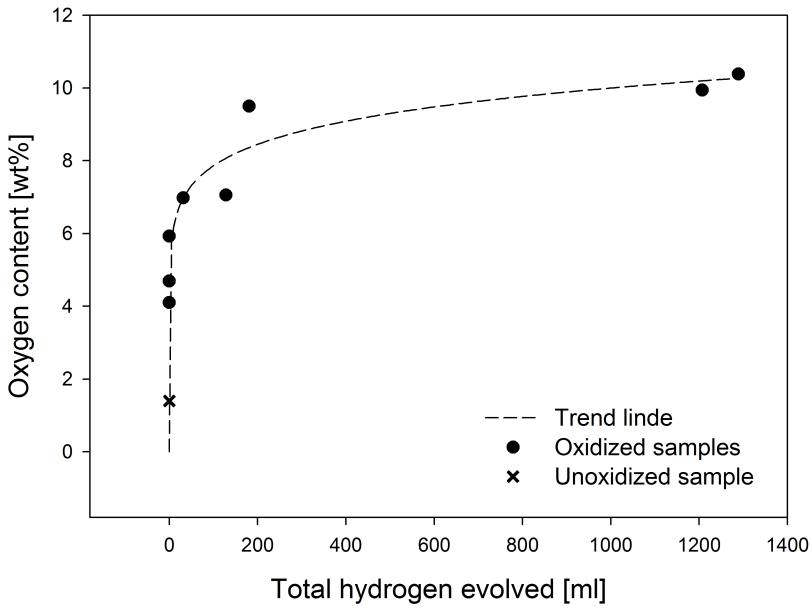

Figure 4.31: *Oxygen content of the oxidized JET1 powders vs. total hydrogen evolved.*

From Figure 4.31 it is observed that the oxygen content increases as a function of total hydrogen evolved, but there is also a great increase even though no hydrogen has evolved. The slope of the increase in oxygen content seems to decline some as the amount of total hydrogen evolved increases.

4.2.6 XRD

An XRD scan of the oxidized silicon powder and the glass-clear rods expected to be amorphous silica was performed.

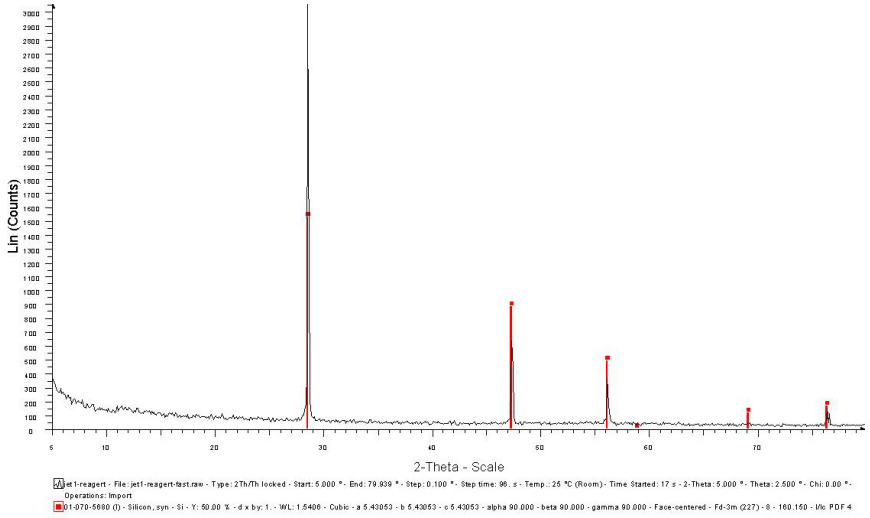

Figure 4.32: *XRD scan of the oxidized JET1 powder.*

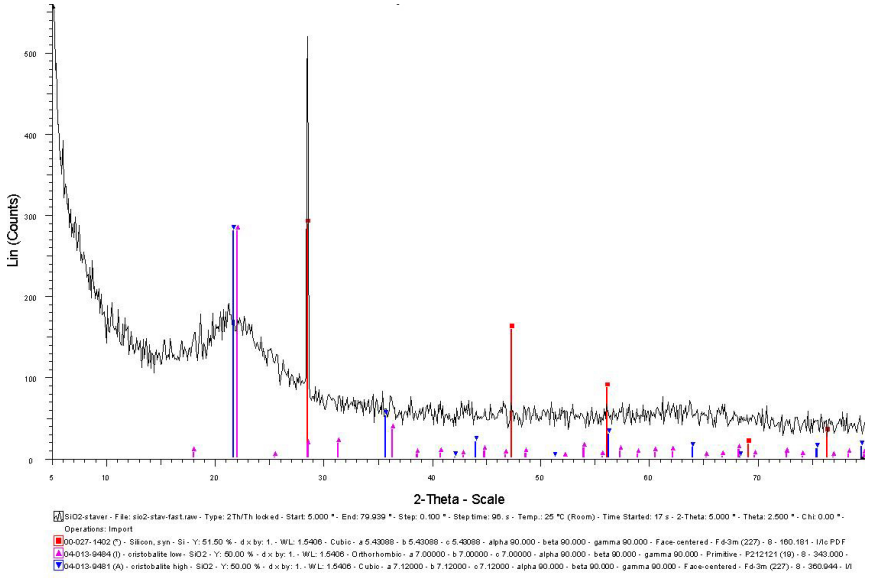

Figure 4.33: *XRD scan of the glass-clear rods, thought to be amorphous silica.*

Figure 4.32 indicates that the oxidized JET1 powder consists of pure

silicon. Some of the peaks are missing, this is due to the fast scanning speed and large step size.

Figure 4.33 indicates that there is some silicon present due to the large peak around 29 Theta on the x-axis. This is most likely a contamination from the dried slurry which the rods were removed from. The broadening of the peak around 22 Theta on the x-axis indicates that an amorphous phase is present. When fitting cristobalite low and high, which are different forms of silica, this fits rather well with the broadened peak. Several of the peaks are missing, but the scan was performed with a large step size.

In short, these scans are very rough with several peaks missing. These measurements were not performed to identify entirely unknown phases, but to confirm assumptions made. Thus there is no need for more accurate measurements.

4.2.7 Colorimetry

Colorimetry was applied to determine the amount of silicic acid in the aqueous solutions from separating the slurries used in the oxidation experiments. Silicic acid is also referred to as dissolved silica. The results from the colorimetry is listed in Table 4.10.

Table 4.10: *Concentration of silicic acid in the aqueous solutions and the respective pH. **The concentration is below the measuring limits of the apparatus which is 0.0002 mmol/l.*

Sample	**Concentration of silicic acid** (mmol/l)	**pH**
10 min	7.5	10.35
30 min	6.2	10.33
40 min	5.6	10.02
60 min	5.2	9.96
90 min	4.7	9.85
90* min	7.6	10.28
120 min	9.2	10.43
240 min	7.8	10.05
Distilled water	0**	6.55

From the results given in Table 4.10, it is clear that the concentration of silicic acid is larger after oxidation compared to the distilled water use to prepare the slurries. The concentration also varies some between the different oxidation experiments. As for the LECO and BET surface area measurements, also the colorimetry measurements are influenced by the JET1 powders problems with reproducing results with respect to the total hydrogen evolved. The concentration of silicic acid is therefore plotted versus total hydrogen evolved in Figure 4.34.

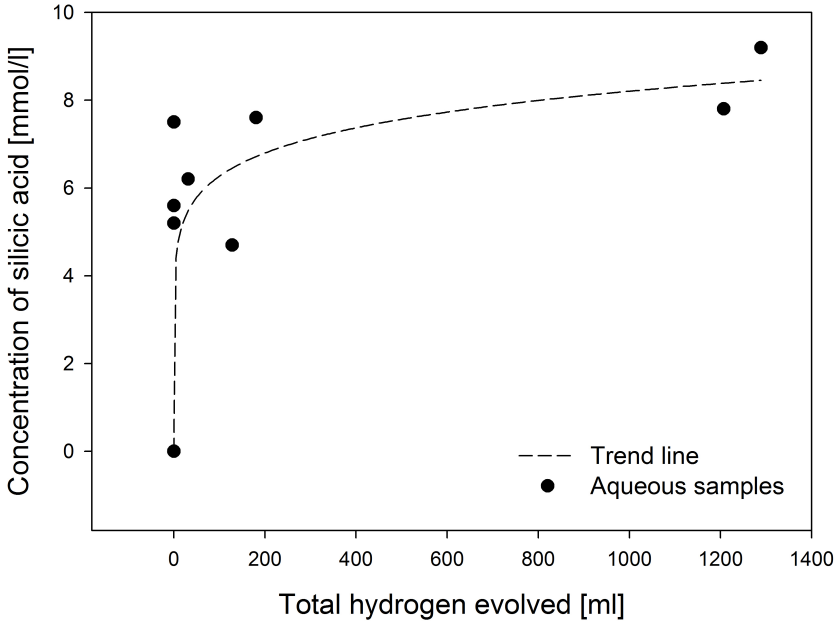

Figure 4.34: *Concentration of silicic acid in the aqueous suspensions vs. total hydrogen evolved.*

Figure 4.34 indicates that the concentration of silicic acid increases although no hydrogen has evolved. As hydrogen evolves, the increase of silicic acid seems to decline, as if a solubility limit was reached. The concentration of silicic acid is plotted against the pH of the aqueous solutions in Figure 4.35.

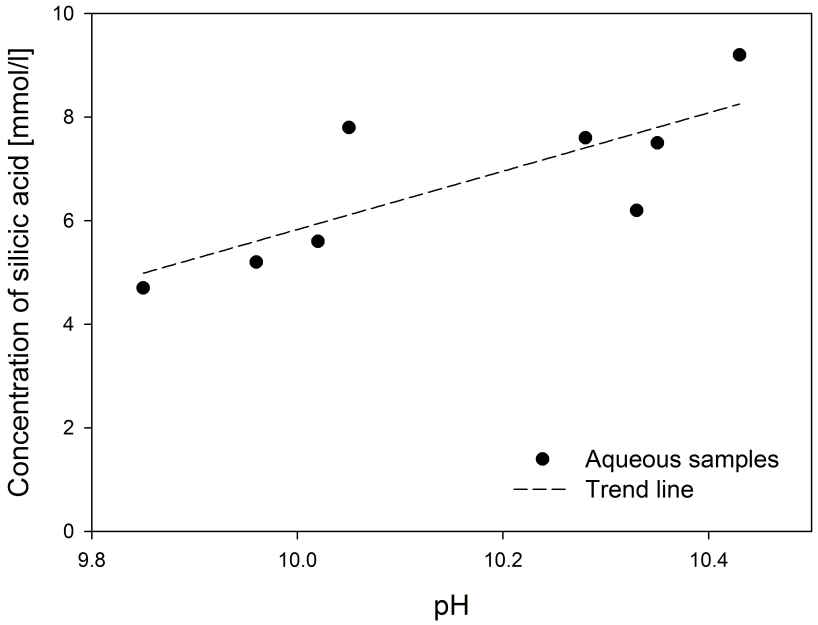

Figure 4.35: *Concentration of silicic acid vs. pH.*

The results from Figure 4.35 predicts that there is a positive linear dependence between pH and concentration of silicic acid. As mentioned earlier, silicic acid is also referred to as dissolved silica. Since silica is an acidic specie, it would need an alkaline environment to dissolve it. A linear positive trend for the increase in concentration of silicic acid and increase in pH is thus plausible.

4.2.8 HR ICP-MS

HR ICP-MS was applied to determine the amount of total silica in the aqueous solutions resulting from the separation of the slurries from the oxidation experiments. The results are listed in Table 4.11.

Table 4.11: *Concentration of total silica in the aqueous solutions.*

Sample	**Concentration of total silica** (mmol/l)
10 min	48.1
30 min	71.5
40 min	53.1
60 min	36.2
90 min	66.5
90* min	76.7
120 min	181.5
240 min	138.5
Distilled water	0.02

The results in Table 4.11 indicates that the concentration of silica in the aqueous solutions have increased compared to the distilled water used for preparing the slurries. The result for the sample with distilled water, was subtracted from the other results so the contribution from natural silica present in the water is removed. As for LECO, BET surface area and colorimetry, the concentration of total silica is plotted against total hydrogen evolved in Figure 4.36.

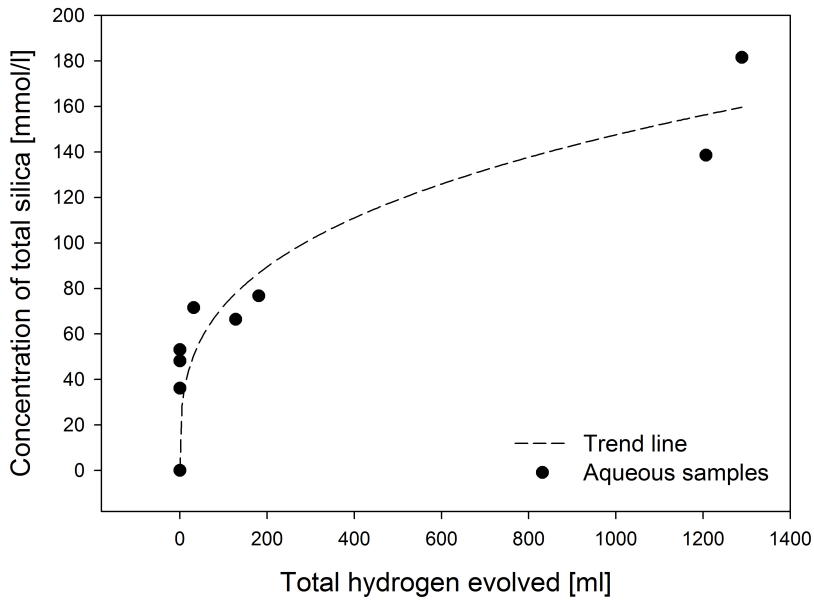

Figure 4.36: *Concentration of total silica vs. total hydrogen evolved*

Figure 4.36 indicates that the total concentration of silica increases even though no hydrogen has evolved. Unlike for the BET surface area, LECO and colorimetry curves, the increase in concentration of total silica does not seem to decline that much.

4.3 Mechanical properties of Silicon

4.3.1 Samples and sample preparations

The prepared samples of single crystal and polycrystalline silicon were studied in the Hitachi S-3400N Scanning Electron Microscope, the results are displayed in Figure 4.37.

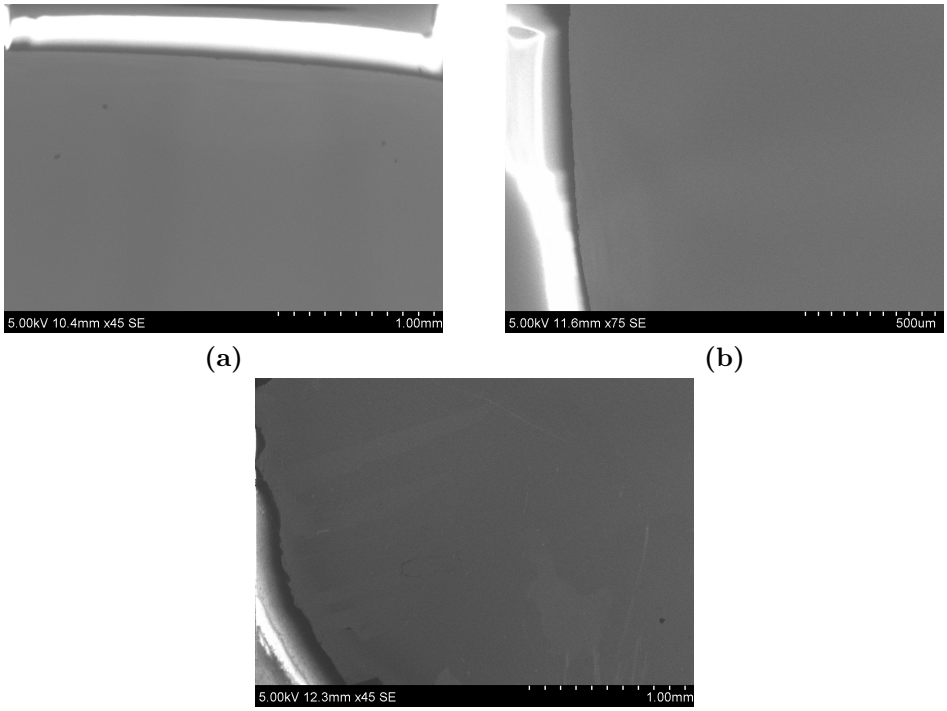

Figure 4.37: *SEM studies of the samples before oxidation (a) Single crystal before oxidation, (b) Single crystal, not to be oxidized, (c) Polycrystalline sample before oxidation.*

The single crystal samples show little of interest, Figure 4.37a and 4.37b. The polycrystalline sample, Figure 4.37c, seems to give an indication of the grains, which in this case are quite large, > 1 cm.

4.3.2 EBSD

The EBSD scan of the chosen surface area of the polycrystalline sample, resulted in the IPF map (Inverse Pole Figure) displayed in Figure 4.38 with the corresponding IPF in Figure 4.39 translating the colours in to crystallographic orientations.

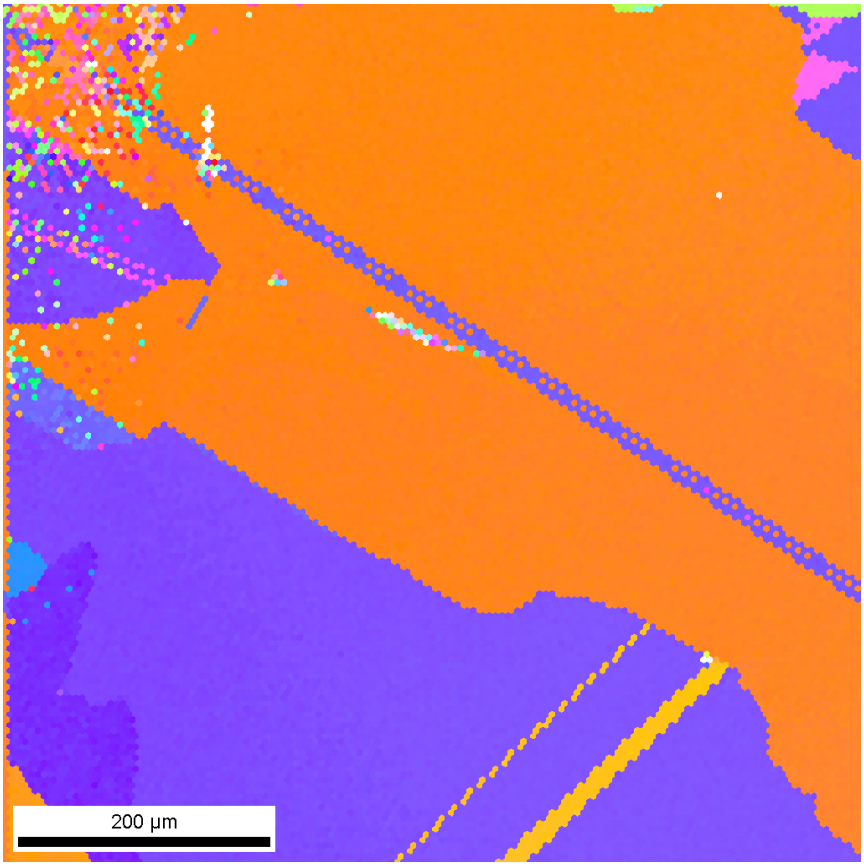

Figure 4.38: *IPF map of the polycrystalline sample.*

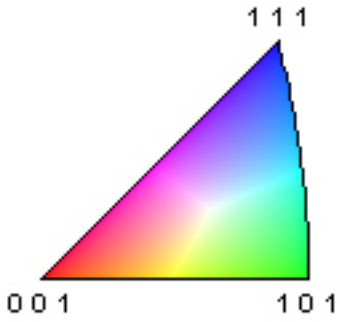

Figure 4.39: *IPF translating the colours of a IPF map in to crystallographic orientations.*

As seen in Figure 4.38, the grain size is quite large, > 1 cm, and the different grains are not homogeneous with respect to crystallographic orientation. This is suggested by the fact that none of the grains consist of a single colour, but have different shades of colour inside the same grain. The translation of the colours in to orientations is given in Figure 4.39. In Figure 4.40 an inverse IPF of the scanned area is displayed.

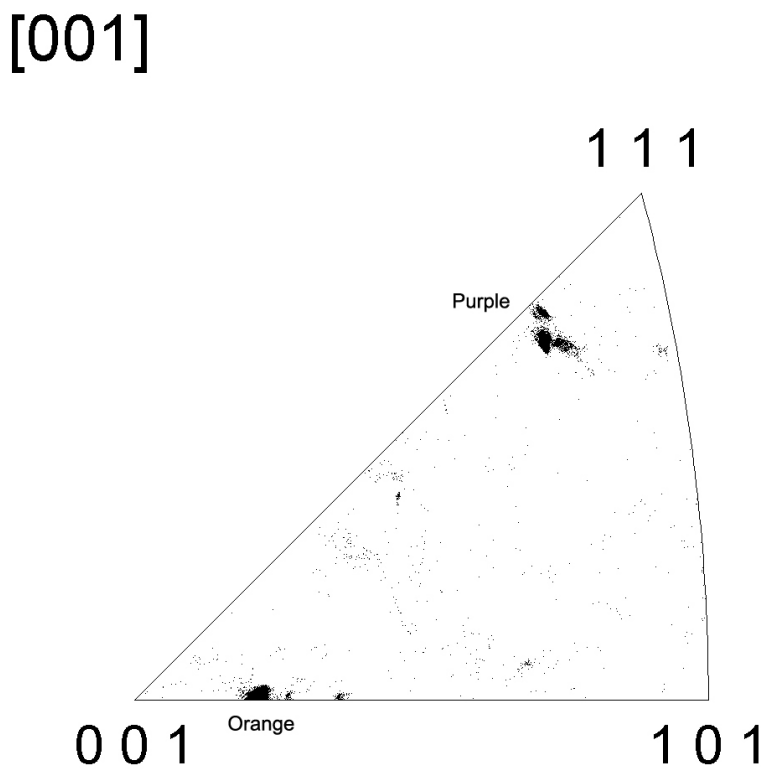

Figure 4.40: *Inverse Pole Figure of the polycrystalline sample.*

The cloud of points at the upper part of the triangle in Figure 4.40, between 001 and 111, corresponds to the purple colour in Figure 4.39. The cloud of points at the lower part of the triangle, adjacent to 001, corresponds to the orange colour in Figure 4.39. As there is some scatter of the points, the grains are not homogeneous with respect

to crystallographic orientation. The orientation of the two grains in respectively orange and purple colour are given in Table 4.12.

Table 4.12: *The crystallographic orientation for the orange and the purple grain.*

Colour	**(hkl)** plane	**[uvw]** direction
Orange	$10\,\bar{6}\,\bar{7}$	$\bar{9}\,\bar{1}\,\bar{1}2$
Purple	$0\,5\,\bar{1}$	$27\ 1\ 5$

4.3.3 Oxidation of samples

The samples were oxidized at different time intervals, the single crystal sample for five hours and the polycrystalline sample for four hours. The amount of hydrogen evolved vs. oxidation time for the single crystal specimen and the polycrystalline specimen is given in Figure 4.41 and 4.42.

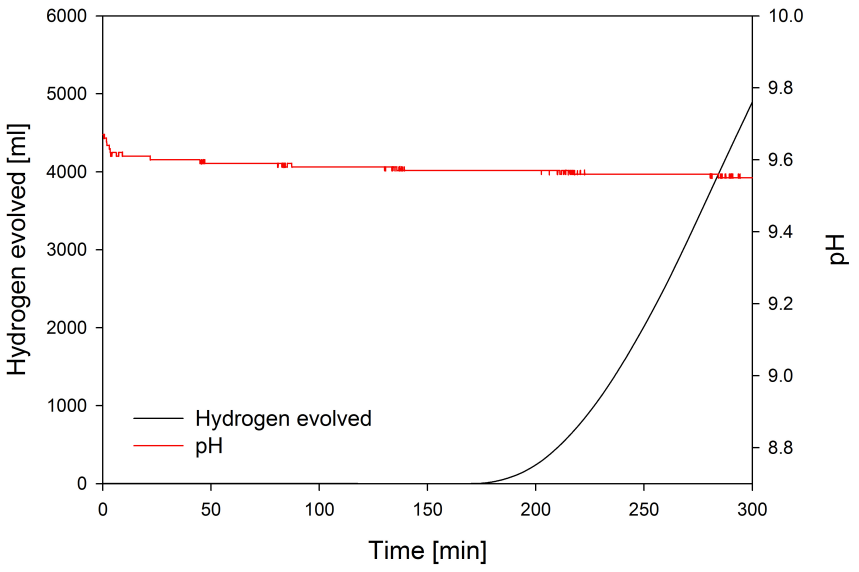

Figure 4.41: *Oxidation of the single crystal sample.*

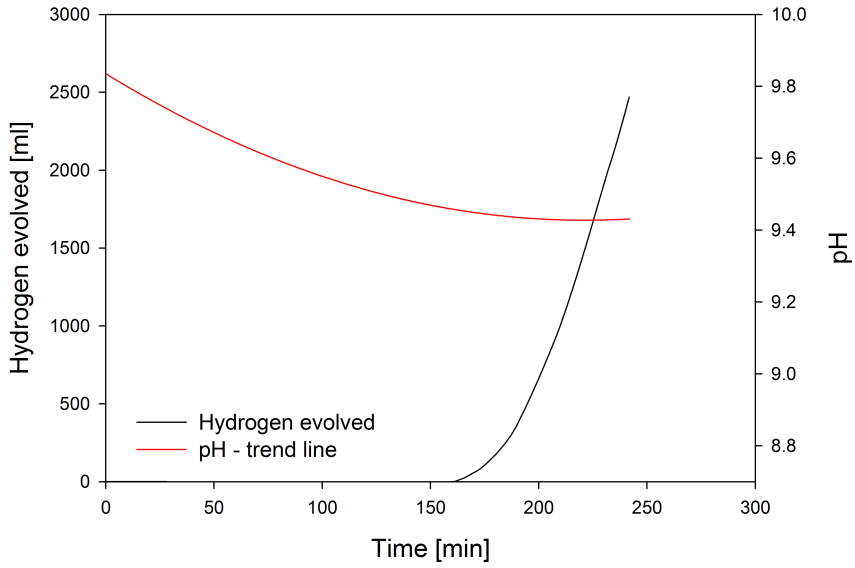

Figure 4.42: *Oxidation of the polycrystalline sample.*

Figure 4.41 and 4.42 predicts that no hydrogen evolution initiated until after 150 min. The decline of pH observed in the previous oxidation experiments is not that clear. The pH curve in Figure 4.41 is not smooth, the reason for this is unknown as the pH electrode was calibrated only minutes before the experiment. The pH curve in Figure 4.42 is a trend line of the original data which contained a lot of scatter. The reason for this was to little reference electrolyte in the pH electrode, but the measurements should be correct even though. The original data is given in Appendix D. In short, these figures do not resemble the oxidation curves of the slurries of JET1 at all. But it is emphasized that the slurries used in the oxidation experiments in section 4.2.1 contained large amount of powder with large surface area, while the single crystal sample and polycrystalline sample are grounded flat. This has an effect on the solubility of silica, and would therefore greatly impair the oxidation of the single crystal and polycrystalline sample. The total amount of hydrogen evolved is given in Table 4.13.

As given in Table 4.13, the oxidized single crystal evolved almost twice as much hydrogen as the polycrystalline sample. But if the oxidation time is taken in to consideration, the single crystal had only produced

Table 4.13: *Total hydrogen evolved from the oxidation of the samples prepared for nanoindentation. Temperature of 60 ℃ and approximately pH 9.8.*

Sample	Time (min)	Total hydrogen evolved (ml)
Single crystal	300	4898
Polycrystalline	240	2470

about 1540 ml of hydrogen after 240 minutes. This would imply that the polycrystalline sample is more oxidized than the single sample after 240 minutes. The Figures of hydrogen flow [ml/min] vs. time [min] are given in Appendix D.

The oxidized samples were examined in a Hitachi S-3400N Scanning Electron Microscope. The results are displayed in Figure 4.43

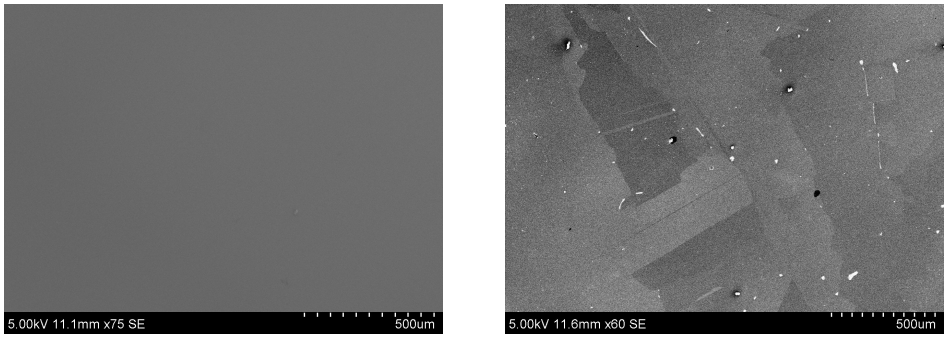

(a) **(b)**

Figure 4.43: *SEM studies of the samples after oxidation (a) Single crystal after oxidation, (b) Polycrystalline sample after oxidation.*

The single crystal sample in Figure 4.43a displays little of interest, no oxidation is observed. The Polycrystalline sample in Figure 4.43b displays no oxidation, but the grains are indicated as for the unoxidized sample in Figure 4.37c.

4.3.4 Nanoindentation

The surface of the different samples were mapped before indentation and after indentation, as displayed in Figure 4.44, 4.45 and 4.46.

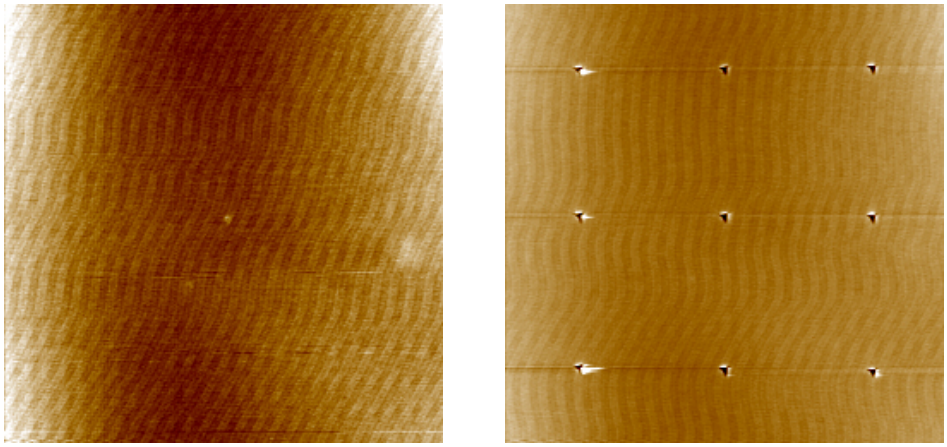

(a) **(b)**

Figure 4.44: *The surface of the unoxidized single crystal sample (a) Before indentation, (b) After indentation.*

For the unoxidized single crystal sample, Figure 4.44a, the surface is quite clean and no contamination of the surface is observed. The wave pattern is probably signal noise. A total number of 12 indents were made, Figure 4.44b.

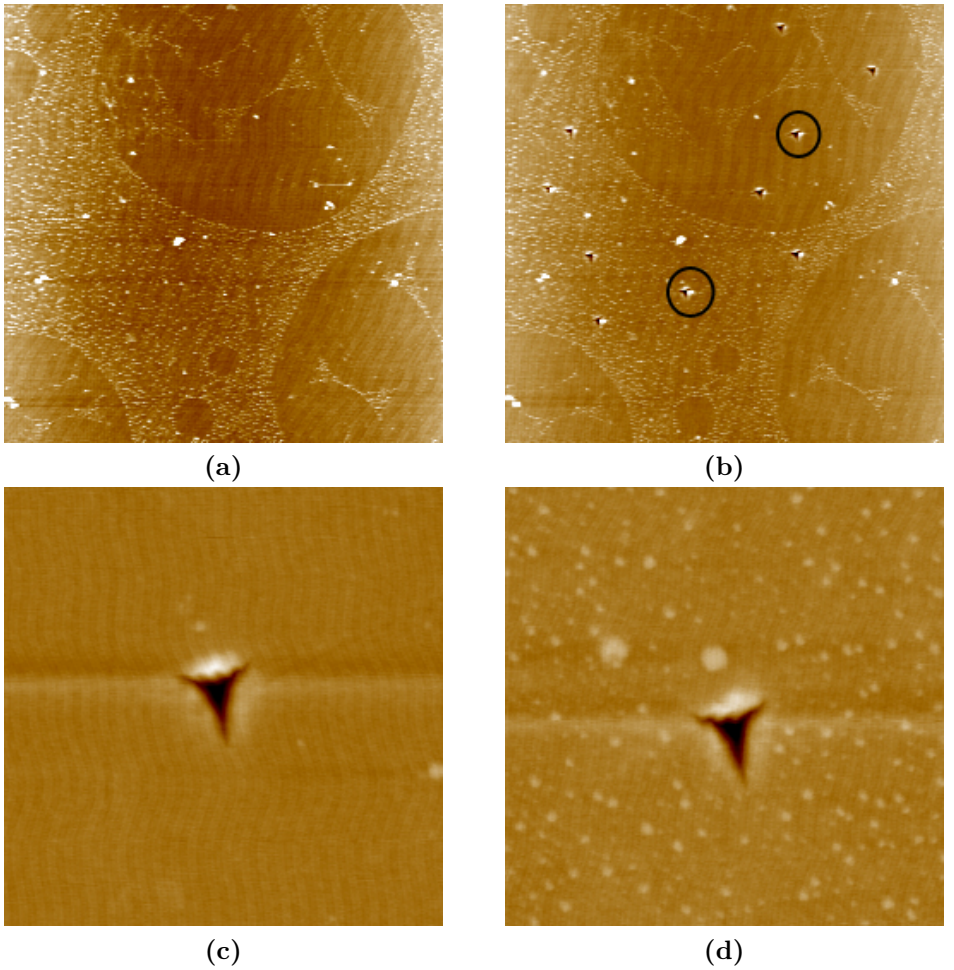

Figure 4.45: *The surface of the oxidized single crystal sample (a) Before indentation, (b) After indentation, c) Close-up of indent in area without oxides, d) Close-up of indent in area with oxides.*

For the oxidized single crystal sample, Figure 4.45a, a pattern of white particles is observed. These particles are believed to be oxide particles consisting of silica. The reason for the characteristic pattern is not known. A total number of 10 indents were made, Figure 4.45b. The black circles in Figure 4.45b indicate which indents the close-ups are from. A close-up of the indent in the area without oxides is displayed in Figure 4.45c and a close-up of the area with oxides is displayed in Figure 4.45d.

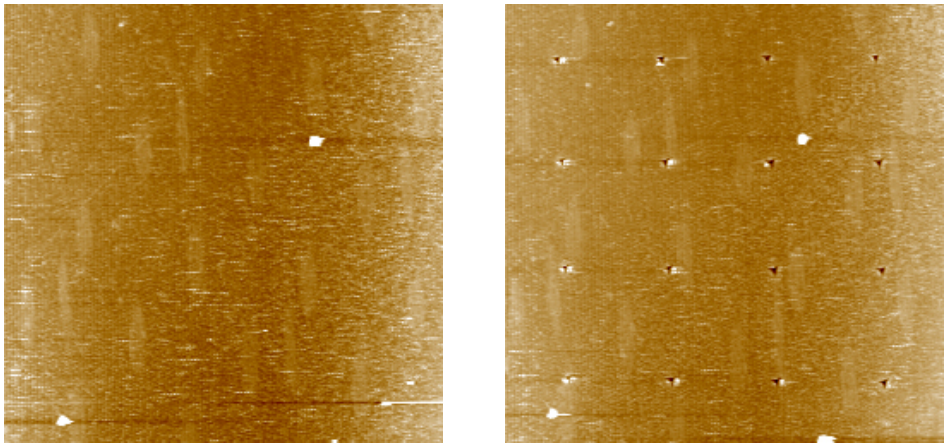

(a) (b)

Figure 4.46: *The surface of the oxidized polycrystalline sample (a) Before indentation, (b) After indentation.*

For the polycrystalline sample, Figure 4.46a, the same white particles as observed on the oxidized single crystal sample in Figure 4.45a is observed on the surface. There is no distinct pattern as compared to the oxidized single crystal sample in Figure 4.45a. A total number of 16 indents were made, Figure 4.46b. The force vs. displacement curve for the three different samples are shown in Figure 4.47, 4.48 and 4.49.

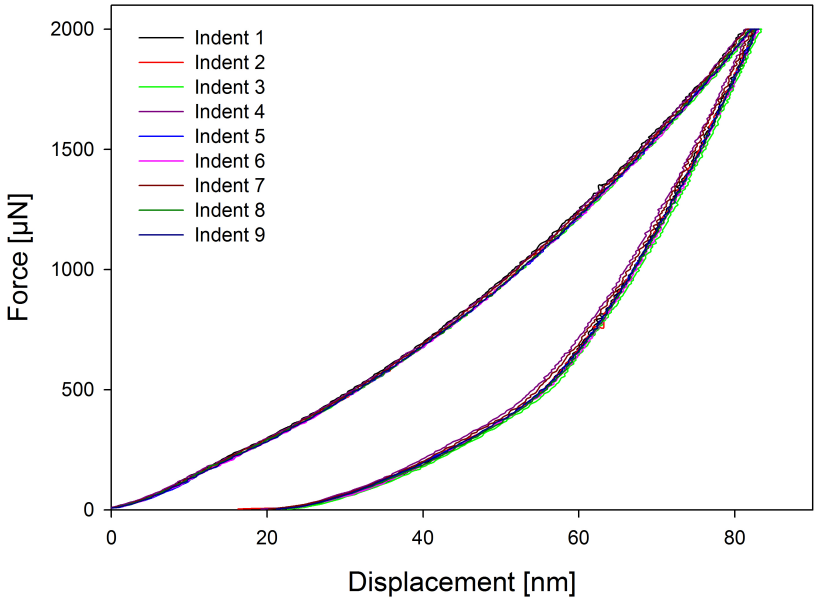

Figure 4.47: *Force vs. displacement curves obtained from the nanoindentation of unoxidized single crystal silicon.*

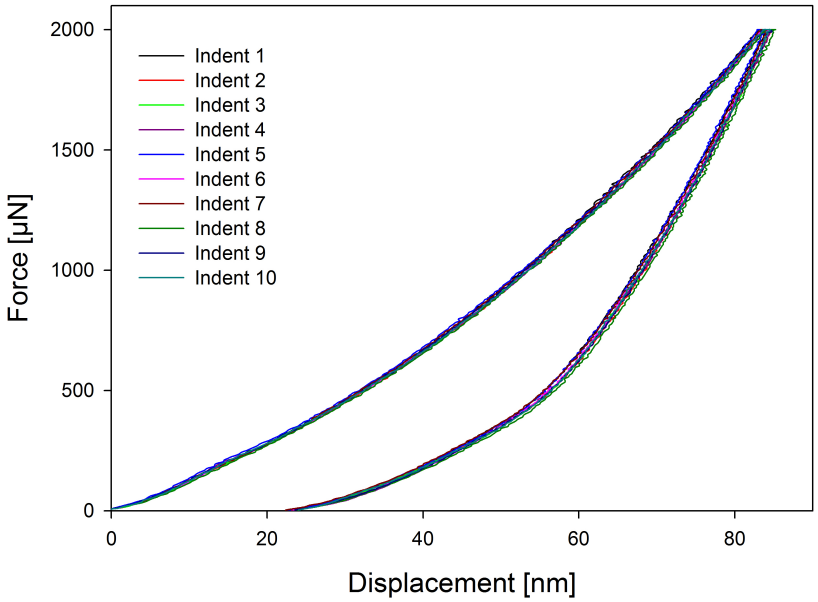

Figure 4.48: *Force vs. displacement curves obtained from the nanoindentation of oxidized single crystal silicon.*

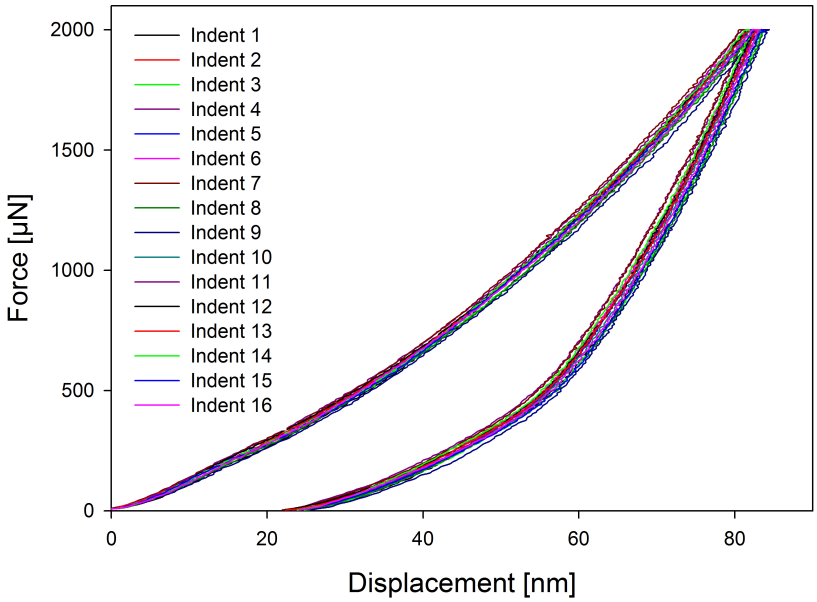

Figure 4.49: *Force vs. displacement curves obtained from the nanoindentation of oxidized polycrystalline silicon.*

Comparing the figures, the curves in Figure 4.47 for the unoxidized single crystal silicon sample seem to overlap, indicating a homogeneous material. The curves in Figure 4.48 are quite overlapping as well. Compared to Figure 4.47, the curves in Figure 4.48 are shifted to the right indicating that the material is more easily indented. The curves in Figure 4.49 are more scattered, indicating that material is not as homogeneous as the single crystal samples.

The average E-modulus and hardness values with standard deviation, obtained from the indentations of each sample are listed in Table 4.14. In Table 4.15, results from [25] is given for the sake of comparison.

The results in Table 4.14 indicates that the E-modulus of the unoxidized single crystal is 10 GPa higher than the E-modulus of the oxidized single crystal. It is also observed that the standard deviation of the oxidized single crystal is over three times as large as the standard deviation for the single crystal sample. The oxidized polycrystal has

Table 4.14: *E-modulus and hardness values for the different samples from the nanoindentation. The values are average values from multiple indentations performed, the standard deviation is stated in parenthesis.*

Sample	E-modulus (GPa)	Hardness (GPa)
Single crystal	175.6 (0.6)	13.0 (0.2)
Oxidized single crystal	165.3 (2.0)	12.7 (0.2)
Oxidized polycrystal	177.0 (1.6)	12.8 (0.3)

Table 4.15: *E-modulus and hardness values for single crystal silicon and fused silica, as given in [25]*

Sample	E-modulus (GPa)	Hardness (GPa)
Single crystal (100)	170	12
Fused silica	72	9

an E-modulus of about the same value as the unoxidized single crystal, but shows a standard deviation about three times larger compared to the unoxidized single crystal. The reason for the large standard deviation of the oxidized single crystal, is the fact that the indents were made in areas with oxides and without oxides, thus is the standard deviation large. The reason for the large standard deviation for the oxidized poly crystal, is that the material is not homogeneous. Comparing the results to values from the literature, Table 4.15, the unoxidized single crystal is 5 GPa higher and the oxidized crystal is 5 GPa lower than literature values. The poly crystal is about 7GPa higher than literature value.

The hardness values for the samples vary some, but if the standard deviation is taken in to account, the variation is not significant and the hardness is therefore about 13 GPa. The results obtained are roughly in order with values found in the literature, Table 4.15.

In short, there is little difference in hardness between the samples, but the E-modulus of the unoxidized and the oxidized single crystal are different by approximately 10 GPa. It is also observed that the single crystal samples seems to be a homogeneous material, resulting

in reproducible values, while there is more scatter in the values for the polycrystalline sample. The large standard deviation for the oxidized single crystal is influenced by the indentation being performed in areas free of oxides and areas with oxides.

Chapter 5

Discussion

In this chapter, the aim is to discuss the results obtained and hopefully give an explanation as to why these results are observed. The main areas discussed are the effect of oxidation on the JET1 silicon powder and the COARSE silicon particles, the challenges with the apparatus and the JET1 powder with respect to achieving reproducible results, the use of nanoindentation to discovered differences between unoxidized silicon and oxidized silicon, the effect of pH on the PSD measurements and how ultrasonification affects the PSD measurements.

5.1 Oxidation experiments - effect on the JET1 powder

In all of the oxidation experiments, a slurry made of water and JET1 powder was used. The slurry was separated after the experiments and the JET1 powder was dried in a furnace at 110 ℃. As this powder is the main contributor to the hydrogen evolution observed in the oxidation experiments, it is important to gain an understanding of how the powder has oxidized. The powder was analyzed by BET surface area and LECO in order to determine the surface area of the oxidized JET1 powder and the oxygen content. The aqueous solutions remaining from the separation of the powder was analyzed by colorimetry to determine amount of silicic acid, also known as dissolved silica, and

by HR ICP-MS to determine the total silica content. It is believed that it is the JET1 powder that has contributed to the silica content in the aqueous solutions, as the surface area of the COARSE particle is negligible compared to the powder. The glass-clear rods discovered after drying of the slurry from the test experiment, was examined with XRD.

The oxide thickness on the JET1 powder for each oxidation experiment was calculated and listed in Table 5.1. The formulas and assumptions needed for these calculations are given in Appendix B.

Table 5.1: *The calculated oxide thickness of the JET1 silica powders from the different oxidation experiments. The calculations are based on a dense oxide layer, in reality the oxide layer would be thicker due to not being a completely dense layer.*

Samples	**Oxide layer thickness** (nm)
10 min	31
30 min	36
40 min	25
60 min	21
90 min	37
90* min	50
120 min	54
240 min	52
Test experiment	31
Jet1 unoxidized	7

Comparing the results in Table 5.1 with the total hydrogen evolved, Table 4.7, the oxide layer thickness seems to have some dependency on the amount of hydrogen evolved.

The BET surface area measurements of the oxidized JET1 powders, 4.30, also indicates that the surface area has changed as the total hydrogen evolution increases. The results obtained could not be used for calculating the oxide layer. It is believed that the surface area results displays the surface area of the silica particles attached to the silicon

particle, rather than the surface area of the whole silicon particle with a silica layer. In short, the BET surface area results agrees with the assumption that the oxidation experiments have lead to the formation of silica on the JET1 silicon powder.

The SEM investigations of the JET1 powder reveals a difference between the unoxidized powder and the oxidized powder, as displayed in Figure 4.6 and 4.18. Any difference between the oxidized powders were not found, as is reasonable since the difference in oxide layer thickness is difficult to detect in the SEM. The important result is that the unoxidized powder consist of particles with smaller particles attached, while the oxidized powder seems to be covered by a "mud-like" layer which is most probably the oxide layer consisting of small silica particles. In short, the SEM investigations agrees with the assumption that the oxide experiments have lead to the formation of silica on the JET1 silicon powder.

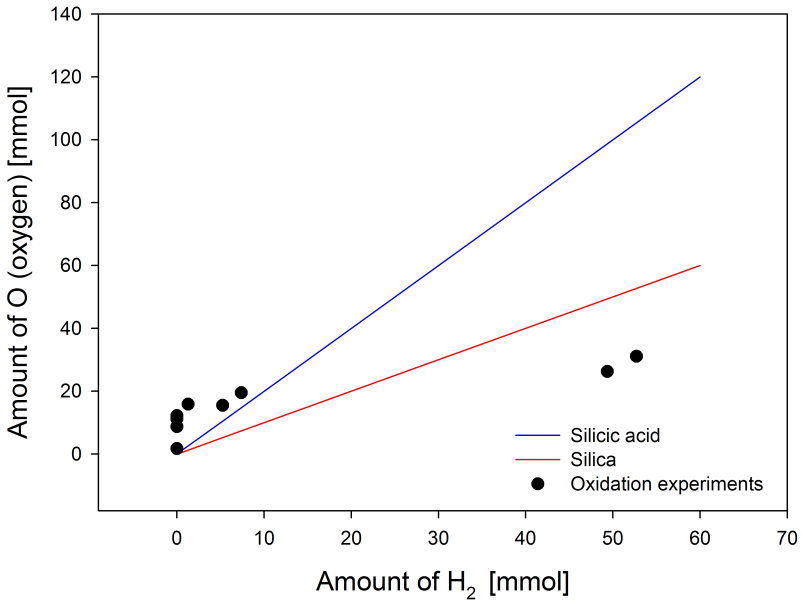

Figure 5.1: *Amount of oxygen (O) vs. amount of hydrogen (H_2) evolved, theoretically and for the experimental results.*

$$Si(s) + 4H_2O(l) = Si(OH)_4(aq) + 2H_2(g) \tag{5.1}$$

$$Si(s) + 2H_2O(l) = SiO_2(s) + 2H_2(g) \tag{5.2}$$

In Figure 5.1 trend lines for the amount of oxygen (O) vs. hydrogen (H_2) for the reactions resulting in silicic acid, Equation 5.1, and the reaction resulting in silica, Equation 5.2, is plotted. The experimental values are plotted, using the amount of total hydrogen evolved and the oxygen content which is the sum of the LECO results and the HR ICP-MS results. It was expected that the experiments with little or no hydrogen evolution at all would lie close to the line of the silicic acid reaction, indicating that the formation of silicic acid is the dominating reaction early in the oxidation. The experimental results supports this, but the amount of oxygen is to high compared to the amount of hydrogen. This is believed to be caused by problems with measuring the hydrogen evolved for experiments evolving little hydrogen and only being run for a small amount of time. As the hydrogen evolved increases, it was expected that experimental results would lie closer to the silica reaction line. This is liable since the silicic acid reaches a solubility limit and thus would the formation of silica through condensation be the dominating reaction. The experimental results lie close to the silica line, indicating a shift in the reactions dominating. The results should have been closer, preferably between the silicic acid line and the silica line. Why the experimental results do not lie between the lines, is not known and any explanations are not found. But it is a fact that the amount of oxygen is too high compared to hydrogen evolved for the experiments evolving little hydrogen, and the amount of oxygen is to low when large amounts of hydrogen is evolved. This could arise from problems with measuring the oxygen and hydrogen amount, but it could also be effects and reactions which cannot be explained by the data collected.

In short, it seems like the formation of silicic acid is the dominating reaction when little hydrogen has evolved, and that the formation of silica is the dominating reaction when much hydrogen has evolved. In reality, it means that silicic acid is formed early in the oxidation until the solubility limit is reached, then colloidal silica is formed due to condensation of silicic acid. The latter is displayed in Figure 2.6.

In order to break the information further down, it is useful to display

how the oxygen content varies with total hydrogen evolved, but emphasizing where the oxygen comes from. Oxygen is present as silica attached to the silicon particles, as silicic acid and colloidal silica dispersed in the aqueous solutions. The oxygen present on the particles was determined by LECO, the silicic acid was determined by colorimetry and the colloidal silica was determined by subtracting the amount of silicic acid from total silica content determined by HR ICP-MS. This is displayed in Figure 5.2.

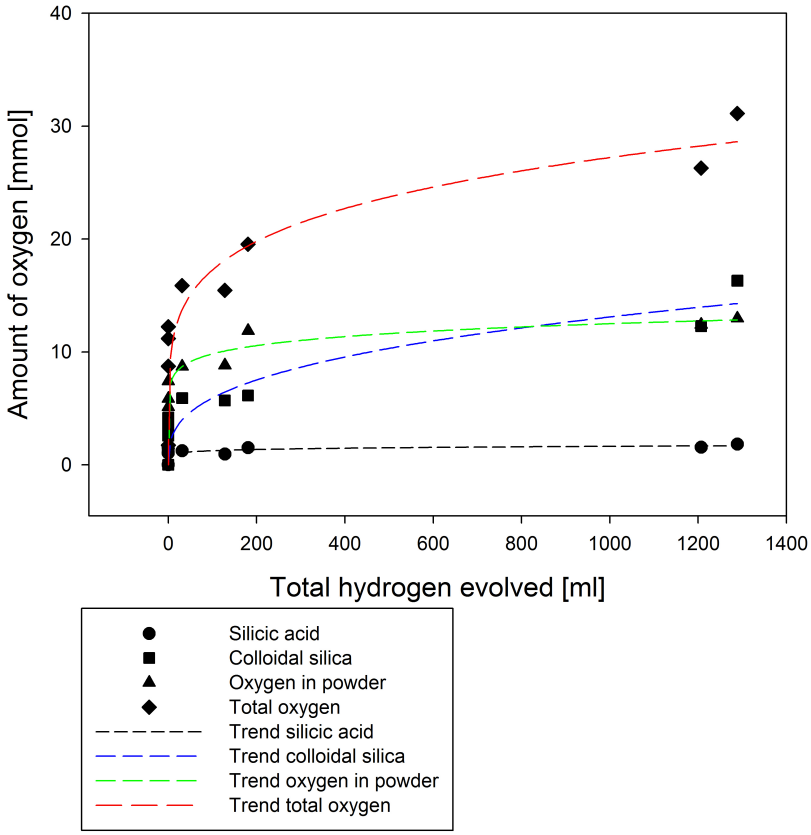

Figure 5.2: *Amount of oxygen vs. total hydrogen evolved, with regards to silicic acid, colloidal silica and oxygen content in the JET1 powder.*

The results indicate that the amount of silicic acid is quite stable regardless of how much hydrogen is evolved, indicating that the solubility limit of silicic acid is reached early in the oxidation experiments. The

small variations can be explained by the variation in pH of the aqueous solutions, as pH is parameter controlling the solubility of silicic acid. When silicic acid has reached its solubility limit, this leads to the condensation of silicic acid in to colloidal silica, which has a steady increase as the hydrogen evolution increases. The oxygen attached to the silicon powder has an increase early on, but seems to decline. This may be due to the surface of the silicon being covered by several layers of adsorbed silica, preventing the adsorption of more silica. It is though important to emphasize that too few experiments have been performed to conclude this, but the results predict a stabilization of the oxygen attached to the silicon powder. The total oxygen content, which is the sum of the silicic acid, colloidal silica and the oxygen attached to the silicon powder displays an increase for all of the experiments, the main contributor seems to be the colloidal silica.

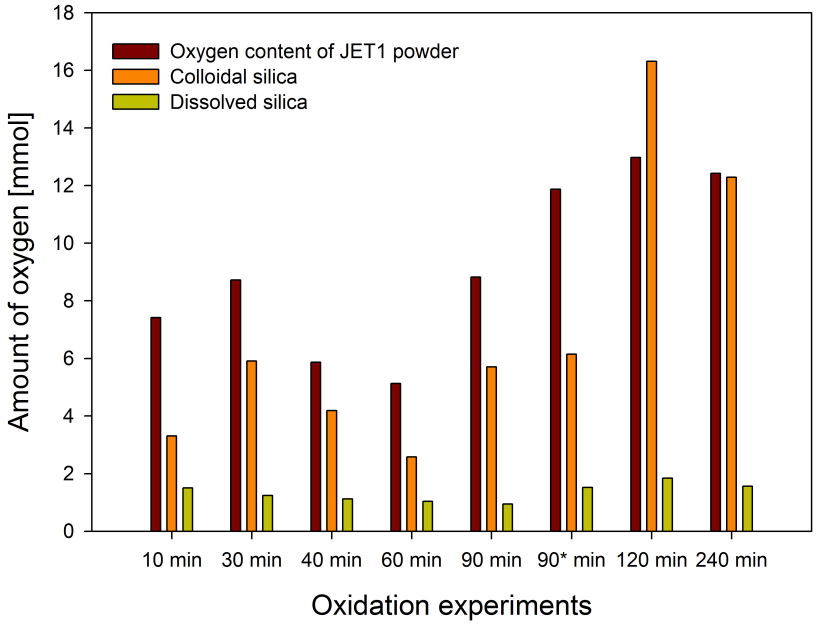

Figure 5.3: *Oxygen content of the JET1 powders from each of the oxidation experiments, divided in to the contributions from oxygen attached to the silicon powder, colloidal silica and the silicic acid.*

Displaying how the oxygen content varies for each of the oxidation experiment samples is also of use, but it is important to remember

that oxidation time is not equivalent with hydrogen evolved, as there are some unexplained issues regarding both the reproducibility of the JET1 silicon powder and the apparatus. The oxygen content of each sample, divided in to the contribution from the oxygen attached to the silicon powder, colloidal silica and silicic acid is displayed in Figure 5.3.

The contribution of oxygen from the silicic acid seems to be rather constant for all of the experiments, indicating that the solubility limit of silica is reached. The colloidal silica varies for all of the experiments, and for the 120 minutes experiment which evolved the most hydrogen, it is the main contributor of oxygen. This is in agreement with theory, as the silicic acid has reached its solubility, a condensation occurs and colloidal silica is formed. The oxygen content of the JET1 powder measured with LECO seems to vary between the experiments, but the increase is rather limited for the 90* min , 120 min and 240 min experiments. This is in agreement with the results in Figure 5.2, indicating that the increase in oxygen content of the powder seems to decline as much hydrogen is evolved.

As mentioned earlier, the glass-clear rods discovered after drying of the silicon slurry from the test experiment were examined by XRD. It was assumed that this was amorphous silica originating from colloidal silica condensed from silicic acid, as the drying of the slurry would lead to precipitation of silica due to decreasing solubility. The XRD examination indicates that these rods were in fact amorphous silica in the form of cristobalite. This supports the results indicating that the aqueous solutions from the separation of the slurries contain colloidal silica and silicic acid.

To summarize, the results indicate that the solubility limit of silicic acid is reached for all of the experiments. This leads to the silicic acid condensing to form colloidal silica. The colloidal silica is first condensed on the silicon particles where it adsorbs to the surface. Continued oxidation will lead to the formation of dispersed colloidal silicon in the suspension, as the silicon surface is fully covered with adsorbed silica. Colloidal silica adsorbed may also detach from the silicon surface and be dispersed in the suspension. The assumption that the oxidation experiments have lead to formation of silica particles on the JET1 silicon

powder surface is also supported by the SEM and the BET surface area analysis. The XRD results supports that silica is present in the aqueous suspensions and is precipitated upon drying as amorphous silica.

A step-by-step explanation of how silicon is oxidized in aqueous media is displayed in Figure 5.4, based on the results obtained from the experimental work combined with theory.

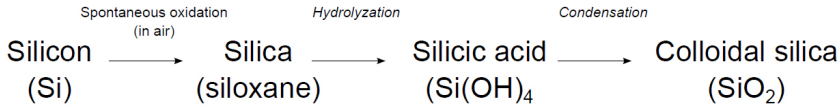

Figure 5.4: *Oxidation of silicon in aqueous media, step-by-step.*

5.2 Oxidation experiments - effect on the COARSE particles

The COARSE particles were oxidized in both the test experiment and the main experiments. The oxidation of the COARSE particles was documented thorough SEM and EDS analysis. For the experiments that did not evolve any hydrogen, no oxide layer was observed on the particle using SEM and EDS to examine the surface. This includes the 10, 20, 30 and 40 minutes COARSE particles from the test experiment, and the 10, 40 and 60 minutes COARSE particles from the main experiment. The EDS analysis of the particles indicated no difference in oxygen content across the particle surface.

For the experiments that evolved hydrogen, an increase in the oxide layer on the COARSE particles is observed as oxidation time increases. It is difficult to divide between the 30, 90 and 120 minutes COARSE particles with respect to which is the most covered with an oxide layer, but the important observation is that the 240 minutes particles seems to be completely covered. Initially it was an important aim to identify the initiation points for oxidation, this proved more difficult than anticipated, and no results exists. A study of initiation points for oxidation would have to imply methods with a high resolution like Atomic

Force Microscopy or Auger Electron Spectroscopy, and the oxidation of the particles would have to be more controllable.

Initiation time for oxidation of the COARSE particles is somewhat complex, as the 30 minutes experiment resulted in an oxidized particle, while the 40 and 60 minutes particle had no oxide layer. The results indicate that the oxidation of the COARSE particles is determined by the oxidation of the JET1 powder, as no oxide layer is seen on COARSE particles when no hydrogen was evolved. It would then be reasonable that the oxide layer would be covering more and more of the particle as the total hydrogen evolved increased. This would imply that the 120 minutes particle should be the most covered particle, but in fact it is the 240 minutes particle that is completely covered. The oxidation time therefore seems to be an important parameter with respect to coverage of the particle with silica. This would indicate that the oxide layer on the COARSE particles is in fact adsorbed colloidal silica, condensed from silicic acid, as explained in the previous section. If no hydrogen is evolved, then little colloidal silica is formed. When hydrogen evolves, the amount of colloidal silica increases and adsorbs to the COARSE particle surface. The amount of adsorption seems to be dependent on oxidation time.

In short, the oxidation of the COARSE particles rely on hydrogen evolution from the JET1 powder in order to display any oxide layer. If no hydrogen has evolved, then there is no visible oxide layer on the COARSE particles. The coverage of the COARSE particle of oxide seems to be dependent on the oxidation time, not the total amount of hydrogen evolved. Thus is the oxidation of the COARSE particles dependent on hydrogen evolution for colloidal silica to be condensed from silicic acid and adsorb on the surface. The growth of the oxide seems to be controlled by the oxidation time, in other words it is the adsorption of colloidal silica which is dependent on the oxidation time.

5.3 Apparatus and JET1 challenges

For the 10, 40 and 60 minutes oxidation experiments a change in BET surface area and oxygen content is displayed, although no hydrogen has

evolved. The 30 minutes oxidation experiment evolved hydrogen even though it was not predicted, as most of the times hydrogen evolution initiated after 50 minutes. It is important to separate these problems in to JET1 powder problems and apparatus problems.

The JET1 powder has proven to be quite unstable resulting in non-reproducible results. Experiments performed within a limited time frame like one day seems to be reproducible within that day. Experiments performed weeks apart with equal parameters with regards to temperature and pH produced totally different results. Powder that was kept in a desiccator for about two weeks evolved more hydrogen and the evolution initiated earlier than previous experiments. Especially the two experiments performed right after the powder was removed from the desiccator, the 30 and 120 minutes experiments, reacted very different from previous experiments. The 240 minutes experiment was performed the next day, the powder was kept in the desiccator overnight. The experiment initiated hydrogen evolution much later than the day before and evolved about 100 ml less of hydrogen than the 120 minutes experiments despite being the performed for twice the time. Figure 4.17 displays this in a good manner, as the 30 and 120 minutes experiments initiate at approximately the same time and with a similar slope with regards to hydrogen evolved. The 240 minutes experiment initiates evolution later and with a much smaller slope, but still earlier initiation and larger slope than the 90 and 90* min experiments.

It is clear that the powder is affected by storage, but the parameters controlling this is unknown. Air humidity seems to be an important factor as the powder gradually initiated hydrogen later and evolved less hydrogen as the winter months passed. A desiccator "restored" the powders ability to produce hydrogen and decreased the initiation time.

The investigation of what parameters that affects the powder "performance" was never a part of this research, but has had a great influence. A more fundamental study of it will performed later by the person continuing this work.

As mentioned earlier, the results might also be affected by problems with the apparatus. The experiments most in question are the 10, 40 and 60 minutes, since the BET surface area analysis, LECO analysis,

colorimetry and HR ICP-MS indicates that the powder has been altered, but no hydrogen evolution is measured. No single reason for this has been discovered, but there are several suggestions. One suggestion is that the hydrogen evolved in the slurry is not released until the slurry is saturated with hydrogen. Another one is that the apparatus needs to be "filled" before the hydrogen is detected. A third is that the hydrogen evolved is such a small amount that it is below the detection limits for the flow meters. All of the experiments have a very rapid flow of hydrogen when it initiates, as displayed in the hydrogen flow vs. oxidation time figures in D. This could indicate that the hydrogen gas is accumulated and then suddenly released, supporting the suggestion of filling of the apparatus of saturation of the slurry. This would indicate that experiments has to be run for a certain amount of time to be reliable with respect to total hydrogen evolved. Nonetheless, further studies are needed, and no single reason can be pointed out.

5.4 Mechanical properties of oxidized silicon

The mechanical properties of unoxidized silicon and oxidized silicon were examined with nanoindentation. The pictures of the surface, rendered by allowing the tip to scan the surface, revealed that the oxidized silicon was covered with small white oxide particles in the size range of 60-120 nm. The nanoindentation therefore gave valuable information about the samples which were not discovered in the SEM. It is emphasized that the oxide particles were too small to be indented for themselves, but seems to have contributed to the results.

The nanoindentation resulted in the E-modulus and hardness values for each of the samples. The E-modulus of the unoxidized single crystal was about 10 GPa higher than the oxidized single crystal. Taking the standard deviation in to account, the oxidized single crystal has a larger variation than the unoxidized single crystal. This is caused by the fact that the indentations of the oxidized single crystal were performed in areas with and without oxides. The decline in E-modulus of the oxidized single crystal is expected since the E-modulus of sil-

ica is considerably lower than the E-modulus of silicon. The hardness values are though not that different, especially when taking the standard deviation in to account. It can be argued that the hardness is calculated from the maximum load applied, hence neglecting the contribution from the oxides and being more influenced by the substrate, while the E-modulus is based on values continually measured during the indentation, thereby making it more sensitive to variations on the surface.

The oxidized polycrystalline sample displayed a similar E-modulus as for the unoxidized single crystal, with a larger standard deviation. As this sample was more or less covered by oxide particles, this indicates that the sample is not homogeneous. The hardness was within the range of the unoxidized and oxidized single crystal. Drawing any conclusions about why the E-modulus was in fact higher than the unoxidized single crystal is difficult. There are several unknown parameters, especially since no unoxidized polycrystalline sample was tested. The most important factors are though that the orientation of the polycrystalline sample was different from the single crystal and that the sample contains more impurities than the single crystal.

In short, nanoindentation of single crystals can give valuable information on the mechanical properties of oxidized silicon and the surface topography. A clear difference in the E-modulus is achieved, hardness values are not that affected. The oxidation time should be increased to obtain more oxides, and preferably particles large enough to be indented themselves. The results for the polycrystalline sample is harder to interpret, and a good explanation of the results cannot be given.

5.5 The effect of pH on PSD measurements

The effect of pH on the PSD measurements was investigated. From theory, it is a well known fact that pH affects the zeta-potential of particles, which is key factor for electrostatic stabilization. The PSD measurements are displayed in Figure 4.2. The measurements also included using Darvan C-N and Polyethyleneimine to disperse the suspensions,

these are dispersing agents which contributes to electrostatic stabilization. It was expected that the Darvan C-N and the polyethyleneimine would give the best dispersion of the suspensions, in short have the highest amount of small particles and less of the large particles. Upon examining the results in Figure 4.2 and Table 4.4, the distilled water with pH 7.3 seems to be the best dispersant on the basis of having the smallest d (0.1), d (0.5) and d (0.9). The electrosteric stabilization of Darvan C-N and polyethyleneimine does not seem to have a big effect, but the pH seems to have a large influence thus yielding electrostatic stabilization as the dominating effect. Thus is it the pH of the Darvan C-N and polyethyleneimine that yields the stabilization of the suspensions they are a part of. In Figure 2.9 the zeta-potential vs. pH for silicon is displayed.

Figure 2.9 indicates an increase of the negative zeta-potential as the pH is increased from a value of 1. The maximum negative zeta-potential of about -75 mV is at about pH 10.5, further increase of the pH decreases the negative zeta-potential making the slurry more unstable. Comparing Figure 4.2 with Figure 2.9, the same trend is observed. The decrease of d (0.5) as a function of pH resembles the increase in negative zeta-potential as function of pH until pH 10.5, with an increase in d (0.5) and decrease in negative zeta-potential at pH 11.5. The distilled water with pH 7.3 does not fit in, as it yields a much smaller d (0.5) than the slurry with pH 10.5, which should be a much more stable slurry. Any good reason for the distilled water yielding the best dispersion is not known. As mentioned earlier, results displaying separate minima of the zeta-potential at pH 4 and 8 have been published. Thus may the good performance of the distilled water come from different surface states of the silicon when dispersed in distilled water versus water with altered pH. The increase in d (0.5) for pH 11.5 is due to the fact that there is to many charged ions in the water. The electrolyte strength therefore shields the charge effect of the particles, in effect leading to agglomeration of the slurry [18].

In short, electrostatic stabilization seems to be the dominating effect, why the distilled water yields the best dispersion of the suspension is unknown. It may arise from different surface states of the silicon powder.

5.6 The effect of ultrasonification on PSD measurements

The effect of various amount of ultrasonification and use of Darvan C-N on the PSD measurements for the JET1 powder was investigated. This was done in order to determine whether or not the use of ultrasonification could break not only the agglomerates, but the silicon particles as well. The PSD measurements are displayed in Figure 4.5 and 4.4. The use of ultrasound to break agglomerates is a well known procedure, but it also increases the chance of generating new agglomerates. This is because when applying ultrasound to a solution, there are two competing processes. One process is the breaking-up of agglomerates, the other one is the formation of new agglomerates because of the kinetic energy added to the particles by the ultrasound [26]. Too long use of ultrasound will in fact introduce more agglomerates rather than remove them, as described in [26].

The measurements without Darvan C-N are displayed in Figure 4.4. The effect seen on the 0 min and 1 min with respect to the increase in large particles is due to agglomeration introduced by the ultrasound. Applying ultrasound for 2 min removed the agglomerates created. The most important result is that after 10 minutes of ultrasound, the distribution is widest compared to the other measurements. This implies that agglomerates have been broken and therefore the distribution has increased with respect to small particles, but it also implies that new agglomerates have been formed since it contains larger particles than the measurements between 2 and 7 minutes. The 10 minutes measurement is therefore a very good example off the two competing processes introduced by the use of ultrasound.

The measurements with Darvan C-N are displayed in 4.5. Of all the measurements, the 10 min measurement is the widest distribution, as for the measurements without Darvan C-N. The formation of agglomerates indicates that the Darvan C-N is not suitable for keeping new agglomerates from being introduced by the ultrasound. The build-up of smaller particles, between 1 to 10 μm, indicates that the Darvan C-N keeps the small particles formed by breaking agglomerates from agglomerating again. The use of Darvan C-N therefore yields a bi-

modal distribution, keeping smaller particles from agglomerating but being unable to prevent the larger particles from agglomerating.

In short will the use of ultrasound deagglomerate a suspension, but prolonged use will introduce more larger agglomerates as well as smaller particles, ultimately resulting in a distribution with larger particles than before applying ultrasound. The use of Darvan C-N is not able to prevent the agglomeration of larger particles, but keeps smaller particles that was formed breaking agglomerates from agglomerating again, and therefore introduces a bimodal distribution. The results obtained are in good agreement with [18] and [26].

Chapter 6

Conclusions

This chapter is devoted to summarize and conclude the results.

The analysis of the oxidized JET1 powder revealed that the powder was covered with an oxide layer, thought to be silica. Combining the information from the powder analysis with the analysis of the aqueous solutions separated from the slurry revealed several results. The content of silicic acid, also known as dissolved silica, seemed to be constant with respect to both total hydrogen evolved and oxidation time. This implies that the solubility limit is reached quite early in the experiments. The solubility of silicic acid is dependent on the pH, as increasing pH gives an increase in solubility. The amount of oxygen in the JET1 powder increases as the total hydrogen evolved increases, but seems to decline as more of the powder is covered with silica condensed from silicic acid. This may be related to problems with adsorbing more layers of colloidal silica. As the oxidation continues the silicic acid will condense to form dispersed colloidal silica in the suspension.

The oxidation of the COARSE particles resulted in an increase of the oxide layer as a function of oxidation time. It was discovered that initiation of oxide formation was dependent on hydrogen evolution from the JET1 powder, but the extent of the oxide coverage was dependent on oxidation time. This is due to the fact that the oxide layer is adsorbed colloidal silica. Thus is hydrogen evolution needed for the colloidal silica to be formed and adsorbed, and the amount of adsorbed silica on the surface is dependent on the oxidation time. Initiation points

for the oxide formation was not found, to obtain this a more controlled oxidation and high resolution examining techniques like Atomic Force Microscopy and Auger Electron Spectroscopy is needed.

The use of nanoindentation to examine oxidized silicon proved useful, as there was a definite variation in E-modulus of the oxidized and unoxidized single crystal samples. The hardness did not vary significantly. Both E-modulus and hardness of the oxidized polycrystalline sample was comparable with the unoxidized single crystal sample. Nanoindentation together with EBSD is capable of providing information about the mechanical properties of polycrystalline samples, but there are many unknown parameters that can affect the result.

There were some difficulties gaining dependable results, these were caused by the fact that the JET1 powder was very sensitive to storage conditions and that the apparatus did not give reliable results for total hydrogen evolved for short oxidation experiments. These problems yielded that the determination of initiation time for oxidation was not possible.

The PSD measurements performed on the 2-10 powder with various pH, were in good agreement with the zeta potential curve in Figure 2.9. This indicated that a higher pH dispersed the powder better, yielding a smaller particle size, but too high pH yielded a larger particle size. Why distilled water with pH 7.4 yielded the smallest particle size is unknown, but literature [16] suggest that different surface states of the silicon powder can yield zeta potential minima at pH 4 and 8.

The effect of ultrasonification on PSD measurements was in good agreement with theory [26]. The results indicated that there are two competing processes, deagglomeration and agglomeration. The use of Darvan C-N indicated that the small particles are prevented from agglomerating once they have been deagglomerated, but it cannot prevent larger particles from agglomerating; yielding a bimodal size distribution as the ultrasonification time is increased.

Chapter 7

Further work

Regarding further work, there are several paths to choose. The most important subject is to investigate how silicon powder is affected by storage. The JET1 powder used did not give reproducible results if the experiments were performed more than a week a part. Thus is a more thorough investigation of how the powder is affected by storage of great importance, in order to get reliable results if more oxidation studies should be conducted. The investigation of what affects the powder during storage is going to be a part of the project thesis for Anne Marthe Nymark, student at NTNU. Studies of the oxide layer on silicon powder using relevant techniques will probably be the area of focus.

As mentioned in the discussion, the apparatus used for oxidation of the slurries and the COARSE particles does not always give results that are reliable. This is especially pronounced when performing short oxidation experiments. It has been suggested that the apparatus may need to be "filled" before the hydrogen evolution is measurable, or that the slurry needs to be saturated with hydrogen before hydrogen can evolve freely. If the apparatus is to be used further on, and especially with short oxidation experiments, less than 60 minutes for JET1, a more detailed study is needed. Any solutions to the problem is not easy to present, but a good start would be to minimize the volume of the flask in which the slurry is oxidized, and the length of pipe before the evolved hydrogen enters the flow meters.

Nanoindentation seems to be a very interesting technique for studying the effect of oxidizing silicon. It would probably be an advantage to focus on single crystal samples to gain knowledge. Later, polycrystalline samples could also be studied, using EBSD to map the crystallographic directions of the different grains prior to nanoindentation. Longer duration of the oxidations would be needed, if hoping to achieve oxide particles large enough to be indented for themselves.

It was a primary objective to determine the initiation point for oxidation on the COARSE silicon particles, in order to achieve this a more controlled oxidation process is needed. The studies of the oxidized particles would probably need to utilize high resolution techniques like Atomic Force Microscopy and Auger Electron Spectroscopy.

Bibliography

[1] Rune Nilsen. Silicon for Si_3Ni_4 bonded sic materials. Technical report, NTNU, 2009.

[2] Haakon Trygve Stroem Joergensen. Silicon for ceramic applications. Technical report, NTNU, 2010.

[3] G. F. Cerofolini and L. Meda. Chemistry at silicon crystalline surfaces. *Applied Surface Science*, 89(4):351–360, 1995.

[4] Harry M. Rong. *Silicon for the direct process to methylchlorosilanes*. PhD thesis, 1992.

[5] Vincent A. Hackley, Ungyu Paik, Bong-Ho Kim, and Subhas G. Malghan. Aqueous processing of sintered reaction-bonded silicon nitride: I, dispersion properties of silicon powder. *Journal of the American Ceramic Society*, 80(7):1781–1788, 1997.

[6] Jordan J Bard AJ, Parsons R and IUPAC. *Standard Potentials in Aqueous Solution*. Marcel Dekker, 1985.

[7] Tina Overton Peter Atkins. *Shriver and Atkins Inorganic Chemistry*. 5 edition, 2009.

[8] R. G. Stephen and F. L. Riley. Oxidation of silicon by water. *Journal of the European Ceramic Society*, 5(4):219–222, 1989.

[9] R. Dillinger, J. Heinrich, and J. Huber. Slip-cast hot isostatically pressed silicon nitride gas turbine components. *Materials Science and Engineering: A*, 109:373–378, 1989.

[10] Qiguo Zhang, Wei Li, Mingyuan Gu, and Yanping Jin. Dispersion and rheological properties of concentrated silicon aqueous suspension. *Powder Technology*, 161(2):130–134, 2006.

[11] Ralph K. Iler. *Solubility, Polymerization, Colloid and Surface Properties and Biochemistry*. John Wiley and Sons, 1979.

[12] E Papirer. *Adsorption on silica surfaces*, volume 90 of *Surfactant science series*. Marcel Dekker, 2000.

[13] Mari-Ann Einarsrud. Personal communication, 2010.

[14] M. N. Rahaman. *Ceramic processing and sintering*. Marcel Dekker, 1995.

[15] Qiguo Zhang and Mingyuan Gu. Rheological properties and gelcasting of concentrated aqueous silicon suspension. *Materials Science and Engineering: A*, 399(1-2):351–357, 2005.

[16] R. Ramachandra Rao, H. N. Roopa, and T. S. Kannan. The characterisation of aqueous silicon slips. *Journal of the European Ceramic Society*, 19(16):2763–2771, 1999.

[17] Rune Nilsen. Silisium for Si_3Ni_4 -bundet sic materialer. Technical report, NTNU, 2008.

[18] David W. Richerson. *Modern ceramic engineering*. Taylor and Francis, third edition, 2006.

[19] R. T. Vanderbilt company. Darvan dispersing agents, 2010. *http://www.rtvanderbilt.com/wwwprd/DARVAN_Dispersing_Agents_TDS_Web.pdf*, 12.14.2010.

[20] Jianying He. Introduction to nanoindentation, 2011.

[21] G.M. Pharr W.C. Oliver. An improved technique for determining hardness and elastic modulus using load and displacement sensing indentation experiments. *Journal of Materials Research*, 7(6):1564–1583, 1992.

[22] Johan P. Svanem. Personal communication, 2010.

[23] Stephen Brunauer, P. H. Emmett, and Edward Teller. Adsorption of gases in multimolecular layers. *J. Am. Chem. Soc.*, 60:309–19, 1938. CAN 32:29289 General and Physical Chemistry.

[24] Jarle Hjelen. *Scanning elektron-mikroskopi*. Compendium. 1989.

[25] Kirsten Ingolf Schiffmann. Determination of fracture toughness of bulk materials and thin films by nanoindentation: comparison of different models. *Philosophical Magazine*, 91(7):1163 – 1178, 2011.

[26] Terry A. Ring. *Fundamentals of Ceramic Powder Processing and Synthesis*. 1996.

[27] Gordon Aylward and Tristan Findlay. *SI Chemical Data, 5th edition*. John Wiley and Sons, 2002.

Appendix A

Particle size calculations

In this section, the formulas and assumptions used to calculate the average diameter of particles, based on the BET surface area results are given. Assuming spherical particles, the radii of the particles can be estimated through the following formulas:

$$S_0 = \frac{m^2}{g} = \frac{4\pi r^2}{g} \tag{A.1}$$

and

$$\rho = \frac{g}{cm^3} = \frac{3g}{4\pi r^3} \tag{A.2}$$

S_0 is the specific surface area given in m^2/g, r is the particle radius, g is the mass and ρ is the crystallographic density.

Combining equation A.1 and equation A.2 gives the following relationship:

$$r = \frac{3}{\rho S_0} \tag{A.3}$$

or given in diameter:

$$D = \frac{6}{\rho S_0} \tag{A.4}$$

The diameter D is given in μm. The crystallographic density for silicon is 2.3 g/cm^3 and silica is 2.6 g/cm^3 [27]. These values were used in calculating the diameters in respectively table 4.2 and 4.8.

The equations and derivations presented in this appendix are based on Appendix B of Rune Nilsens master thesis [1].

Appendix B

Oxide layer thickness calculations

In this section, the formulas and assumptions used to calculate the oxide thickness on the JET1 particles are given. It is assumed that the oxide layer is completely dense and that all of the oxygen is present as silica. Using the oxygen content determined by LECO and the density of silica, the volume of the oxide was calculated using Equation B.1. Using the volume of the oxide and the surface area of the unoxidized JET1 powder, the thickness of the oxide layer was calculated using Equation B.2.

$$V_o = \frac{f_o}{\rho_o} \tag{B.1}$$

V_o is the volume of the oxide, f_o is the weight fraction of the oxide and ρ_o is the density of the silica with the denomination $\frac{cm^3}{g}$.

$$L_o = \frac{V_o}{S_0} \tag{B.2}$$

L_o is the thickness of the oxide given in m and S_0 is the surface area of the unoxidized JET1 powder given in m^2/g. The oxygen content of the oxidized JET1 powders are listed in Table 4.9 and the surface area of the unoxidized JET1 powder is listed in Table 4.2. The real

thickness of the oxide layer would be larger, as the oxide layer is not dense as assumed in the calculations.

Appendix C

BET surface area plot

In this section, the BET surface area plot for every sample measured is displayed.

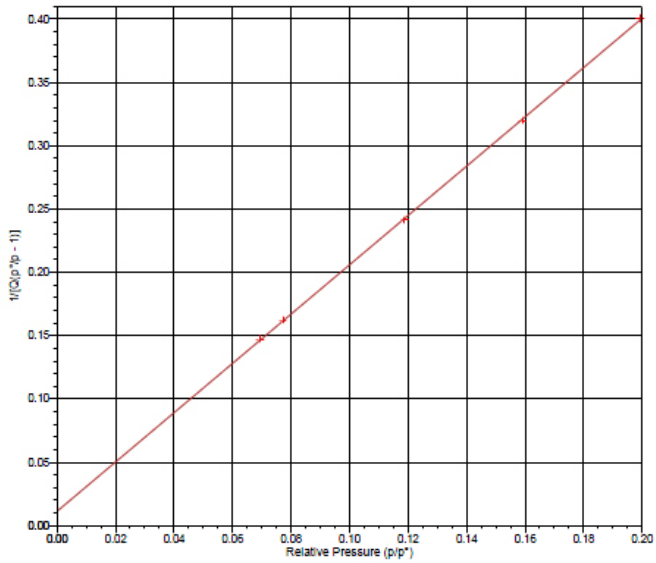

Figure C.1: *BET surface area plot for JET1 silicon powder unoxidized. Degas temperature of 150 ℃.*

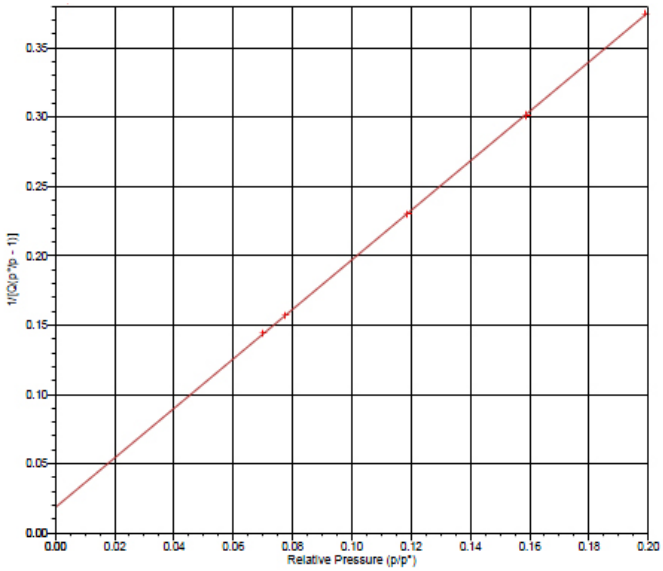

Figure C.2: *BET surface area plot for 2-10 silicon powder unoxidized. Degas temperature of 150 ℃.*

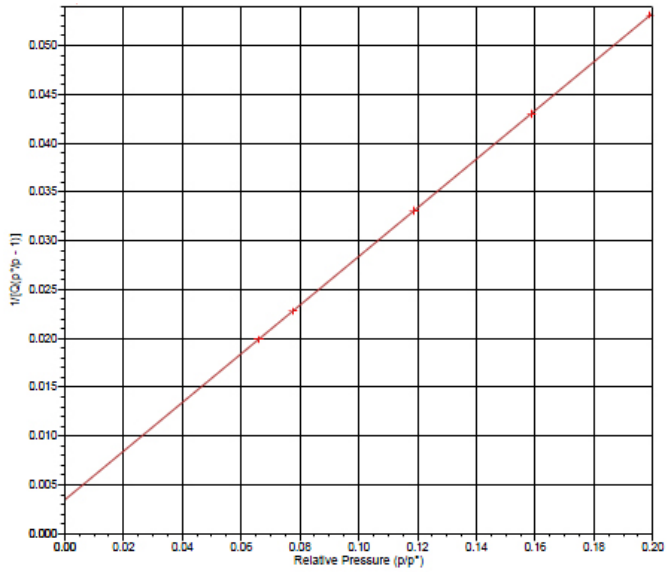

Figure C.3: *BET surface area plot for the 10 minutes oxidation experiment. Degas temperature of 150 ℃.*

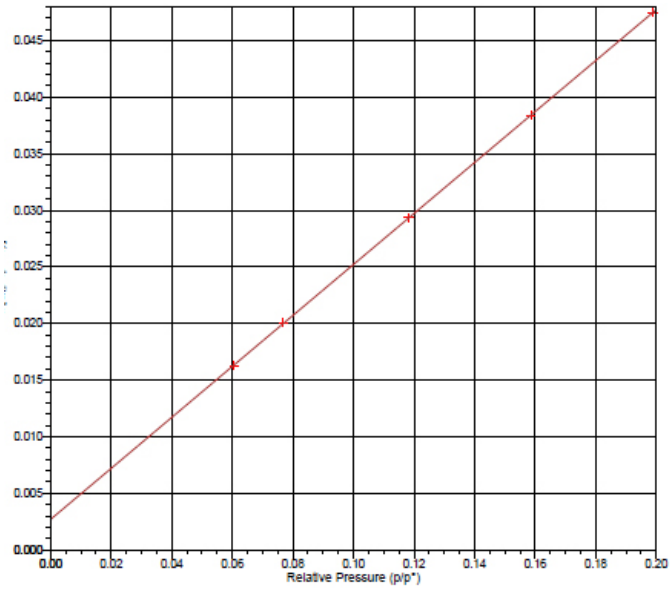

Figure C.4: *BET surface area plot for the 10 minutes oxidation experiment. Degas temperature of 300 ℃.*

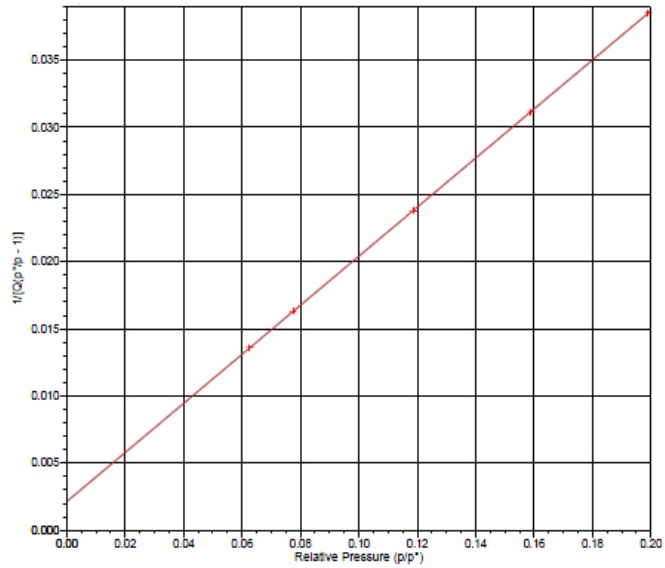

Figure C.5: *BET surface area plot for the 30 minutes oxidation experiment. Degas temperature of 150 ℃.*

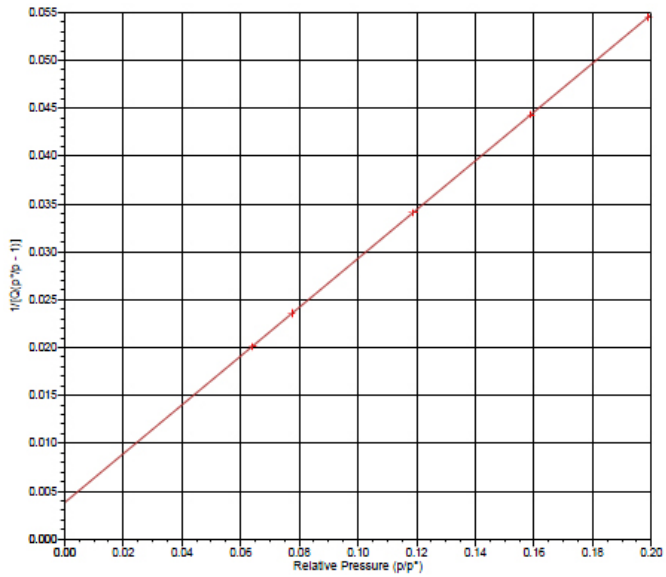

Figure C.6: *BET surface area plot for the 40 minutes oxidation experiment. Degas temperature of 150 ℃.*

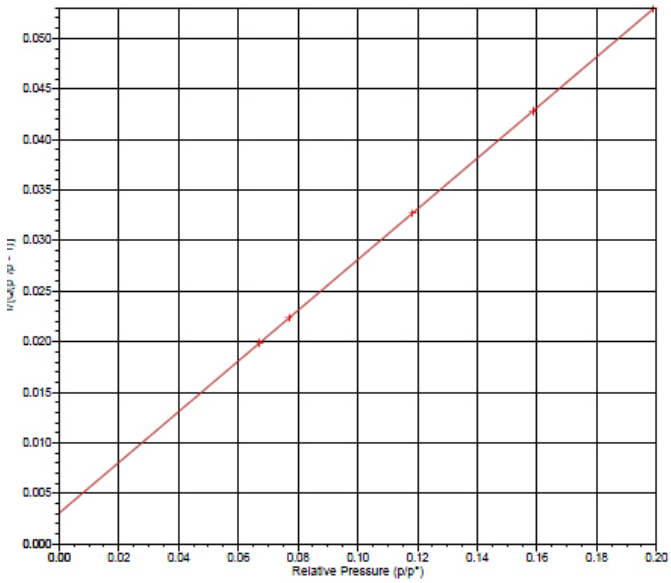

Figure C.7: *BET surface area plot for the 40 minutes oxidation experiment. Degas temperature of 300 ℃.*

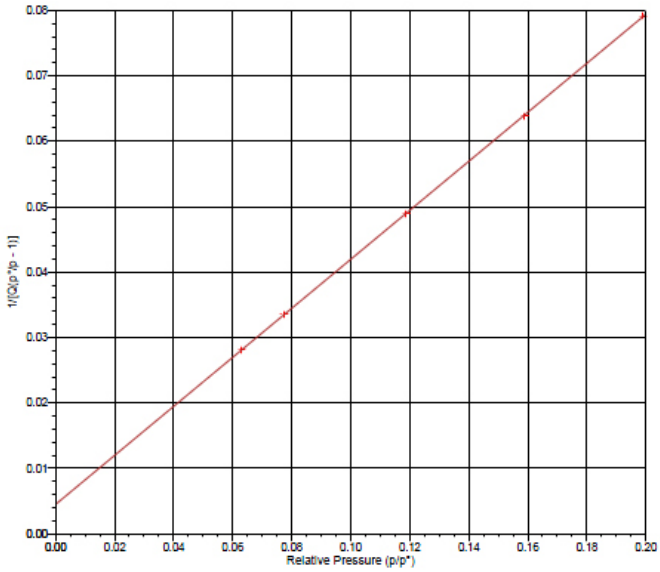

Figure C.8: *BET surface area plot for the 60 minutes oxidation experiment. Degas temperature of 150 ℃.*

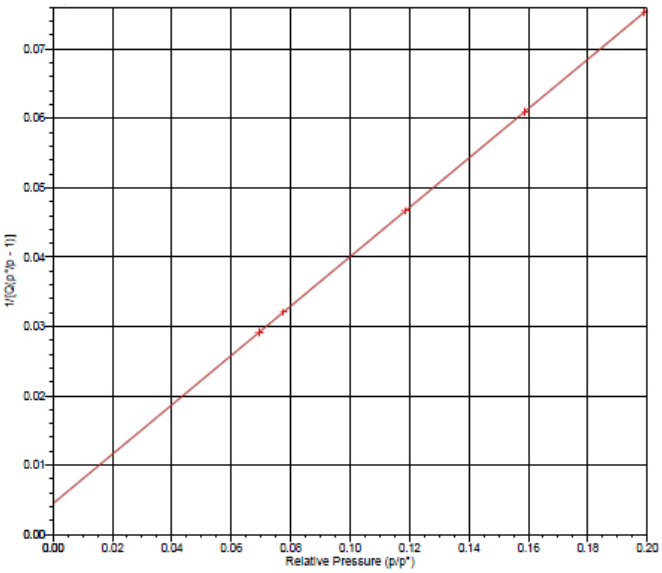

Figure C.9: *BET surface area plot for the 60 minutes oxidation experiment. Degas temperature of 300 ℃.*

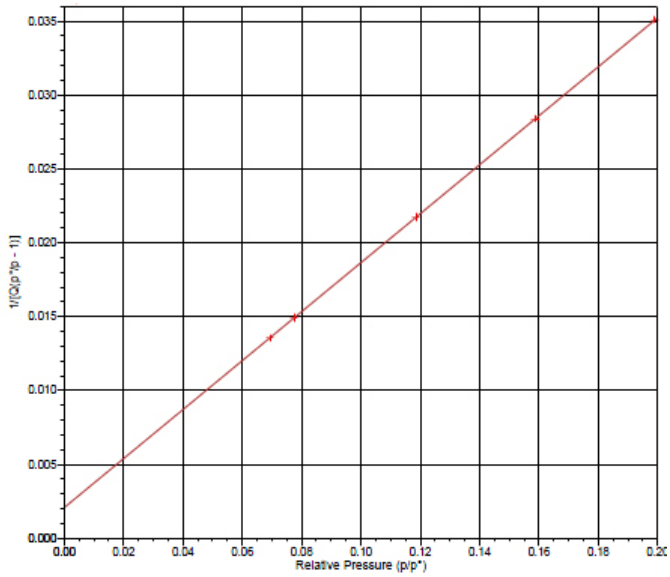

Figure C.10: *BET surface area plot for the 90 minutes oxidation experiment. Degas temperature of 150 ℃.*

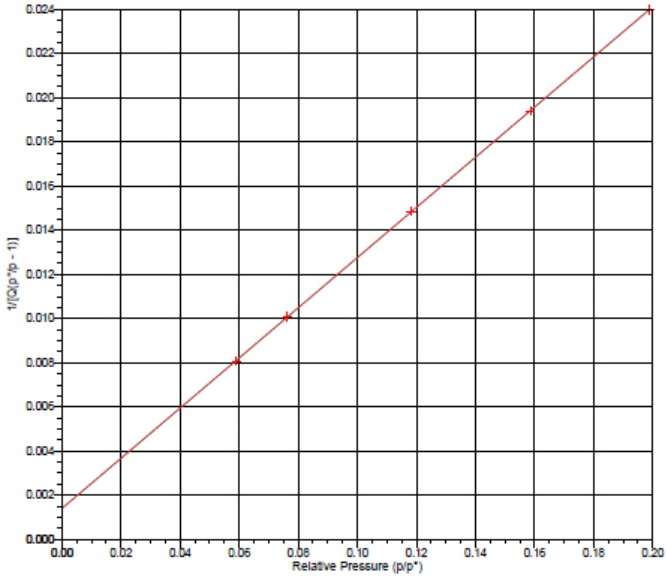

Figure C.11: *BET surface area plot for the 90* minutes oxidation experiment, performed without a COARSE particle. Degas temperature of 150 ℃.*

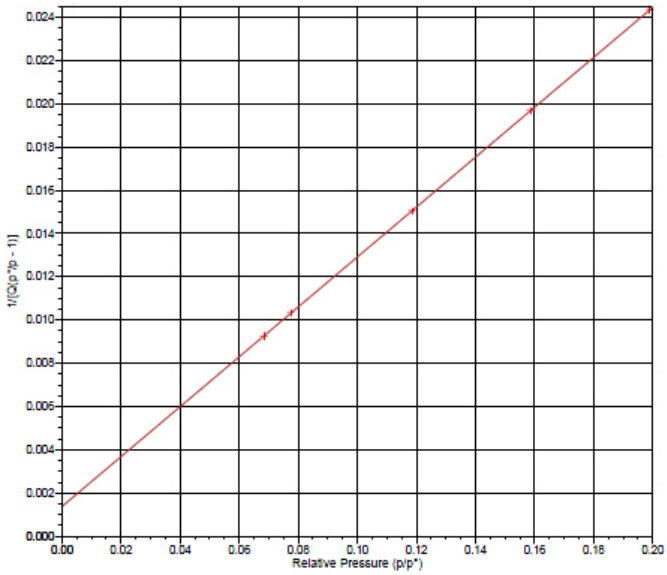

Figure C.12: *BET surface area plot for the 120 minutes oxidation experiment. Degas temperature of 150 °C.*

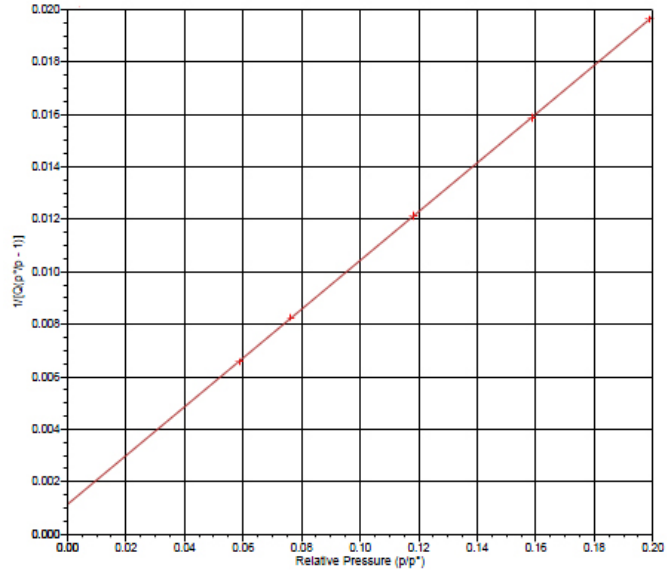

Figure C.13: *BET surface area plot for the 240 minutes oxidation experiment. Degas temperature of 150 °C.*

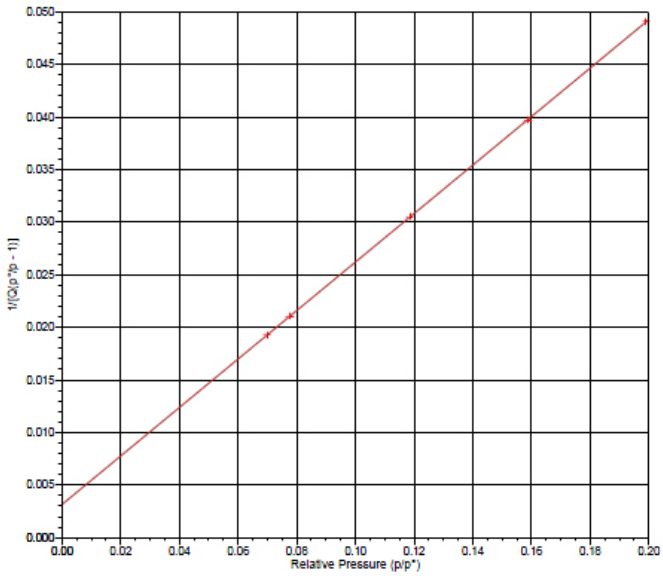

Figure C.14: *BET surface area plot for the test oxidation experiment, using six COARSE particles. Degas temperature of 150 ℃.*

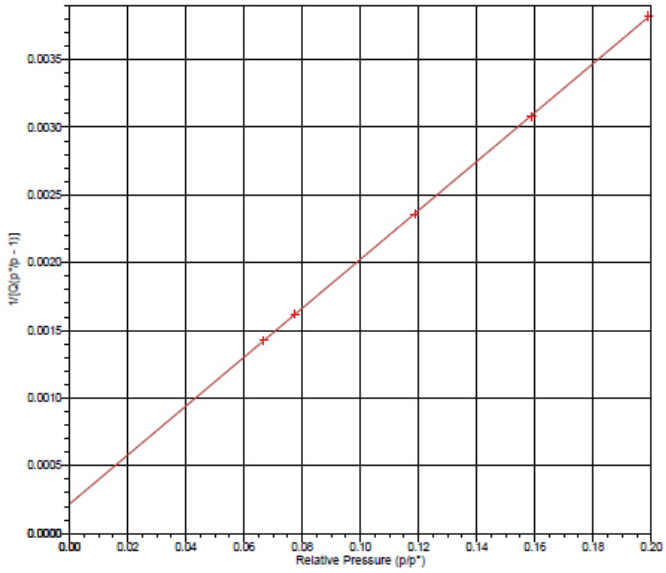

Figure C.15: *BET surface area plot for the amorphous silica. Degas temperature of 150 ℃.*

Appendix D

Hydrogen flow vs. oxidation time

In this section, the hydrogen flow vs. oxidation time for every oxidation experiment which evolved hydrogen is displayed.

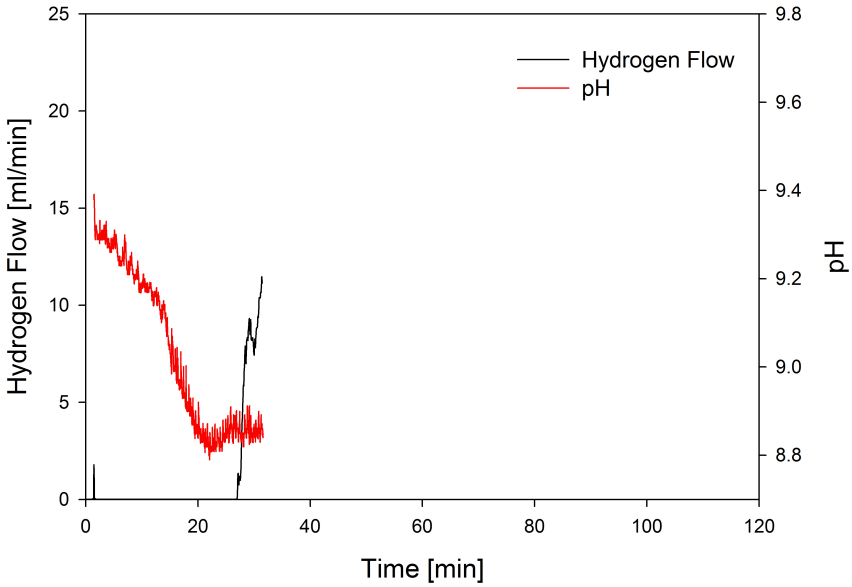

Figure D.1: *Hydrogen flow [ml/min] vs. oxidation time [min] for the 30 minutes oxidation experiment.*

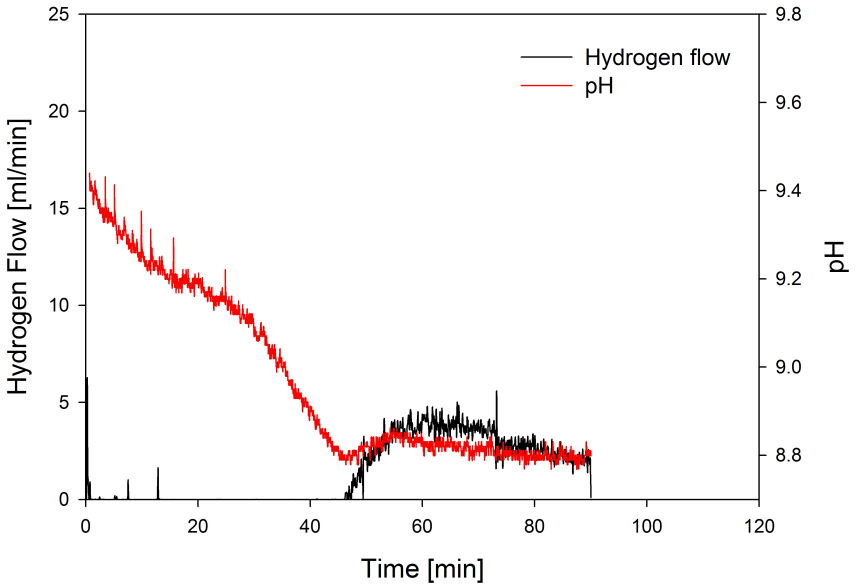

Figure D.2: *Hydrogen flow [ml/min] vs. oxidation time [min] for the 90 minutes oxidation experiment.*

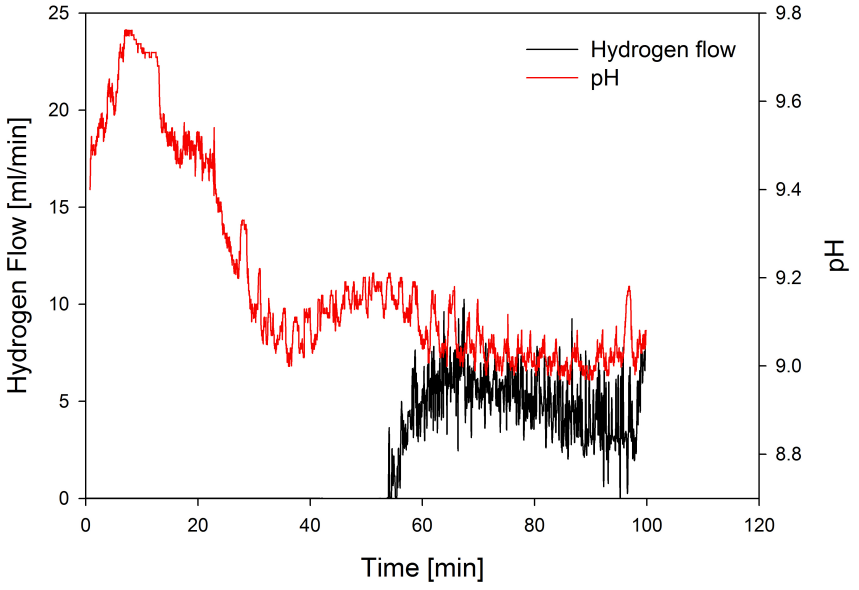

Figure D.3: *Hydrogen flow [ml/min] vs. oxidation time [min] for the 90* minutes oxidation experiment, this was performed without a COARSE particle.*

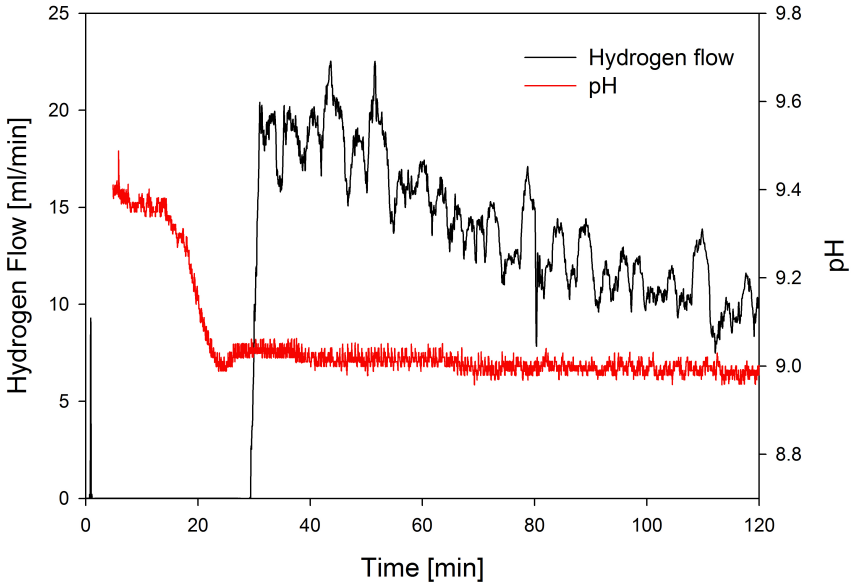

Figure D.4: *Hydrogen flow [ml/min] vs. oxidation time [min] for the 120 minutes oxidation experiment.*

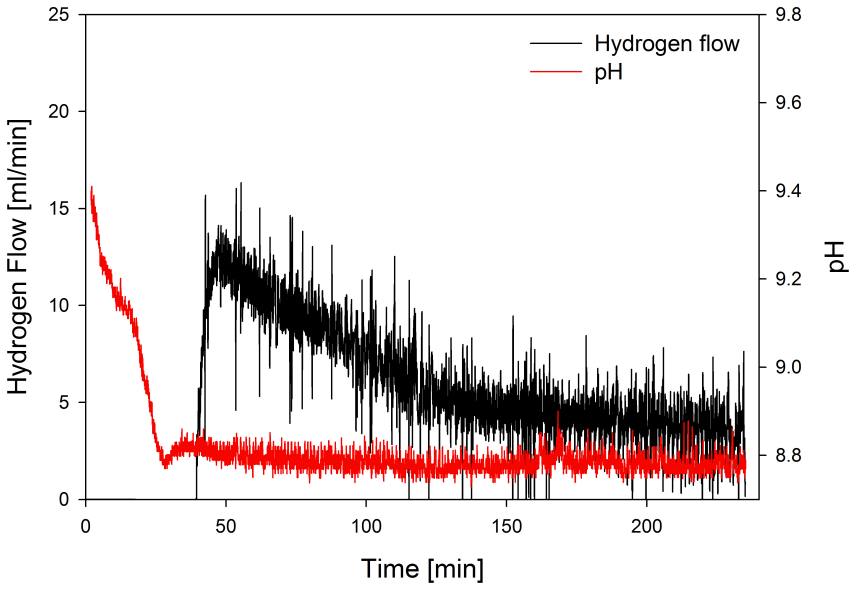

Figure D.5: *Hydrogen flow [ml/min] vs. oxidation time [min] for the 240 minutes oxidation experiment.*

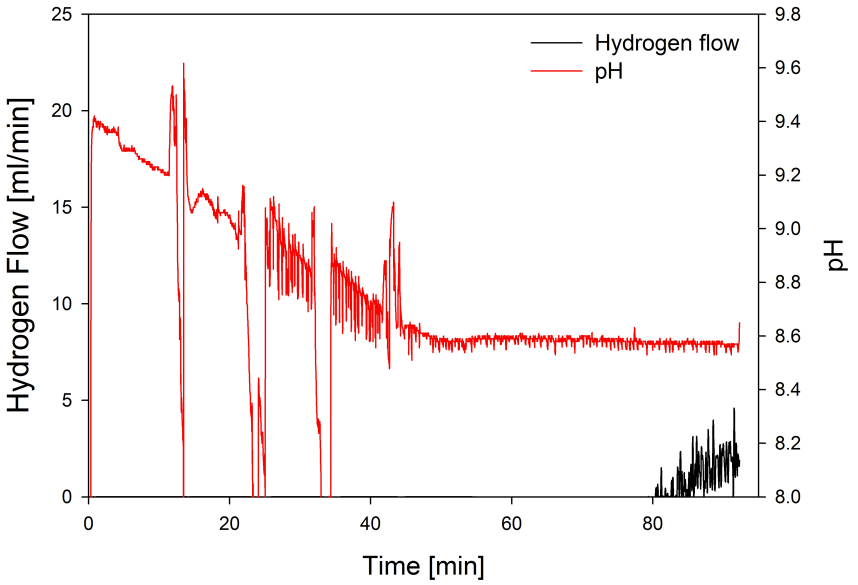

Figure D.6: *Hydrogen flow [ml/min] vs. oxidation time [min] for the test oxidation experiment, using six COARSE particles.*

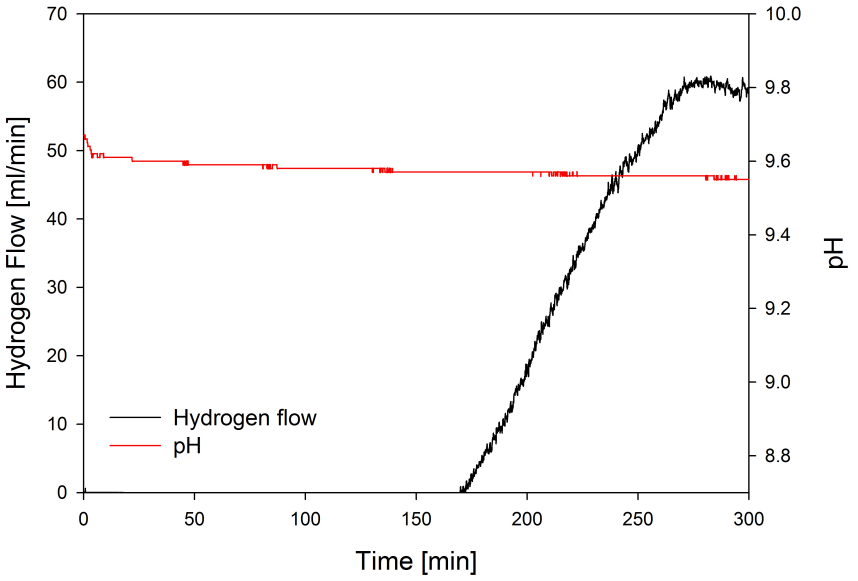

Figure D.7: *Hydrogen flow [ml/min] vs. oxidation time [min] for oxidation of the silicon single crystal sample used for nanoindentation.*

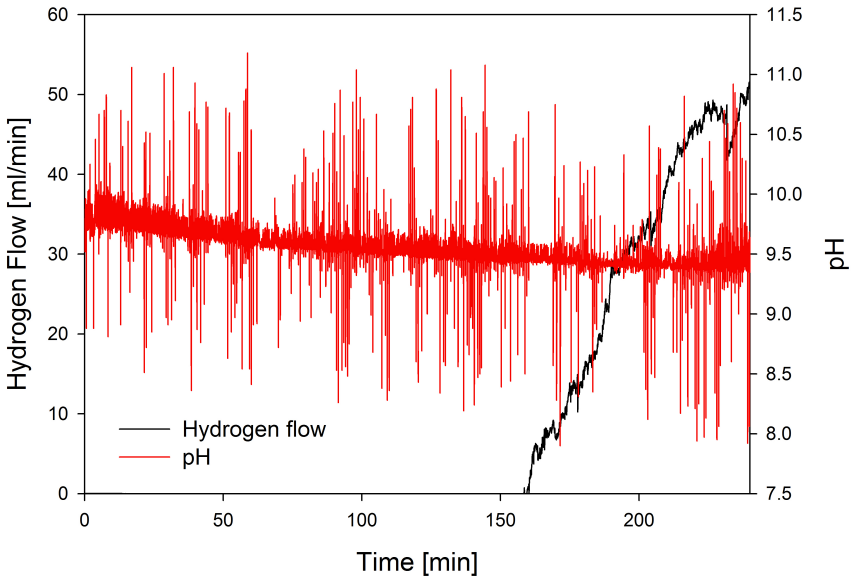

Figure D.8: *Hydrogen flow [ml/min] vs. oxidation time [min] for oxidation of the silicon polycrystalline sample used for nanoindentation. The large variations in the pH measurements is probably an effect of too little reference electrolyte in the pH-electrode.*

Appendix E

Development of the oxidation apparatus

The oxidation apparatus used in the project thesis [2] had several limitations and the results gained were not reproducible. The original apparatus is displayed in Figure E.1. The results produced by this apparatus was characterised by much scatter and sudden variations, with respect to the hydrogen flow [ml/min] vs. oxidation time [min] curves.

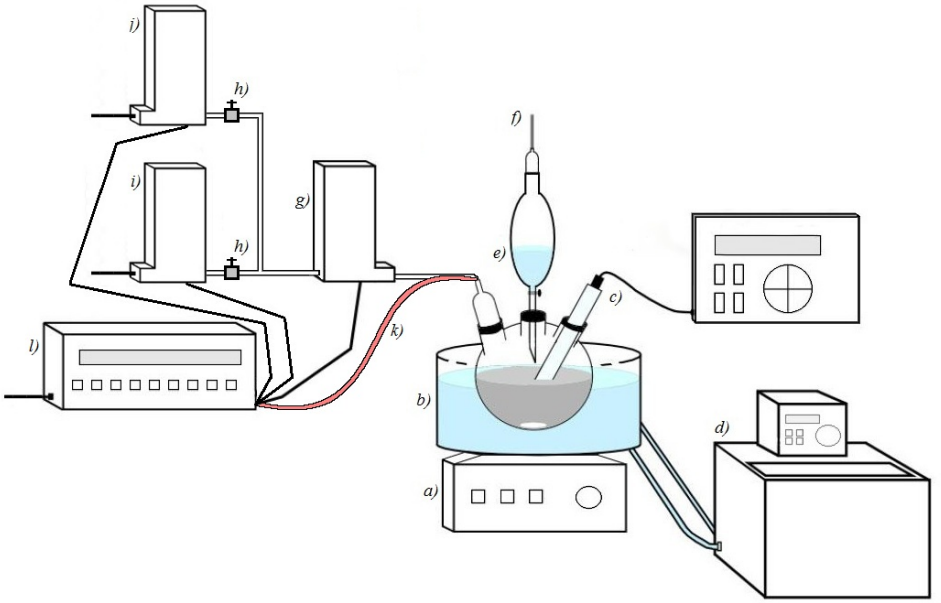

Figure E.1: *The oxidation apparatus used in the project thesis. a) Magnetic stirrer, b) Water bath with fixed temperature, c) pH-meter, d) Heat circulator, e) Titration burette with ammonium hydroxide, f) Nitrogen input, g) Pressure sensor, h) Ball valve, i) Flow meter with small range, j) Flow meter with larger range k) Thermocouple type K l) Data logger with computer output.*

Before the apparatus could be used in this current thesis, a total rebuild and extensive testing was needed. It was decided that water vapour could condense inside the flow meters, thereby affecting the measurements. To prevent this a cold trap using liquid nitrogen was installed. Testing of the apparatus revealed that the results were not satisfying, even with the installation of the cold trap. After much discussion, it was decided to connect the flow meters in series instead of parallel. This gave satisfying results with less scatter and no sudden variations, as displayed in the D. It was also decided to install a pH-meter with a data connection so the pH of the solution could be continuously logged. The titration burette was removed, since the use of a pipette gave better control over the addition of ammonium hydroxide. The improved apparatus is displayed in Figure E.2.

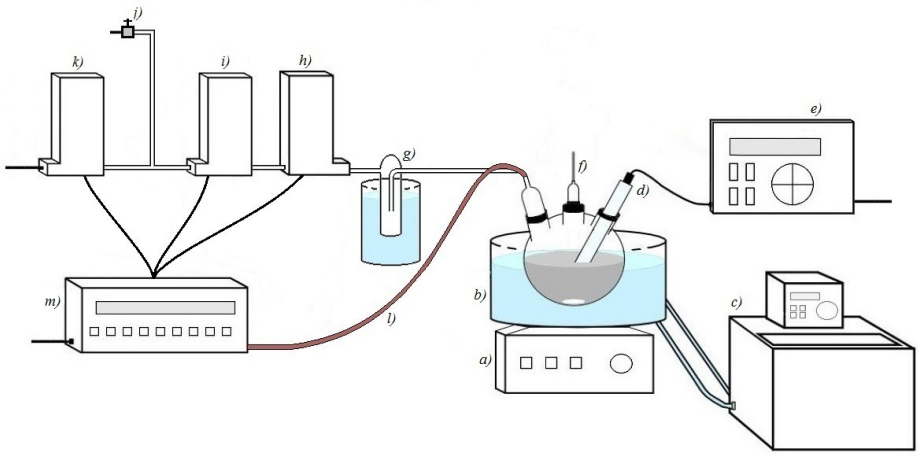

Figure E.2: *The improved apparatus for oxidation of silicon slurries. a) Magnetic stirrer, b) Water bath with fixed temperature, c) Heat circulator, d) pH-electrode), e) pH-meter with computer output, f) Nitrogen input, g) Cold trap, h) Pressure sensor, i) Flow meter with large range, j) Ball valve, k) Flow meter with small range, l) Thermocouple type K, m) Data logger with computer output.*

The apparatus was used extensively throughout the work with this thesis and some problems have been noted. The measuring of hydrogen seems to be inappropriate when the oxidation experiments are run for a short time, which is less than 50 minutes for the JET1 powder. Whether it is the slurry that retains the hydrogen until it is saturated or some shortcomings with the apparatus is unknown. Some of the problems are also related to the JET1 powder not providing reproducibility for experiments performed more than a week apart. It is of importance that these problems are investigated in order to use this apparatus for further experiments. Thoughts about how to improve the apparatus is described in the further work section of the thesis.